João Francisco Martinho Lêdo Guerreiro
Licenciado em
Engenharia Electrotécnica e de Computadores

Maximum Likelihood Detection for OFDM signals with strong nonlinear distortion effects

Dissertação para obtenção do Grau de Mestre em
Engenharia Electrotécnica e de Computadores

Orientador: Rui Miguel Henriques Dias Morgado Dinis,
Professor Auxiliar com agregação, FCT-UNL
Co-orientador: Paulo Miguel de Araújo Borges
Montezuma de Carvalho, Professor Auxiliar, FCT-UNL

Júri:

Presidente:	Prof. Doutor Luís Filipe Lourenço Bernardo
Arguente:	Prof. Doutor Nuno Manuel Branco Souto
Vogais:	Prof. Doutor Rui Miguel Henriques Dias Morgado Dinis
	Prof. Doutor Paulo Miguel de Araújo Borges Montezuma de Carvalho

Julho 2012

Maximum Likelihood Detection for OFDM signals with strong nonlinear distortion effects

Dedication

to the memory of my dear mother, God bless her soul.

Acknowledgements

Firstly, I would like to express my sincere gratitude to my supervisors Rui Dinis and Paulo Montezuma for all the scientific knowledge that they gave me along the realisation of this thesis. In addition, I would like to thank for their patient and availability to help me whenever I need. Without their support, this work could not be developed. In addition, I must express my gratitude to other teachers of the Telecommunications Section, namely, Luis Bernardo and Rodolfo Oliveira for their sympathy and academic support.

I would like to thank to all my family. But, with all my heart, I would like to express my gratitude to my grandparents Carminda and António for all the love, education, support and encouragement during my entire life. There are simply no words to describe all that you have done for me. For all these reasons, it would not make sense if my master degree is not dedicated to you. A special reference also to my uncle Paulo and to my kids Pedro, Miguel and Leonor that make me smile all the time.

From the Department of Electrical Engineering, I would also like to give my special thanks to my colleagues and friends Mauro Ramires, João Pires and Carlos Raposo for their friendship, fellowship and for the stimulating discussions that we had during these five years.

Looking back in these 23 years, I must also thank my friends along the way: José Félix, Miguel Cardoso, Gonçalo Silva, Miguel Castel-Branco, Pedro Castel-Branco, João Serafim, José Marques, Vanessa Guerreiro, Jonas Richter, Tânia Silva, Jorge Simão, Margarida Simão, Daniela Machado, Andreia Dias, and José Mestre that help me one way or another but, specially, for all the fun moments that we shared, for their friendship in the good and bad moments and for always believe in my work and capabilities. I am also very grateful to Teresinha, for all the support, strength and affection that she gives me, sometimes, only with her smile.

Even without being physically present, I would like to dedicate all the work that make possible the achievement of my master degree to my mom, Ilda. She is my *guiding light*, a constant source of encouragement, strength and love. For now, I think that she will be proud of me and (eventually) she would not scolding me due to my bad marks as when I was a kid.

Resumo

Nos dias de hoje, observa-se que os sistemas de comunicações móveis são muito solicitados. Novos serviços como transmissão de dados e vídeo precisam de ritmos elevados para que se garanta o rendimento desejado pelos utilizadores. As técnicas de transmissão por blocos são frequentemente usadas para estes sistemas, visto que preenchem a maior parte dos seus requisitos. Dentro destas técnicas, esquemas como o Orthogonal Frequency Division Multiplexing (OFDM) são bastante utilizados, pois conseguem lidar com canais fortemente seletivos na frequência e atingir uma elevada eficiência espectral. Contudo, os sinais OFDM são muito sensíveis aos efeitos não lineares devido às suas elevadas flutuações de envolvente. Foram propostas várias técnicas para reduzir de forma eficiente estas flutuações. A que apresenta resultados mais promissores consiste em aplicar uma operação não linear para remover os picos de amplitude, seguida de uma operação de filtragem no domínio da frequência para eliminar a radiação fora da banda.

Nas implementações convencionais do OFDM, o termo de distorção linear é visto como ruído que leva a uma degradação na desempenho. Nestas condições, para atingir o melhor desempenho deve-se usar um receptor de máxima verosimilhança, pois este tem em conta toda a informação associada aos sinais com distorção não linear. Esta tese foca-se no estudo de receptores de máxima verosimilhana para sinais OFDM com fortes efeitos não lineares. É demonstrado que, ao contrário do que se poderia esperar, a existência de distorção não linear não implica que haja uma degradação na desempenho, pois o rácio distância Euclideana/energia de bit será maior do que sem a existência de efeitos não lineares. De facto, verifica-se que o desempenho do receptor óptimo que lida com sinais não linearmente distorcidos pode mesmo ser melhor que a desempenho do OFDM convencional com transmissores lineares. Para provar isto, o desempenho assintótica do receptor óptimo é obtida por simulação e teoricamente. Além disso, devido à grande complexidade que este receptor apresenta, quatro receptores sub-ótimos e menos complexos são propostos e avaliados, sendo também estudado o efeito do uso de técnicas iterativas de clipping e filtragem e uso de esquemas de diversidade no seu desempenho.

Palavras chave: Sinais OFDM , efeitos de distorção não linear, deteção de máxima verosimilhança, avaliação de desempenho, diversidade

Abstract

Nowadays, the wireless communication systems are in great demand. New multimedia services such as data and video need reliable high-speed data rates to guarantee the desired throughput to the mobile users. The block transmission techniques are commonly used in these systems since they fulfil the most part of the requirements. Among these techniques, multicarrier schemes like Orthogonal Frequency Division Multiplexing (OFDM) are widely used since they can deal with strong frequency selective channels and also present high spectral efficiency. However, OFDM signals are very prone to nonlinear distortion effects due to their high envelope fluctuations. Therefore, several techniques were proposed to efficiently reduce these fluctuations. The most promising technique is employing a nonlinear operation to reduce the amplitude peaks followed by a frequency-domain filtering operation to reduce the spectral broadening. In typical OFDM implementations, the resulting nonlinear distortion component is treated as a noise-like term that leads to performance degradation. Under these conditions, to achieve optimum performance should be employed a ML (Maximum Likelihood) receiver that considers all the information associated to nonlinear components.

This thesis focus on the study of maximum likelihood receivers for OFDM signals with strong nonlinear distortion effects. It is shown that, contrarily to the one could expect, the nonlinear distortion does not necessary imply a performance degradation because the ratio minimum distance between bit energy of nonlinearly distorted signals is higher than without nonlinear distortion. In fact, the performance of the optimum receiver can be better than with conventional linear transmitters. To prove this, the asymptotic performance of the optimum receiver is evaluated both theoretically and by simulation. In addition, since the optimum receiver presents very high complexity, four less complex sub-optimal receivers are proposed and evaluated, being also studied the impact of employing iterative clipping and filtering techniques and diversity schemes in their BER performance.

Keywords: OFDM signals, nonlinear distortion effects, maximum likelihood detection, performance evaluation, diversity

Contents

List of Acronyms

ADC	**A**nalog to **D**igital **C**onverter
AWGN	**A**dditive **W**hite **G**aussian **N**oise
BER	**B**it **E**rror **R**ate
CCDF	**C**omplementary **C**umulative **D**ensity **F**unction
CIR	**C**hannel **I**mpulsive **R**esponse
CP	**C**yclic **P**refix
DAC	**D**igital to **A**nalog **C**onverter
DFT	**D**iscrete **F**ourier **T**ransform
DR	**D**ynamic **R**ange
DVB	**D**igital **V**ideo **B**roadcasting
FDE	**F**requency **D**omain **E**qualization
FDF	**F**requency **D**omain **F**ilter
FDM	**F**requency **D**ivision **M**ultiplexing
FFT	**F**ast **F**ourier **T**ransform
FT	**F**ourier **T**ransform
HPA	**H**igh **P**ower **A**mplifier
IBI	**I**nter **B**lock **I**nterference
IDFT	**I**nverse **D**iscrete **F**ourier **T**ransform
IMP	**I**nter **M**odulation **P**roduct
ISI	**I**nter **S**ymbol **I**nterference
LINC	**LI**near amplification with **N**onlinear **C**omponents
LS	**L**east **S**quare
MAP	**M**aximum **A** **P**osteriori
MC	**M**ulti **C**arrier
MMSE	**M**inimum **M**ean **S**quare **E**rror
ML	**M**aximum **L**ikelihood
MT	**M**obile **T**erminal
OFDM	**O**rthogonal **F**requency Division **M**ultiplexing
PAR	**P**eak to **A**verage **R**atio
PDF	**P**robability **D**ensity **F**unction

PSD	**P**ower **S**pectral **D**ensity
PMPER	**P**eak to **M**ean **E**nvelope **P**ower **R**atio
QAM	**Q**uadrature **A**mplitude **M**odulation
QPSK	**Q**uadrature **P**hase **S**hift **K**eying
SIMO	**S**ingle **I**nput **M**ultiple **O**utput
RF	**R**adio **F**requency
SNR	**S**ignal to **N**oise **R**atio
SP	**S**erial to **P**arallel
SSPA	**S**olid **S**tate **P**ower **A**mplifier
TWTA	**T**ravelling **W**ave **T**ube **A**mplifier
ZP	**Z**ero **P**adding

List of Symbols

A	amplitude of QPSK symbols
$A(\cdot)$	AM-AM characteristic of a nonlinear function
B	bandwidth of $G_x(f)$
$\mathfrak{D}^2$	Euclidean distance between to nonlinearly signals
$d(t)$	distortion component of the non-linearity output
E_b	bit energy
F	frequency separation
F_k	equalization factor for the k^{th} sub-carrier
f	frequency variable
f_0	central frequency of the spectrum
$\mathfrak{G}$	asymptotic gain of nonlinear OFDM
$G_x(\tau)$	power spectral density of the input signal $x(t)$
$G_y(\tau)$	power spectral density of the output signal $y(t)$
$G_d(\tau)$	power spectral density of the distortion component d(t)
H_k	channel impulsive response for the k^{th} sub-carrier
$\hat{H}_k$	estimated channel impulsive response for the k^{th} sub-carrier
$h_R(t)$	impulsive response of the reception filter
$h_T(t)$	impulsive response of the after sampling reconstruction filter
$h_W(t)$	impulsive response of the shaping filter
I	average power of the interference at the non-linearity output
L	number of clipping and filtering iterations
k	frequency index
$\mathcal{M}$	number of constellation points
M	oversampling factor
N	number of data sub-carriers
N_0	PSD of the channel noise
N_k	frequency-domain noise factor for the k^{th} sub-carrier
N_{Rx}	number of receiver antennas
n	time index

P_b	bit error probability
P_{out}	average power at the non-linearity output
$P_{2\gamma+1}$	power associated with inter modulation product of order $2\gamma + 1$
$R_x(\tau)$	autocorrelation of input signal $x(t)$
$R_y(\tau)$	autocorrelation of nonlinearity output $y(t)$
$R_d(\tau)$	autocorrelation of self-interference component $d(t)$
$S_{k,m}$	transmitted symbol for k^{th} frequency in m^{th} burst
S_k	transmitted symbol for k^{th}frequency
S	average power of the non-linearity output
$S_m(f)$	frequency-domain signal associated to m^{th} data block
$s(t)$	time-domain OFDM signal
s_n	n^{th} time-domain sample of OFDM signal
s_n^M	n^{th} time-domain sample of the oversampled OFDM signal
$s^{(P)}(t)$	time-domain periodic function associated to an OFDM block
$s_m(t)$	time-domain signal associated to m^{th} data block
t	time variable
T_B	OFDM block duration
T_G	cyclic prefix duration
T	useful duration of the OFDM block
$W(f)$	Fourier transform of $w(t)$
w_n	n^{th} time-domain sample of the support pulse
$w(t)$	OFDM support pulse
$w'(t)$	rectangular window
$x(t)$	complex envelope of non-linearity input
Y_k	frequency-domain output for the k^{th} sub-carrier
$y(t)$	nonlinearity output
α	scaling factor of the nonlinearity useful component
y_n	n^{th} time-domain output sample of OFDM signal

$\Theta(\cdot)$	AM-PM characteristic of a nonlinear function
σ^2	variance of OFDM time-domain complex samples
μ	number of different bits between two data sequences
$\delta(t)$	Dirac delta function
ρ	roll-off factor

Matrix Symbols

$\mathbf{E}$	frequency-domain data error sequence
$\boldsymbol{\varepsilon}$	time-domain error samples
$\mathbf{D}$	frequency-domain nonlinear distortion component
$\mathbf{N}$	frequency-domain noise sequence
$\mathbf{I}_N$	$N \times N$ identity matrix
$\mathbf{X}$	frequency-domain transmitted data sequence
$\mathbf{x}$	time-domain transmitted samples
$\hat{\mathbf{X}}$	frequency-domain estimated data sequence
$\mathbf{Y}$	frequency-domain nonlinearly distorted data sequence
$\mathbf{y}$	time-domain nonlinearly distorted samples
$\mathbf{H}$	frequency-domain channel response
$\mathbf{G}$	frequency-domain filter response
$\mathbf{Z}$	frequency-domain received data sequence
$\mathbf{F}_{NM}$	NM-size DFT matrix

List of Figures

Chapter 1

Introduction

1.1 Context

Wireless communications are today widely used due to the growing demand for users mobility. Nevertheless, these kind of communications continue to be a challenging area due to the constant demand of higher data rates and spectral efficiencies. Moreover, it is desired that wireless devices have long battery life (i.e., low power consumption) as well as low complexity for ease manufacture.

To achieve high-speed data transmission in wireless environments it is necessary to develop techniques that overcome the radio channel problems as frequency and time selectivity, the multipath propagation or the Doppler Effect. Orthogonal Frequency Division Multiplexing (OFDM) [1][2] based schemes are excellent candidates for broadband wireless communications mainly due to their good performance over severely time-dispersive channels without the need for complex receiver implementations. However, this multicarrier scheme has a key issue: presents high sensitivity to nonlinear distortion effects.

In time-domain, OFDM signals are characterized by high envelope fluctuations, which make them susceptible to nonlinear distortion effects. Both the transmitter and receiver, have stages that don't present a completely linear behaviour, however the main source of nonlinear distortion is usually the high power amplifier (HPA), specially a high power efficiency is desired in the radio frequency (RF) amplification. To avoid nonlinear distortion in signals with large dynamic range (DR), the HPA should be overdimensioned to assure an operation far away from

the saturation point. In the uplink direction this is a severe issue, since it is intended that the mobile terminals (MT) have low power consumption for a longer battery life. Therefore, many methods to reduce the envelope fluctuations by means of signal processing have been proposed. These methods can work both in frequency and time-domain. In the frequency-domain, a reasonable amount of redundancy can be used to avoid high amplitude peaks [3]. However, there is an issue associated with this method since when the number of subcarriers is high, the code rate of the required frequency-domain codes becomes also very low (i.e. the redundant information is very high). Another technique implemented in the frequency-domain is the use of multiple symbol representations [4][5]. The main problem of this technique is the very high computational complexity. Other methods are defined in the time-domain, such as those that consider a nonlinear operation to avoid amplitude peaks [6][7]. A new class of promising low complexity and spectrally efficient schemes combine a nonlinear operation in the time-domain, for example a clipping operation, with a frequency-domain filtering operation to remove the out-of-band radiation associated to the intermodulation products [9][8][10][11]. Although the significant reduction on the envelope fluctuations of OFDM achieved by the clipping technique, it is still need to employ quasi-linear amplifiers. On the other hand, it would be desirable to employ nonlinear amplifiers since they are simpler, cheaper, have higher output power and higher amplification efficiency. A promising technique that allows the use of nonlinear amplifiers is the two-branch LInear amplification with Nonlinear Components (LINC) [12][13][14]. In addition, the LINC and clipping techniques can be used in another multicarrier schemes or with other nonlinear devices [15][16][17][18].
This work focuses on the study of nonlinear OFDM schemes, with special focus on the study of optimal and suboptimal receivers that use the distortion components to improve the performance.

According to the central limit theorem [19], when the number of subcarriers is high, an OFDM signal can be modelled by a complex Gaussian process which allows the decomposition of the transmitted nonlinearly signal as the sum of two uncorrelated components: an useful component that is proportional to the original signal and a distortion component [21].

In conventional receiver implementations the distortion component is regarded as an additional noise-like term that can lead to performance degradation. In that sense, several techniques were proposed to improve the performance of nonlinear OFDM transmissions. One of them

employs iterative receivers that try to estimate and cancellate the nonlinear distortion component [22][23]. Nevertheless, the estimation of this component is not easy and, in fact, for low values of signal-to-noise ratio (SNR) the performance of these receivers can even be worse than the conventional OFDM receivers. Moreover, the distortion component has information about the transmitted signal that can be used to improve the performance [24] which suggests the use of an optimum receiver. The optimum receiver is a maximum likelihood (ML) receiver that compares the Euclidean distance between the received signal and all the possible transmitted signals selecting the estimated data that have smaller distance relative to the received signal. It is clear that the ML receiver takes into account not only the useful component but also the information inherent to the nonlinear component. The main problem associated to an ML receiver relies in its complexity that grows exponentially with the number of subcarriers. However, it is possible to develop suboptimal ML receivers that have good performance and present less complexity [25] [26]. This thesis focuses on the study of optimal and suboptimal ML-based receivers that deal with nonlinear distorted signals. Besides the characterization of the performance of these receivers both by simulation and theoretically, it is also shown that, the optimum ML and the sub-optimum performance of nonlinearly distorted OFDM can be better than considering conventional OFDM that deals with linear transmitters. As consequence, the proposed receivers are specially adequate for wireless systems that face propagation problems or underwater communications [27], due to the lower requirements for the data rates.

Conventions

Bold letters denote matrices or vectors and italic letters denote scalars. Capital letters are associated to the frequency-domain and small letters are associated to the time-domain. $[\mathbf{X}]_{i,j}$ denotes the $(i,j)^{th}$ element of $\mathbf{X}$, i.e., the element at the i^{th} line and the j^{th} column of the matrix $\mathbf{X}$ and $[\mathbf{X}]_i$ denotes the i^{th} element of the vector $\mathbf{X}$. diag($\mathbf{X}$) denotes a diagonal matrix with $(i,i)^{th}$ element equal to $[\mathbf{X}]_i$ and $||\mathbf{X}||$ denotes the Euclidean norm of the vector $\mathbf{X}$. $\mathbf{I}_N$ is the $N \times N$ identity matrix. $(\cdot)^T$ and $(\cdot)^H$ denote the transpose and Hermitian (i.e., complex conjugate of the transpose) operators, respectively. The PDF of the random variable x, $p_x(x)$, is simply denoted by $p(x)$ when there is no risk of ambiguity.

1.2 Organization

After the introduction made before in this chapter, this thesis is organized as follows: in Chapter 2 is made an analytical characterization of OFDM signals in time and frequency-domains. The transmitter and receiver structures that are commonly used are also described. In the last section of the chapter, based on a statistical approach, we present a theoretical characterization of the nonlinear effects. Chapter 3 concerns about the potential performance of an ideal ML receiver that deals with nonlinearly distorted signals. Here, the achievable gains are analysed analytically and by simulation, and both results are compared. Chapter 4 presents several suboptimal ML-based receivers as well as their performance results. Finally, Chapter 5 resumes this thesis and presents perspectives for future work.

1.3 Major Contributions

The major contribution of this thesis is to present a new vision for systems that lead with nonlinearly distorted OFDM signals. It is shown that the performance of the ML and ML-based receivers can be improved even in the presence of nonlinear distortion. The achievable gains are analysed and quantified both by simulation and theoretically. Additionally, a closed expression for the Euclidean distance between two distorted signals that are behind the achievable gain of nonlinear OFDM is derived.

Meantime, several papers have resulted from the developed research work:

Accepted:

- João Guerreiro, Rui Dinis and Paulo Montezuma, "Approaching the Maximum Likelihood Performance with Nonlinearly Distorted OFDM Signals, published in *IEEE VTC2012 (Spring)*, Yokohama, May 2012.
- João Guerreiro, Rui Dinis and Paulo Montezuma, "Optimum and Sub-Optimum Receivers for OFDM Signals with Iterative Clipping and Filtering", to be presented at *IEEE VTC2012 (Fall)*, Quebec City, Canada, Sep. 2012.

- João Guerreiro, Rui Dinis and Paulo Montezuma, "ML-Based Receivers for Underwater Networks Using OFDM Signals with Strong Nonlinear Distortion Effects", to be presented at *MILCOM 2012*, Florida, USA, Oct. 2012.

Submitted:

- João Guerreiro, Rui Dinis and Paulo Montezuma, "Optimum and Sub-Optimum Receivers for OFDM Signals with Strong Nonlinear Distortion Effects", submitted to *IEEE Transactions on Communications*.

Chapter 2

OFDM Schemes

The multi-carrier (MC) modulation OFDM was selected for several systems, such as Digital Video Broadcasting (DVB) [28], wireless broadband access technologies IEEE 802.16a/d/e [29, 30] and fourth generation networks as the Long Term Evolution (LTE) [31].

In this chapter, a brief introduction to OFDM signals is carried out. This introduction includes the characterization of the signals both in time and frequency-domain as well as the definition of the transmitter and receiver structure suitable for these signals. As these signals are very prone to nonlinear distortion effects due to their high envelope fluctuations, the nonlinear effects associated to polar memoryless nonlinearities are also studied.

This chapter is organized as follows: in Section 2.1 is presented an characterization of OFDM signals and its key properties. Section 2.2 characterizes the transmitter and receiver structure that are typically used in OFDM schemes. Finally, in Section 2.3 is made a theoretical analysis of the nonlinear effects in OFDM signals based on a Gaussian approximation. This theoretical analysis includes the signal characterization at the nonlinearity output both in time and frequency-domain.

2.1 Signal Characterization

The main concept of MC schemes is to split the available bandwidth B into N smaller sub-channels spaced at F. In other words, the initial frequency selective wideband channel is divided in smaller and approximately flat frequency sub-channels, mitigating the need to perform a complex equalization. The main data stream is also divided into N individually low

rate streams that will be transmitted in parallel on the different subcarriers. Since OFDM's subcarriers are orthogonal, thus, it is possible to recover the data even if their spectrum overlap. When compared with other FDM schemes, the overlapping of the subcarriers is a key advantage, because it allows a compression of the spectrum. The complex envelope of an OFDM signal can be expressed as a sum of data bursts spaced at T_B,

$$s(t) = \sum_{m} s_m(t - mT_B), \tag{2.1}$$

where T_B is the burst duration and $s_m(t)$ denotes the m^{th} burst that is defined as

$$s_m(t) = \sum_{k=0}^{N-1} |S_{k,m}| \cos\left(2\pi(f_0 + kF)t + \arg\{S_{k,m}\}\right) w(t), \tag{2.2}$$

with $S_{k,m} = |S_{k,m}| \exp\left(\arg\{S_{k,m}\}\right)$ denoting the complex symbol selected from a given constellation (e.g. Quadrature Amplitude Modulation (QAM)) that modulate the k^{th} subcarrier of the m^{th} burst, F representing the subcarrier spacing, f_0 denoting the central frequency and $w(t)$ representing the support pulse. Note that the time-domain signal $s_m(t)$ can also be written as

$$s_m(t) = \Re\left\{s_m(t) \exp\left(j2\pi f_0 t\right)\right\}, \tag{2.3}$$

with

$$\tilde{s_m}(t) = \sum_{k=0}^{N-1} S_{k,m} \exp\left(j2\pi kFt\right) w(t), \tag{2.4}$$

Applying the Fourier Transform (FT) (denoted by $\mathcal{F}(\cdot)$ operator) to both sides of (2.4) and using the modulation property of the referred transform, we get

$$S_m(f) = \sum_{k=0}^{N-1} S_{k,m} W(f - kF), \tag{2.5}$$

where $W(f) = \mathcal{F}\{w(t)\}$. Therefore, we note that the spectrum of an OFDM signal is defined by the complex symbols that are transmitted sequentially and individually in the frequency domain during the time interval T. To ensure an Inter Symbol Interference (ISI) free transmission, the Fourier transform of the support pulse $w(t)$ must verify the orthogonality condition

$$\int_{-\infty}^{+\infty} W(f - kF) W^*(f - k'F)\, \mathrm{d}f = 0, \qquad k \neq k', \tag{2.6}$$

where $(\cdot)^*$ denotes complex conjugate. Using Parseval theorem we can rewrite (2.6) as

$$\int_{-\infty}^{+\infty} |w(t)|^2 \exp\left(-j2\pi(k-k')Ft\right)\, \mathrm{d}t = 0, \qquad k \neq k'. \tag{2.7}$$

The transmitted pulse associated to conventional OFDM schemes $w(t)$ is

$$w(t) = \begin{cases} 1, & 0 \leq t \leq T \\ 0, & \text{otherwise,} \end{cases} \tag{2.8}$$

and, although the condition (2.6) is not verified by the support pulse defined in (2.8), the subcarriers can be assumed to be orthogonal in the interval [0,T]. Using (2.7) and (2.8) we may write

$$\int_{-\infty}^{+\infty} |w(t)|^2 \exp\left(-j2\pi(k-k')Ft\right)\, \mathrm{d}t \quad = \tag{2.9}$$

$$= \begin{cases} T, & k = k' \\ 0, & k \neq k'. \end{cases} \tag{2.10}$$

Note that considering the support pulse defined in (2.8), we can write (2.5) as

$$S_m(f) = \sum_{k=0}^{N-1} S_{k,m} \mathrm{sinc}(f - kF), \tag{2.11}$$

where $\mathrm{sinc}(a) = \frac{\sin(\pi a)}{\pi a}$. Therefore, it can be shown that the Power Spectral Density (PSD) of the OFDM signal is proportional to $\sum_{k=0}^{N-1} |\mathrm{sinc}(f - kF)|^2$ as depicted in the Figure 2.1.

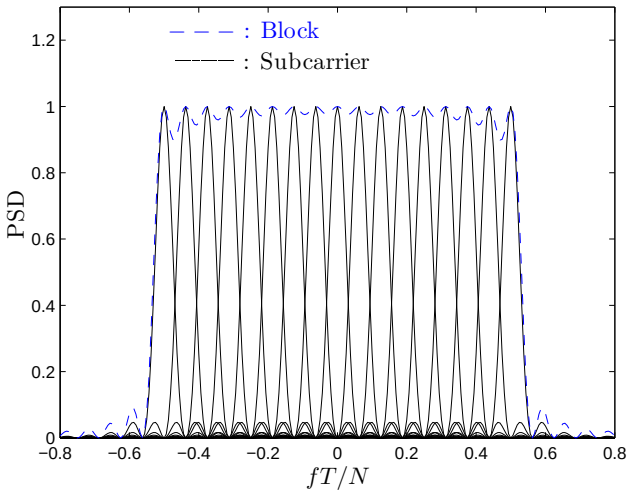

FIGURE 2.1: PSD of the OFDM complex envelope considering N=16 subcarriers.

In time dispersive channels, the OFDM bursts can overlap leading to existence of Inter Block Interference (IBI). To solve this problem, a guard interval between adjacent blocks can be used. If this interval is bigger than the channel impulse response (CIR) (i.e., the delay of last multipath ray), all the copies of the original transmitted block that arrive at the receiver will fall into this interval. Note that this interval can be achieved by extending each OFDM burst with a fixed sequence, for example, a cyclic prefix (CP) or a zero-padding (ZP) sequence. In this work, it is considered the first case, being the overall pulse duration defined as $T_B = T_G + T$, where T_G is the duration of CP and T is the useful part of the block. A typical value for T_G is $0.2T$, however, is important to mention that there is not an optimal duration for CP, since it depends directly on the channel impulsive response CIR, i.e., varies from channel to channel. It is also important to point out that the use of this technique has also some drawbacks: since the CP is an overhead, each burst will have redundant information which can compromise the service bit rate and the power efficiency. Moreover, as CP will occupy some subcarriers, the spectral efficiency is lower, which is a relevant issue since the band is a limited and expensive resource.

2.2 Transmitter and Receiver Structure

Let us now consider the transmitter structure for OFDM signals. The first task performed by the receiver is to split the high data rate input stream in N lower data rate streams through

a serial-to-parallel (SP) converter. Subsequently, the data bits are mapped into the complex symbols $\{S_k; k = 0, 1, \ldots, N-1\}$, according to the adopted constellation. The next procedure consists in multiplying the complex data symbols by the generated subcarriers and sum all the resultant signals to build the data block $s^{(P)}(t)$ defined as

$$s^{(P)}(t) = \sum_{k=0}^{N-1} S_{k,m} \exp(j2\pi kFt). \tag{2.12}$$

Note that (2.4) can also be written as

$$s_m(t) = s^{(P)}(t)w(t). \tag{2.13}$$

Since $s^{(P)}(t)$ is a periodic function in t, with period $T = 1/F$, i.e.,

$$s^{(P)}(t+T) = \sum_{k=0}^{N-1} S_{k,m} \exp(j2\pi kF(t+T)) = \sum_{k=0}^{N-1} S_{k,m} \exp(j2\pi kFt) \underbrace{\exp(j2\pi k)}_{1 \ \forall \ k}, \tag{2.14}$$

we can say that the complex envelope of the OFDM block during T_G (i.e., during the CP) is a repetition of the last part of the transmitted block, i.e.,

$$s_m(t) = s_m(t+T), \qquad -T_G \leq t \leq 0, \tag{2.15}$$

as illustrated in the Figure 2.2.

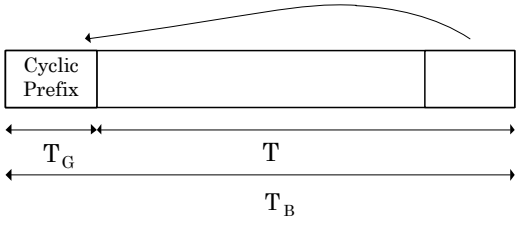

FIGURE 2.2: OFDM block structure with the Cyclic Prefix

Applying the FT to both sides of (2.12) we obtain

$$S^{(P)}(f) = \sum_{k=0}^{N-1} S_{k,m}\delta(f - kF), \tag{2.16}$$

where $\delta(f) = \mathcal{F}\{1\}$ represents the Delta dirac function. Summing all the spectral components it is clear that the bandwidth occupied by $S^{(P)}(f)$ is $NF = N/T$. According to the sampling theorem and assuming that the maximum frequency is $N/2T$, the signal can be recovered when sampled at a rate of $2N/2T = N/T$ in the interval [0,T]. The resultant samples can be written as

$$s_n^{(P)}(t) = s^{(P)}(t)|_{t=\frac{nT}{N}} = \sum_{k=0}^{N-1} S_{k,m} \exp\left(j2\pi k \frac{n}{N}\right), \qquad n = 0, 1, ..., N-1. \tag{2.17}$$

Looking at (2.17), are obvious the similarities with the inverse discrete Fourier transform (IDFT). This operation transforms the frequency-domain block $\{X_k; k = 0, 1, \ldots, N-1\}$ into the time-domain samples $\{x_n; n = 0, 1, \ldots, N-1\}$, with

$$x_n = \frac{1}{\sqrt{N}} \sum_{k=0}^{N-1} X_k \exp\left(j2\pi k \frac{n}{N}\right), \tag{2.18}$$

where N is the size of the considered data block. If we define s_n as

$$s_n = \frac{1}{\sqrt{N}} s_n^{(P)}(t), \tag{2.19}$$

it is clear that the block of time domain samples $\{s_n; n = 0, 1, \ldots, N-1\}$ is the IDFT of the frequency domain block $\{S_k; k = 0, 1, \ldots, N-1\}$, i.e.,

$$s_n = \text{IDFT}\{S_k\}. \tag{2.20}$$

This means that a sampled version of $s^{(P)}(t)$ on the interval T can be obtained through the IDFT of the block of transmitted symbols, which can be efficiently implemented using the Fast Fourier Transform (FFT). This algorithm reduces the required operations to compute the IDFT from N^2 to $N \log_2(N)$ (N must be a power of 2) [32]. In addition, with an N-point FFT, the complexity of transmitter is reduced, since N multipliers and oscillators that would be necessary to generate the multicarrier signal are avoided. At the FFT's output, a CP of N_G samples is added at the beginning of each N-size OFDM block. In order to obtain $s(t)$, the time-domain samples s_n must be multiplied by the samples of the support pulse. The resultant samples are then converted into an analog signal that will be sent through the RF link. To do that conversion, the time-domain samples are submitted to a Digital to Analog

Converter (DAC). The DAC is followed by a reconstruction filter, to suppress the spectral replicas at its output. The reconstructed complex envelope, $s(t)$, can be written as

$$\begin{aligned} s(t) &= \left(\sum_{n=-\infty}^{+\infty} s_n \; w_n \delta\left(t - \frac{nT}{N}\right) \right) * h_T(t) \\ &= \sum_{n=-\infty}^{+\infty} s_n \; w_n h_T\left(t - \frac{nT}{N}\right), \end{aligned} \tag{2.21}$$

where $h_T(t)$ is the impulsive response of the reconstruction filter that has a bandwidth of $\frac{N'}{2T}(1+\rho)$, with ρ being the roll-off factor that varies from 0 to 1.

If a sampling rate of N/T is used, the spectrum of the sampled signal is free of aliasing effects. However, after the sampling operation, it is desired that the baseband spectrum is far away from its first spectral replica, allowing the realization of a smooth filter to recover the baseband signal. For this purpose, the signal $s^{(P)}(t)$ is usually sampled at a rate greater than N/T (the Nyquist rate), which increases the bandwidth of the sampled signal. Therefore, the complexity of the reconstruction filter can be reduced since it can have a lower order.

Note that the augmented sampling rate can be $\frac{MN}{T} \geq \frac{N}{T}$, with M representing the oversampling factor that is greater than one and not necessarily integer. In fact, the oversampling operation can be performed by the addition of $(M-1)N$ idle subcarriers to the original data block $\{S_k; k = 0, 1, \ldots, N-1\}$, half of them in the beginning and the other half in the end. This operation also ensures the desired space between the original spectrum and the first replica. Note that the block will have a total of MN subcarriers, however, only N of them are useful subcarriers. The corresponding time-domain samples are given by

$$s_n^M(t) = s^{(P)}(t)|_{t=\frac{nT}{NM}} = \sum_{k=0}^{N-1} S_{k,m} \exp\left(j2\pi k \frac{n}{NM}\right), \qquad n = 0, 1, ..., NM-1. \tag{2.22}$$

The complex envelope of the oversampled analog signal is

$$s(t) = \sum_{n=-\infty}^{+\infty} s_n \; w_n h_T\left(t - \frac{nT}{N'}\right). \tag{2.23}$$

It should be mentioned that this signal doesn't represent exactly the original OFDM analog signal expressed in (2.13). However, the difference is small, specially for a large number of subcarriers and/or a high oversampling factor (i.e., when $M \to \infty$). To reduce the out-of-band radiation levels, it is common to use a square-root raised-cosine window for $w(t)$, instead of

a rectangular one [11]. This type of windowing makes the amplitude go smoothly to zero at the symbol boundaries, allowing a compression of the spectrum and increases the spectral efficiency. The considered window is obtained through the convolution with shaping filter $h_W(t)$, i.e.,

$$w(t) = w'(t) * h_W(t), \tag{2.24}$$

where

$$h_W(t) = \frac{\pi}{2T_W} \cos\left(\frac{\pi t}{T_W}\right) \text{rect}\left(\frac{t}{T_W}\right), \tag{2.25}$$

and $w'(t)$ is a rectangular window with duration $T_B = T + T_G + T_W$. The result of the convolution operation, $w(t)$, is a square-root raised-cosine pulse with duration $T_B + T_W$. The transmitter structure is shown in the Figure 2.3.

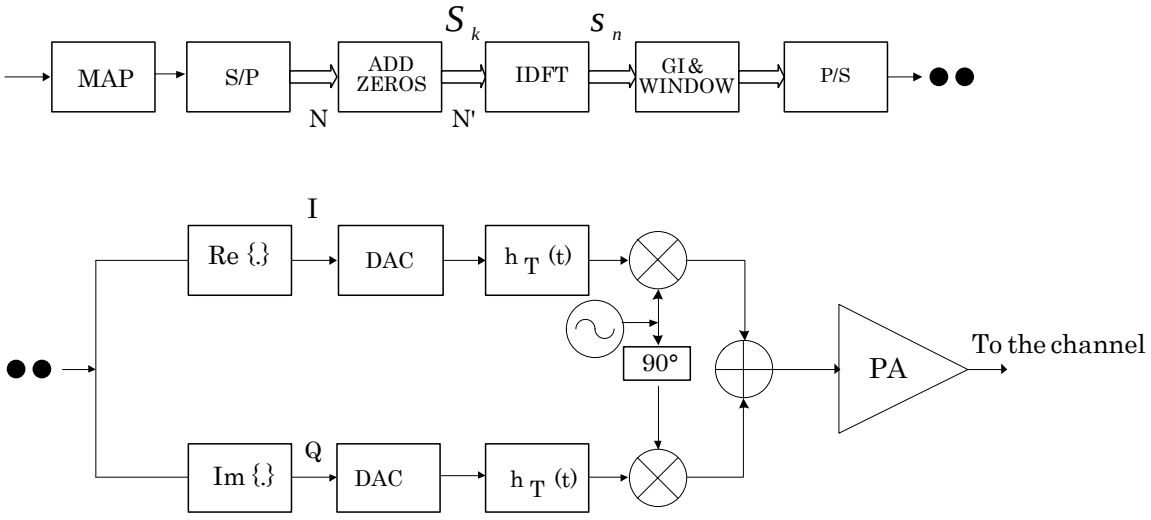

FIGURE 2.3: OFDM transmitter structure

Let us now consider the receiver. The first thing that the receiver does is the RF down conversion, obtaining the baseband signal through an orthogonal demodulator. Since OFDM schemes are multicarrier modulations, they are more sensitive to the Doppler effect and, thus, an accurate frequency synchronization and estimation is required. After the down conversion, the signal is multiplied by the reception filter $H_R(f)$, that has a bandwidth of $\frac{NM}{2T}(1+\rho)$, where ρ represents the roll-off factor, i.e., the excess bandwidth of the filter. If the CIR is characterized by $h(\tau, t)$ and the noise is modelled by $n(t)$ then the output $y(t)$ at the receiver

can be written as

$$y(t) = \int_{-\infty}^{+\infty} s(t-\tau)h(\tau,t)\ \mathrm{d}\tau + n(t). \tag{2.26}$$

This signal is sampled with the same oversampling factor used in the transmitter (i.e., the sampling rate is NM/T) and submitted to an analog to digital (ADC) converter. The ADC output are the time-domain samples $\{y_n; n = -N_G, 0, 1, \ldots, NM-1\}$.

As well as the signal generation can be performed using a IDFT, the signal processing scheme on the receiver side can be implemented using a discrete Fourier transform (DFT). Before applying the DFT operation, the N_G samples that belong to CP are removed to avoid the overlapping of consecutive bursts (that is restricted to the guard interval T_G). Consequently, the null IBI is achieved, since all the corrupted samples are ignored by the receiver. Without the CP, the DFT input is $\{y_n; n = 0, 1, \ldots, NM-1\}$ and the frequency-domain signal $\{Y_k; k = 0, 1, \ldots, NM-1\}$ at the DFT output is given by

$$Y_k = \sum_{n=0}^{NM-1} y_n \exp\left(-j2\pi k \frac{n}{NM}\right), \qquad k = 0, 1, ..., NM-1. \tag{2.27}$$

Also due to CP usage, the output Y_k can be seen as the result of a circular discrete convolution instead of a linear discrete convolution, due to the periodicity introduced by the CP in the OFDM block. As result, (2.27) can be also written as

$$Y_k = S_k H_k + N_k, \tag{2.28}$$

where H_k and N_k represent the channel frequency response and the noise for the k^{th} subcarrier, respectively. It is assumed that the samples N_k are assumed to be independent and Gaussian distributed on both the in-phase and quadrature components.

In Figure 2.4 it is shown the frequency response for a frequency selective channel considering $N = 64$ useful subcarriers and an oversampling factor of $M = 4$. Looking at (2.28), we note that each subcarrier can be treated individually in the frequency-domain which suggests that the equalization process can also be done in frequency-domain. Under these conditions, the equalization performed by the receiver is a simple multiplication of the received signal by the factor F_k defined as follows

$$F_k = \frac{1}{\hat{H}_k} = \frac{\hat{H}_k^{\,*}}{|\hat{H}_k|^2}, \qquad k = 0, 1, ..., N-1, \tag{2.29}$$

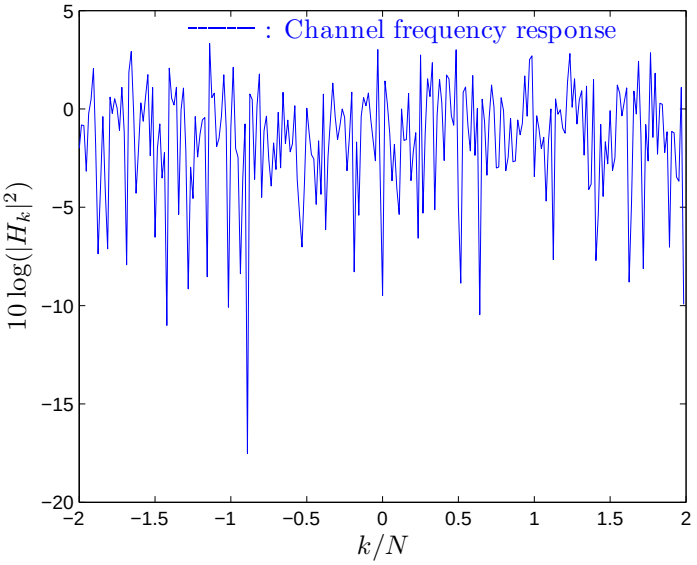

FIGURE 2.4: Channel frequency response

where $\hat{H}_k$ is the estimated frequency response of the channel for the k^{th} subcarrier. The resultant equalized sequence can be expressed as

$$\tilde{S_k} = S_k H_k F_k + F_k N_k, \qquad k = 0, 1, ..., N-1. \tag{2.30}$$

After the equalization process, the equalized signal $\{\tilde{S_k}; k = 0, 1, \ldots, N-1\}$ is submitted to the decision device that will estimate the transmitted symbols $\{\hat{S_k}; k = 0, 1, \ldots, N-1\}$. The receiver structure is depicted in Figure 2.5. (S/H - Sample and Hold, S/P - Serial to Parallel, CP Rem - CP removal)

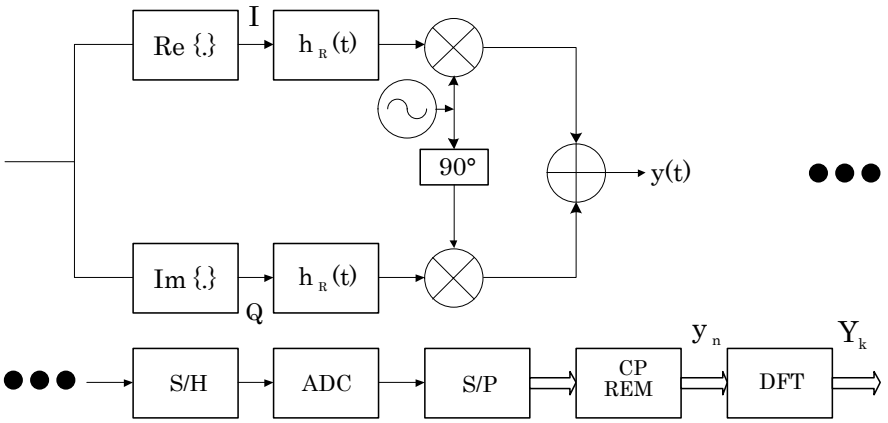

FIGURE 2.5: OFDM receiver structure

2.3 Nonlinear effects in OFDM signals

The OFDM complex envelope results from a sum of N subcarriers, each one modulated by independent data symbols as is expressed in (2.12). Therefore, the resultant signal has high envelope fluctuations even when each sub channel uses a low envelope modulation. This behaviour is evident in Figure 2.6, where it is shown the absolute value of the time-domain samples of an OFDM signal with $N = 64$ in-band subcarriers, an oversampling factor of $M = 4$ and a QPSK constellation.

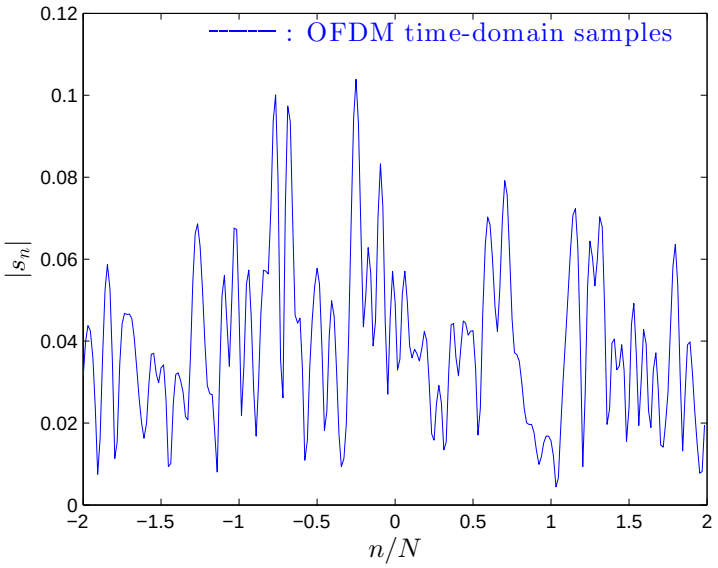

FIGURE 2.6: Amplitude of the time-domain samples of and OFDM signal with $N = 64$ and $M = 4$.

From the figure it is clear that in the time-domain, the OFDM signal present an high dynamic range even for small constellations, which can lead to amplification difficulties. One of the most promising solution for this issue is to clip the signal, however, this can bring severe non-linear distortion effects.

From the point of view of signal processing schemes, it would be appreciated that the nonlinearly distorted signals could be characterized in a theoretical way. In fact, for a high number of subcarriers, the central limit theorem [19] states that the OFDM complex envelope can be assumed to be a stationary complex Gaussian process. Therefore, a Gaussian approximation can be employed for performance evaluation of the nonlinearly distorted OFDM signals [11, 17], substituting the usually used Monte Carlo simulations that require large times of computation.

In this section, we will focus on the study of polar memoryless nonlinearities (i.e. the ones whose output for the instant t depends only on the input at the same instant) and it will be shown how we can obtain the statistical characterization of the signals that are passed through these type of nonlinearities. The expressions for the power and the PSD associated with the useful component and the distortion component of the nonlinearly distorted OFDM signal are presented. The analytical characterization includes also the out-of-band radiation due to the existence of intermodulation products (IMP).

Let us start by verifying the accuracy of the Gaussian approximation for the OFDM complex envelope that is assumed in the following theoretical analysis. In Figure 2.7 it is shown the PDF of the imaginary part of the OFDM time-domain samples, i.e., $\Im(s_n)$, for different values of N and an oversampling factor of $M = 4$. From the figure, its clear that even for a moderate values of N, the distribution of the imaginary part of the samples tends to the normal distribution with zero mean and $\sigma^2 = 0.5$, which leads us to conclude that, this approximation is accurate in almost all of the cases. Of course, the same result is obtained for the real part of the samples, $\Re(s_n)$.

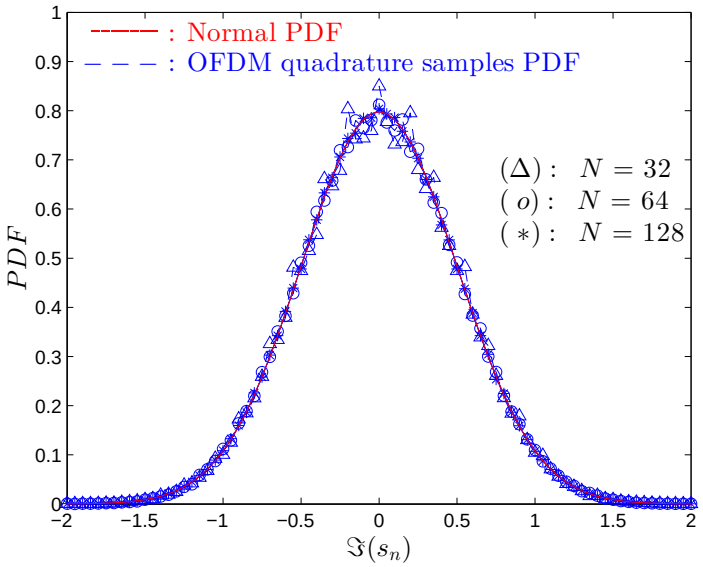

FIGURE 2.7: PDF of the $\Im(s_n)$ with different values of N and $M = 4$.

As the OFDM complex envelope is defined as

$$R = |s_n| = \sqrt{\Re(s_n)^2 + \Im(s_n)^2}, \tag{2.31}$$

we can expect a Rayleigh distribution for R, since both the in-phase and quadrature samples are assumed to be normal distributed.

In Figure 2.8 it is shown the PDF of the OFDM complex envelope samples considering different values of in-band subcarriers and an oversampling factor of $M = 4$. As it can be seen in figure, the distribution of the complex envelope samples is almost equal to the Rayleigh distribution with $\sigma^2 = 1$, even with $N = 16$. For this reason, in this work, the OFDM complex envelope is often modelled by a Rayleigh distribution.

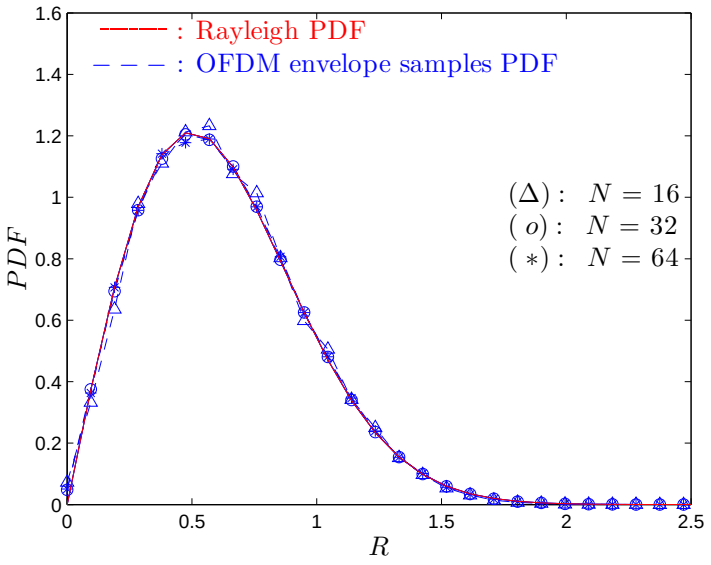

FIGURE 2.8: PDF for OFDM complex envelope samples with different values of N and $M = 4$.

Let us consider a bandpass signal described by

$$x_{BP}(t) = \mathrm{Re}\left\{x(t)\exp\left(2\pi f_c t\right)\right\}, \tag{2.32}$$

where f_c is the frequency of the carrier wave and $x(t)$ is the complex envelope defined in the polar form as

$$x(t) = R(t)\exp\left(\varphi(t)\right), \tag{2.33}$$

where $R(t)$ denotes the absolute value and $\varphi(t)$ represents the argument of $x(t)$. Replacing (2.33) in (2.32), we have

$$\begin{aligned} x_{BP}(t) &= \mathrm{Re}\left\{R(t)\exp\left(\varphi(t)\right)\exp\left(2\pi f_c t\right)\right\} \\ &= \mathrm{Re}\left\{R(t)\exp\left(\psi(t)\right)\right\} \\ &= R(t)\cos\left(\psi(t)\right), \end{aligned} \tag{2.34}$$

with

$$\psi(t) = \varphi(t) + 2\pi f_c t. \tag{2.35}$$

If the bandpass signal, $R(t)\exp\psi(t)$, is submitted to the nonlinear device depicted in Figure 2.9, which models a polar memoryless nonlinearity, the output $y(t)$ is given by

$$y(t) = g_I\left(R(t)\cos\left(\psi(t)\right)\right) - g_Q\left(R(t)\sin\left(\psi(t)\right)\right), \tag{2.36}$$

where $g_I(\cdot)$ and $g_Q(\cdot)$ are odd real functions. It is important to note that since $y(t)$ is a

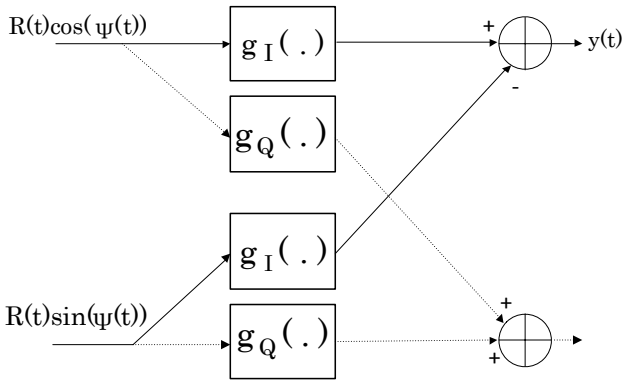

FIGURE 2.9: Memoryless nonlinearity model with a bandpass input.

periodic function of $\psi = \psi(t)$ it can be expanded in Fourier series as

$$y(t) = \sum_{l=-\infty}^{+\infty} c_l\left(R\left(t\right)\right)\exp\left(jl\psi\right), \tag{2.37}$$

with c_l denoting the complex Fourier coefficient defined as

$$\begin{aligned} c_l &= \frac{1}{2\pi} \int_0^{2\pi} g_I\left(R(t)\cos(\psi)\right) - g_Q\left(R(t)\cos(\psi)\right)\exp(-jl\psi)\ \mathrm{d}\psi \\ &= a_l + jb_l, \end{aligned} \tag{2.38}$$

where,

$$a_l = \mathrm{Re}(c_l) = \frac{1}{2\pi} \int_0^{2\pi} g_I\left(R\cos(\psi)\right)\cos(l\psi)\ \mathrm{d}\psi, \tag{2.39}$$

and

$$b_l = \mathrm{Im}(c_l) = \frac{1}{2\pi} \int_0^{2\pi} g_Q\left(R\cos(\psi)\right)\sin(l\psi)\ \mathrm{d}\psi. \tag{2.40}$$

The signal $x_{BP}(t)$ has typically a much smaller bandwidth than the carrier frequency f_c. However, the nonlinearity output will have spectral components centred at $\pm l f_c$. To remove all these components except the one at the carrier frequency, a filter must be used. The filtered output is written as

$$y_f(t) = g(R)\exp(j\psi) = f(R)\exp(j\psi), \tag{2.41}$$

i.e., the nonlinear effect depends only on the absolute value of the input signal $R = R(t) = |x(t)|$ and $f(R) = A_I(R) + j\ A_Q(R)$, with

$$A_Q(R) = 2\ \mathrm{Re}(c_l) = \frac{1}{\pi} \int_0^{2\pi} g_I\left(R\cos(\psi)\right)\cos(\psi)\ \mathrm{d}\psi, \tag{2.42}$$

and

$$A_I(R) = 2\ \mathrm{Im}(c_l) = \frac{1}{\pi} \int_0^{2\pi} g_Q\left(R\cos(\psi)\right)\sin(\psi)\ \mathrm{d}\psi. \tag{2.43}$$

The nonlinear characteristic $f(R)$ is modelled as

$$f(R) = A(R)\exp(j\Theta(R)), \tag{2.44}$$

with $A(R)$ being the AM/AM conversion characteristic, that represents the effect on the output amplitude as a function of the input amplitude and $\Theta(R)$ denoting the AM/PM characteristic curve, that represents the effect on the output phase caused by the input amplitude. Replacing

(2.44) in (2.41) we may write

$$y(t) = A(R)\exp\left(j\left(\Theta(R) + \psi\right)\right), \tag{2.45}$$

Clearly, the effect of the memoryless nonlinearity on the input $x(t)$, corresponds, together with the referred filter, to the effect on $x_{BP}(t)$ when it is submitted to a polar memoryless nonlinearity described by its AM/AM and AM/PM conversion functions as depicted in the Figure 2.10.

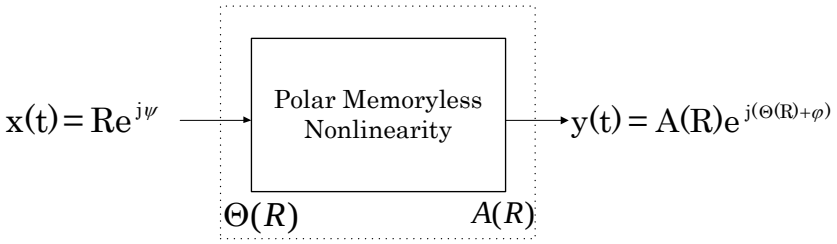

FIGURE 2.10: Memoryless polar nonlinearity model

An example of a bandpass memoryless nonlinearity is an Solid State Power Amplifier (SSPA) that can be modelled with $\Theta(R) \approx 0$ and $A(R)$ defined in [20] as

$$A(R) = A_M \frac{\frac{R}{s_M}}{\sqrt[2p]{1 + \left(\frac{R}{s_M}\right)^{2p}}}, \tag{2.46}$$

where $\frac{A_M}{s_M}$ is the small signal gain (i.e., $\lim_{R\to 0} \frac{A(R)}{R} = \frac{A_M}{s_M}$) and A_M is the saturation value (i.e., $\lim_{R\to+\infty} A(R) = A_M$). In Figure 2.11 we have the AM/AM characteristic function for this amplifier, considering several values of p, $A_M = 4$ and $s_M = 5$. As we can see, the transition between the linear region and the saturation tends to be smoother for low values of p. In the limit, i.e., $p = +\infty$, the SSPA is equivalent to a clipping device.

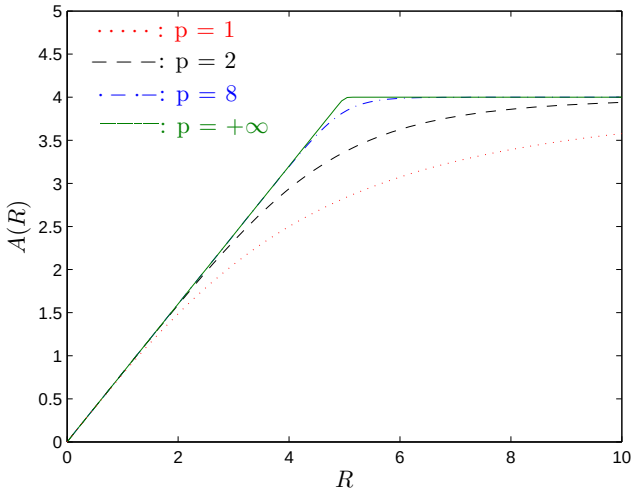

FIGURE 2.11: AM/AM characteristic of a SSPA

Note that this device limits the output to be A_M from a certain value of R, leading to an existence of severe nonlinear distortion effects. Another example of a polar memoryless nonlinearity is the Travelling Wave Tube Amplifier (TWTA), characterized by the AM/AM and AM/PM functions defined in [20] as

$$A(R) = 2\frac{A_M\left(\frac{R}{s_M}\right)}{1+\left(\frac{R}{s_M}\right)^2}, \tag{2.47}$$

and

$$\Theta(R) = 2\frac{\theta_M\left(\frac{R}{s_M}\right)^2}{1+\left(\frac{R}{s_M}\right)^2}. \tag{2.48}$$

As verified before, when the number of subcarriers is high, we can make a Gaussian approximation for the OFDM signal. Using the Bussgang theorem [21], that can also be obtained as a variation of the Price theorem [33], it can be shown that the nonlinear distorted signal that results from a Gaussian input, is decomposable as the sum of two uncorrelated components: an useful component that is proportional to the input signal and a distortion component. Thus, for the input $x(t)$ we may write

$$y(t) = \alpha x(t) + d(t), \tag{2.49}$$

where α is a scaling factor, $d(t)$ denotes the self-interference component and $y(t)$ represents the output of the polar memoryless nonlinearity.

Let us assume that $R = R(t)$ represent a realization of a random process that models the absolute value of the OFDM complex envelope, i.e., is associated to $|x(t)|$. Note that this realization is composed by a set of samples that are associated with a Rayleigh distribution as seen in Figure 2.8, since the magnitude of the real and imaginary parts of each sample are uncorrelated and normally distributed with the same variance, σ^2. Moreover, since it is assumed a stationary complex Gaussian process, the PDF of the sample at t_1 is the same for the sample at $t_1 + \tau$, resulting that the scaling factor α is time independent. As the two components are uncorrelated, we have $\mathbb{E}[x(t)d(t)] = 0$ (where $\mathbb{E}[\cdot]$ is the expectation operator). Therefore, using the expectation operator properties we can write

$$\begin{aligned}\mathbb{E}[y(t)x(t)] &= \mathbb{E}[(\alpha x(t) + d(t))x(t)] \\ &= \mathbb{E}[\alpha x^2(t)] + \mathbb{E}[x(t)d(t)] \\ &= \alpha\mathbb{E}[x^2(t)].\end{aligned} \tag{2.50}$$

Solving in order to α, we may write

$$\begin{aligned}\alpha &= \frac{\mathbb{E}[y(t)x^*(t)]}{\mathbb{E}[x(t)x^*(t)]} \\ &= \frac{\mathbb{E}[A(R)\exp(j\Theta(R))\exp(j\varphi)R\exp(-j\varphi)]}{\mathbb{E}[R^2]} \\ &= \frac{\mathbb{E}[RA(R)\exp(j\Theta(R))]}{\mathbb{E}[R^2]} \\ &= \frac{\mathbb{E}[Rf(R)]}{\mathbb{E}[R^2]},\end{aligned} \tag{2.51}$$

Recalling that the PDF of Rayleigh distribution is given by

$$p(R) = \frac{R}{\sigma^2}\exp\left(-\frac{R^2}{2\sigma^2}\right), \qquad R > 0, \tag{2.52}$$

the expected value of R is

$$\mathbb{E}[R] = \int_{-\infty}^{+\infty} R\frac{R}{\sigma^2}\exp\left(-\frac{R^2}{2\sigma^2}\right)\mathrm{d}R, \tag{2.53}$$

or, more generally, the expected value of an arbitrary function of R, say $\phi(R)$, is

$$\mathbb{E}[\phi(R)] = \int_{-\infty}^{+\infty} \phi(R) \frac{R}{\sigma^2} \exp\left(-\frac{R^2}{2\sigma^2}\right) \mathrm{d}R. \tag{2.54}$$

Using (2.54), equation (2.51) can be rewritten as

$$\alpha = \frac{\mathbb{E}[RA(R)\exp(j\Theta(R))]}{\mathbb{E}[R^2]} \tag{2.55}$$

$$= \frac{\int_{-\infty}^{+\infty} RA(R)\exp(j\Theta(R))\ p(R)\ \mathrm{d}R}{\int_{0}^{+\infty} R^2\ p(R)\ \mathrm{d}R} \tag{2.56}$$

$$= \frac{1}{2\sigma^2} \int_{0}^{+\infty} RA(R)\exp(j\Theta(R))\ p(R)\ \mathrm{d}R \tag{2.57}$$

$$= \frac{1}{2\sigma^4} \int_{0}^{+\infty} RA(R)\exp(j\Theta(R))\ R\exp\left(-\frac{R^2}{2\sigma^2}\right)\ \mathrm{d}R, \tag{2.58}$$

but, since $\mathbb{E}[R^2]$ can also be written as

$$\mathbb{E}[R^2] = \mathbb{E}\left[R\exp(j\varphi(t))R\exp(-j\varphi(t))\right] = \mathbb{E}\left[x(t)x^*(t-\tau)\right]\Big|_{\tau=0} = R_x(\tau)\Big|_{\tau=0}, \tag{2.59}$$

and the autocorrelation $R_x(\tau)$ forms a Fourier pair with the PSD of $x(t)$, i.e.,

$$R_x(\tau) = \int_{-\infty}^{+\infty} G_x(f)\exp(j2\pi f\tau)\mathrm{d}f, \tag{2.60}$$

we can note that

$$R_x(\tau)\Big|_{\tau=0} = \int_{-\infty}^{+\infty} G_x(f)\ \mathrm{d}f, \tag{2.61}$$

which is equal to the power of the input signal, $2\sigma^2$, that appears in the denominator of (2.55). Looking at (2.49), we note that the average power of the useful component, S, is given by

$$S = 2|\alpha|^2\sigma^2, \tag{2.62}$$

on the other hand, the total average power at the output of the nonlinearity is

$$P_{out} = \mathbb{E}[|f^2(R)|] = \frac{1}{2\sigma^2} \int_0^{+\infty} A^2(R)\ R \exp\left(-\frac{R^2}{2\sigma^2}\right) \mathrm{d}R. \tag{2.63}$$

Using (2.62) and (2.63) we can define the average power of the self-interference component as

$$I = P_{out} - S \tag{2.64}$$

To characterize in the frequency-domain the nonlinear effects at the PSD of the nonlinearity output, $G_y(f)$, we can find the output autocorrelation $R_y(\tau)$ since, as mentioned before, they form a Fourier pair. In Appendix A it is shown that the autocorrelation of the output $y(t)$ is given by (A.38)

$$R_y(\tau) = 2\sum_{\gamma=0}^{+\infty} P_{2\gamma+1} \frac{R_x(\tau)^{\gamma+1} R_x^*(\tau)^{\gamma}}{R_x(0)^{2\gamma+1}}, \tag{2.65}$$

with $P_{2\gamma+1}$ denoting the total power associated to the IMP of order $2\gamma+1$, which can be obtained with (A.36)

$$P_{2\gamma+1} = \frac{1}{4\sigma^6(\gamma+1)} \left| \int_0^{+\infty} R^2 f(R) \exp\left(-\frac{R^2}{2\sigma^2}\right) L_{\gamma}^{(1)}\left(\frac{R^2}{2\sigma^2}\right) \mathrm{d}R \right|^2, \tag{2.66}$$

where $L_{\gamma}^{(1)}$ denotes the generalized Laguerre polynomial of order γ, defined as

$$L_{\gamma}^{(1)}(x) = \frac{1}{\gamma!} x^{-1} \exp(x) \frac{d^{\gamma}}{dx^{\gamma}} \left(\exp(-x)\, x^{\gamma+1}\right). \tag{2.67}$$

Using (2.66) for $\gamma = 0$ we get $P_1 = |\alpha|^2\sigma^2$ (which is the useful power of the output, expressed in (2.62)). Thus, the first IMP is proportional to the input signal and we conclude that the IMP from order $\gamma = 1$ to $+\infty$ are the responsible for the power of the distortion component I. In addition, since the useful and self-interference components are uncorrelated, we can write

$$R_y(\tau) = |\alpha|^2 R_x(\tau) + R_d(\tau), \tag{2.68}$$

with $R_d(\tau)$ denoting the PSD of the distortion component, which is given by

$$R_d(\tau) = \mathbb{E}[d(t)d^*(t-\tau)] = 2\sum_{\gamma=1}^{+\infty} P_{2\gamma+1} \frac{R_x(\tau)^{\gamma+1} R_x^*(\tau)^{\gamma}}{R_x(0)^{2\gamma+1}}, \tag{2.69}$$

and

$$I = R_d(\tau)\Big|_{\tau=0} = 2\sum_{\gamma=1}^{+\infty} P_{2\gamma+1}. \tag{2.70}$$

The power spectral density of $y(t)$ is simply obtained by calculating the Fourier Transform of (2.65) , i.e.,

$$\begin{aligned} G_y(f) &= \mathcal{F}\{R_y(\tau)\} \\ &= 2\sum_{\gamma=0}^{+\infty} \frac{P_{2\gamma+1}}{R_x(0)^{2\gamma+1}} \underbrace{G_x(f) * \cdots * G_x(f)}_{\gamma+1} \underbrace{G_x(-f) * \cdots * G_x(-f)}_{\gamma}, \end{aligned} \tag{2.71}$$

recalling that $\mathcal{F}\{a(t) \times b(t)\} = A(f) * B(f)$ and $\mathcal{F}\{a^*(t)\} = A(-f)$. Once again, we can decompose the PSD of the nonlinearity output in two components, i.e.,

$$G_y(f) = |\alpha|^2 G_x(f) + G_d(f), \tag{2.72}$$

with $G_d(f)$ denoting the PSD of the self-interference component, defined as

$$\begin{aligned} G_d(f) &= \mathcal{F}\{R_d(\tau)\} \\ &= 2\sum_{\gamma=1}^{+\infty} \frac{P_{2\gamma+1}}{R_x(0)^{2\gamma+1}} \underbrace{G_x(f) * \cdots * G_x(f)}_{\gamma+1} \underbrace{G_x(-f) * \cdots * G_x(-f)}_{\gamma}. \end{aligned} \tag{2.73}$$

Looking at (2.71) it is easy to understand that the nonlinearity will cause a spectral outgrowth, since the expression contains several convolutions between the PSD of the input signal. More concretely, if the PSD of the input signal has bandwidth B, $G_y(f)$ will have a bandwidth of $(2\gamma + 1)\ B$. The spectral outgrowth is justified by the existence of IMP that appears when signals with different frequencies are passed through a nonlinear device. Clearly, the existence of an undesired out-of-band radiation can lead to interferences with neighbouring communication systems, which is a relevant problem. However, this radiation can be attenuated using an adequate frequency filtering operation.

Chapter 3

Maximum-Likelihood Receivers for nonlinearly distorted OFDM signals

In previous chapter, it was verified that in OFDM schemes the received signal is equalized in the frequency-domain, which allows the realization of simple receivers. In this chapter, we will study the last and the most important task performed by the receiver - the data detection. After the equalization procedure, the receiver must estimate the data that, even with a perfect equalization, is still corrupted by noise (otherwise stated, we will assume that the channel corrupts the transmitted signal with Additive White Gaussian Noise (AWGN)) and nonlinear distortion.

There are a large variety of techniques for doing data detection. One of them consists in applying a simple hard-detection, according to the decision threshold of the complex symbols in the adopted constellation. Although this technique brings very low complexity, it also has low performance, i.e., high BER values, specially for signals with high nonlinear distortion effects (which are the main target of this work). To have an optimal performance, it is necessary to employ an ideal Maximum Likelihood ML receiver. This receiver tries to minimize the error probability by selecting the data estimate with smallest Euclidean distance relatively to the received signal. As will be seen later, these receivers consider the overall nonlinear distorted signal, taking advantage of the information that is present in the distortion component, instead of regarding it as a noise-like term.

This chapter is organized as follows: in Section 3.1 are presented the reasons behind the

improvements in nonlinear OFDM. In Section 3.2 the main principle of ML detection is explained. Section 3.3 characterizes analytically the ML receivers and it is also derived a closed expression for the Euclidean distance between two nonlinearly distorted signals. Finally, in Section 3.4 it is presented the achievable performance of ML receivers dealing with nonlinear OFDM signals.

3.1 Achievable gain for nonlinear OFDM

To understand how the nonlinear distortion can improve the performance, let us consider an OFDM signal with $N = 64$ data symbols selected from a QPSK constellation. The data blocks are represented by $\mathbf{X} = [X_0\, X_1 \ldots X_{NM-1}]^T \in \mathbb{C}^{NM}$, i.e., in addition to the data symbols, the block also contains a set of $(M-1)N$ zeros. As seen before in Section 2.2, adding these zeros is formally equivalent to add $(M-1)N/2$ idle subcarriers (i.e. subcarriers that don't carry any data) at each edge of the band. This means that the time-domain block $\mathbf{x} = [x_0\, x_1 \ldots x_{NM-1}]^T \in \mathbb{C}^{NM}$ can be regarded as an oversampled version of the original OFDM block with an oversampling factor M (in this case, it is considered an oversampling factor of $M = 4$ that is enough to avoid aliasing effects in the nonlinearly distorted signal). In Figure 3.1 it is shown the considered scenario.

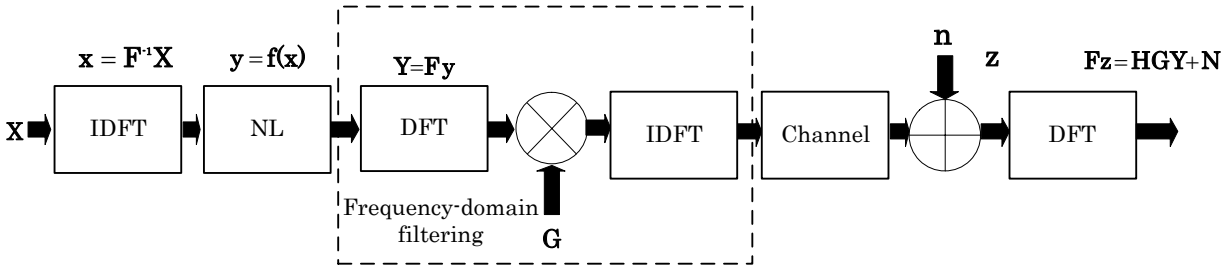

FIGURE 3.1: Signal processing scheme associated to the considered scenario

At the transmitter, the input time-domain signal $\mathbf{x} = [x_0\, x_1 \ldots x_{NM-1}]^T \in \mathbb{C}^{NM}$ is distorted by the memoryless nonlinearity $\mathbf{f}(.)$ which corresponds to a clipping device characterized by the normalized clipping level $s_M/\sigma = 0.5$. Note that this function distorts the magnitude but

not the phase of the elements of $\mathbf{x}$ (i.e., it is assumed a null AM/PM conversion characteristic). Its AM/AM conversion is given by

$$f(R) = \begin{cases} R, & R \leq s_M \\ s_M, & R > s_M, \end{cases} \tag{3.1}$$

where $R = |\mathbf{x}| = [R_0\, R_1 \ldots R_{NM-1}]^T \in \mathbb{C}^{NM}$ is a vector composed by Rayleigh distributed random variables that models the absolute value of time-domain samples that are obtained through an IDFT. This operation is considered as a matrix multiplication, with $\mathbf{F}_{NM}$ being a unitary matrix that denotes the NM-size DFT and whose the element of the i^{th} line and j^{th} column is defined as

$$[\mathbf{F}_{NM}]_{i,l} = \frac{1}{\sqrt{NM}} \exp\left(-\frac{j2\pi il}{NM}\right). \tag{3.2}$$

The IDFT operation is represented as a multiplication by the matrix $\mathbf{F}_{NM}^{-1} = \mathbf{F}^H$ (since $\mathbf{F}$ is unitary, its inverse is equal to the conjugate transpose). The signal $\mathbf{x}$ is hence given by $\mathbf{F}_{NM}^{-1}\mathbf{X}$ (in the following it will be simply used $\mathbf{F}^{-1}$ and $\mathbf{F}$ when there is no risk of ambiguity). The nonlinearly distorted signal is represented by $\mathbf{y} = \mathbf{f}(\mathbf{x}) = [y_0\, y_1 \ldots y_{NM-1}]^T \in \mathbb{C}^{NM}$ and, in the frequency-domain, we have

$$\mathbf{Y} = \mathbf{F}\left(\mathbf{f}\left(\mathbf{F}^{-1}\mathbf{X}\right)\right). \tag{3.3}$$

It is assumed that the samples of $\mathbf{x}$ have a Gaussian nature and, according to (2.49), the nonlinearity output $\mathbf{Y}$ can be decomposed in two uncorrelated components as

$$\begin{aligned} \mathbf{Y} &= \mathbf{F}\mathbf{y} \\ &= \mathbf{F}\left(\alpha\mathbf{x} + \mathbf{d}\right) \\ &= \alpha\mathbf{X} + \mathbf{D}, \end{aligned} \tag{3.4}$$

where α is the scaling factor defined in (2.51) and $\mathbf{D} = [D_0\, D_1 \ldots D_{NM-1}]^T \in \mathbb{C}^{NM}$ is the frequency-domain version of the distortion component. After appending an appropriate cyclic prefix to the time-domain block $\mathbf{F}^{-1}\mathbf{G}\mathbf{Y}$, the resulting samples are transmitted through the wireless channel. At the receiver, the cyclic prefix is removed, leading to the time-domain block $\mathbf{z} = [z_0\ z_1\ \ldots\ z_{NM-1}]^T \in \mathbb{C}^{NM}$ (without loss of generality we assume the same oversampling

factor at the transmitter and the receiver). The block $\mathbf{Z} \in \mathbb{C}^{NM}$ represents the frequency-domain version of the received signal that can be defined using (3.3) and (3.4) as

$$\begin{aligned} \mathbf{Z} &= \mathbf{Fz} \\ &= \mathbf{HGY} + \mathbf{N} \\ &= \mathbf{HGFf}(\mathbf{F}^{-1}\mathbf{X}) + \mathbf{N} \\ &= \alpha\mathbf{HGX} + \mathbf{HGD} + \mathbf{N}, \end{aligned} \tag{3.5}$$

where $\mathbf{N} = [N_0\ N_1\ ...\ N_{MN-1}]^T \in \mathbb{C}^{NM}$ represents the noise vector, with $[\mathbf{N}]_k$ denoting the k^{th} frequency-domain noise component, and $\mathbf{H}$ represents the channel response defined as

$$\mathbf{H} = \text{diag}\left([H_0\ H_1\ ...\ H_{MN-1}]^T\right), \tag{3.6}$$

where $[\mathbf{H}]_{k,k}$ is the channel frequency response for the k^{th} subcarrier.

We shall now consider two nonlinearly distorted sequences $\mathbf{Y}^{(1)}$ and $\mathbf{Y}^{(2)}$ that are generated by passing the time-domain version of $\mathbf{X}^{(1)}$ and $\mathbf{X}^{(2)}$ through a clipping device. In addition, let us consider that the data block $\mathbf{X}^{(2)}$ differs from $\mathbf{X}^{(1)}$ in only one bit at the middle subcarrier of the spectrum. In the Figure 3.2 is shown the magnitude of the two sequences $\mathbf{Y}^{(1)}$ and $\mathbf{Y}^{(2)}$ and the absolute value of the difference between them. It is clear that this difference has energy in the entire band (in-band and out-of-band part of the spectrum) and not only in the subcarrier where the bit was modified.

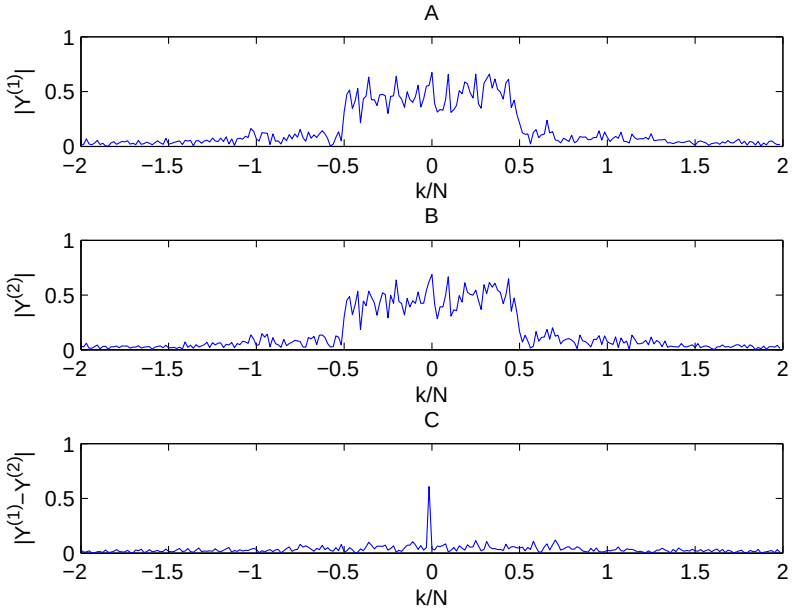

FIGURE 3.2: Absolute value of the transmitted frequency-domain signal for two OFDM data blocks differing in a single bit that are submitted to an envelope clipping with clipping level $s_M/\sigma = 0.5$ ((A) and (B)) and the absolute value of the difference between them (C).

It is important to note that the scaling factor of $\frac{1}{\sqrt{NM}}$ in the definition of the DFT in (3.2), makes this transform unitary. This implies that the energy is preserved, i.e.,

$$\sum_{k=0}^{NM-1} \left| [\mathbf{X}]_k \right|^2 = \sum_{i=0}^{NM-1} \left| [\mathbf{x}]_n \right|^2, \tag{3.7}$$

therefore, the energy is the same in the time-domain and frequency-domain (or, in other words, the same in the input and output of the DFT). If we take advantage of this DFT definition, the average bit energy that is typically defined using the time-domain samples can also be defined in the frequency-domain. In addition, the SNR, the ratio between the average bit energy, the squared Euclidean distances and other related parameters defined in frequency-domain are identical to the ones defined in time-domain.

Let us now focus our analysis in the frequency-domain samples. Using (3.4), we can define the average bit energy for a nonlinear transmitter as

$$\begin{aligned} E_b &= \frac{1}{2N} \sum_{k=0}^{NM-1} \mathbb{E}[|[\mathbf{Y}]_k|^2] \\ &= \frac{1}{2N} \sum_{k=0}^{NM-1} \left(|\alpha \mathbb{E}[[\mathbf{X}]_k] + \mathbb{E}[[\mathbf{D}]_k|\right)^2 . \end{aligned} \tag{3.8}$$

Another way to obtain the average bit energy is to consider the output power of the nonlinearity as in (2.63). For example, using the clipping function defined in (3.1), we have

$$\begin{aligned} E_b &= A^2 \frac{\mathbb{E}[f(R)^2]}{\mathbb{E}[R^2]} \\ &= A^2 \frac{\int_{-\infty}^{+\infty} f(R)^2 \frac{R}{\sigma^2} \exp\left(-\frac{R^2}{2\sigma^2}\right) \mathrm{d}R}{\int_{0}^{+\infty} R^2 \frac{R}{\sigma^2} \exp\left(-\frac{R^2}{2\sigma^2}\right) \mathrm{d}R} \\ &= \frac{A^2}{\sigma^2}\left(1 - \exp\left(-\frac{s_M^2}{2\sigma^2}\right)\right). \end{aligned} \tag{3.9}$$

Figure 3.3 shows the average bit energy computed from (3.9) as a function of the normalized clipping level s_M/σ, considering $A = 1$ (A is the amplitude of the symbols in the QPSK constellation) and $\sigma^2 = 1$. Its clear that $E_b \ll A^2$, especially for lower values of s_M/σ.

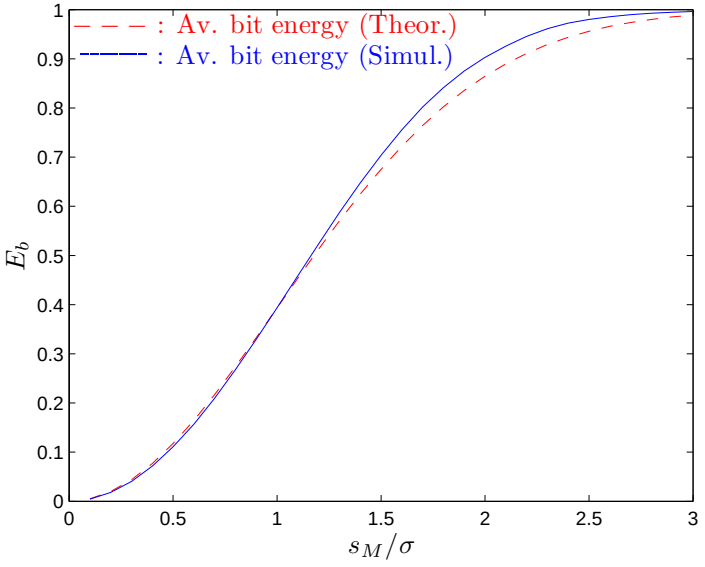

FIGURE 3.3: Evolution of average bit energy considering different values for the normalized clipping level s_M/σ.

When higher values clipping levels are considered, E_b gets closer to A^2 (the value for linear transmitters), which means very low distortion levels. Still in the frequency-domain, as the Euclidean distance between two nonlinearly signals is given by the squared euclidean norm

between them, we have

$$\begin{aligned}\mathfrak{D}^2 &= \left|\left|\mathbf{Y}^{(1)}-\mathbf{Y}^{(2)}\right|\right|^2 \\ &= \sum_{k=0}^{NM-1}\left|[\mathbf{Y}]_k^{(1)}-[\mathbf{Y}]_k^{(2)}\right|^2 \\ &= \sum_{k=0}^{NM-1}\left|\alpha[\mathbf{X}]_k^{(1)}+[\mathbf{D}]_k^{(1)}-\alpha[\mathbf{X}]_k^{(2)}-[\mathbf{D}]_k^{(2)}\right|^2. \end{aligned} \tag{3.10}$$

Considering Figure 3.2 and using (3.10), the Euclidean distance between the sequences $\mathbf{Y}^{(2)}$ and $\mathbf{Y}^{(1)}$ is

$$\mathfrak{D}^2 = \left|\left|\mathbf{Y}^{(2)}-\mathbf{Y}^{(1)}\right|\right|^2 \approx 7.7E_b$$

which means that the quantity $\mathfrak{D}^2/E_b$ between the two signals that are submitted to this clipping device is greater than without this nonlinear distortion effect (for a linear transmitter is $\mathfrak{D}^2/E_b = 4$). Since the asymptotic behaviour of the BER performance is closely related to the ratio $\mathfrak{D}^2/E_b$ (where $\mathfrak{D}^2$ is the minimum distance between any two signals that belong to transmitted signals set) and we note that Euclidean distance is many times greater than E_b, an improvement can be achieved. It is important to point out that (3.10) takes into account the $M(N-1)$ out-of-band subcarriers. However, the radiation associated to them must not overlap with neighbours spectra and, thus, must be removed. As in [11], to eliminate the out-of-band radiation, a subsequent frequency-domain filtering operation can be performed. In the considered signal processing scheme, the frequency domain filter (FDF) is represented by the diagonal matrix $\mathbf{G} \in \mathbb{C}^{NM}$ which is defined as

$$\mathbf{G} = \operatorname{diag}\left(\left[\underbrace{0.....0}_{(M-1)N/2}\ \underbrace{1.....1}_{N}\ \underbrace{0.....0}_{(M-1)N/2}\right]\right). \tag{3.11}$$

This filter removes the $(M-1)N$ subcarriers that not belong to the in-band spectrum weighing them by 0. However, the N in-band subcarriers will remain unchanged after this operation. Naturally, if no frequency-domain filter is employed, the matrix $\mathbf{G}$ is defined as

$$\mathbf{G} = \mathbf{I}_{NM}. \tag{3.12}$$

It should be pointed out that using a FDF leads to a reduction in the Euclidean distance between the signals (since a lower number of subcarriers are considered in (3.10)). Therefore,

since the ratio $\mathfrak{D}^2/E_b$ will be smaller, there is a reduction in the achievable gain.

Let us now quantify the asymptotic gain defined as

$$\mathfrak{G} = \frac{\mathfrak{D}^2}{4E_b}. \tag{3.13}$$

It is expected that the asymptotic gain $\mathfrak{G}$ is almost always higher than one (the value for the linear transmitter), especially in the presence of strong nonlinear distortion effects. This is explained as follows: since for lower values of s_M/σ, E_b also assumes very low values as shown in Figure 3.3, $\mathfrak{D}^2$ will be higher than $4E_b$, which makes the gain higher than one as depicted in Figure 3.4. In this figure it is considered an OFDM signal with $N = 64$ and data sequences that differ in only one bit. From the figure, its clear that when lower values of s_M/σ are adopted, the asymptotic gain $\mathfrak{G}$ assume values greater than one. This behaviour is justified because the higher $\mathfrak{D}^2/E_b$ that results from consider strong nonlinear distortion effects.

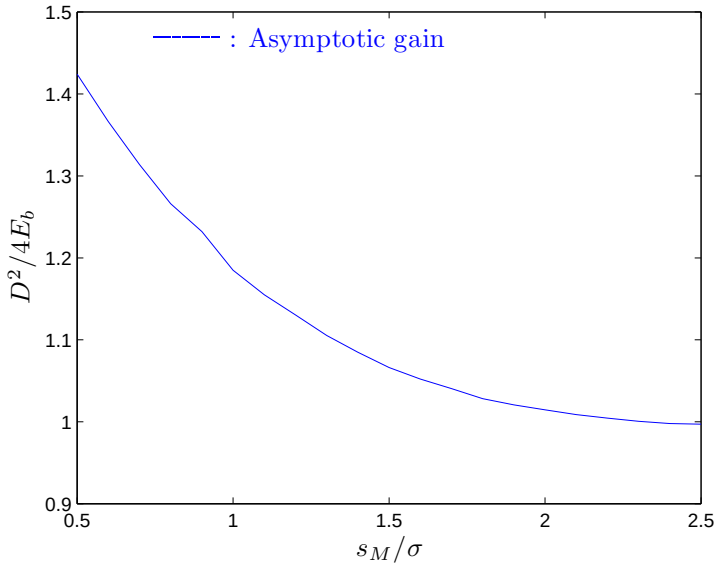

FIGURE 3.4: Evolution of $\mathfrak{G}$ for different values of the normalized clipping level s_M/σ.

3.2 Maximum-Likelihood Detection

It is well known that the asymptotic performance on communication systems is closely related to the minimum distance between any two transmitted signals. Intuitively, if the signals are well spaced, it is easier for the receiver to perform the data detection a lower number of errors

and, consequently, lower BER values. As referred previously, the distance between the nonlinearly distorted signals is many times higher than the average bit energy when comparing to the linear case, which seems to justify the improvements in the performance of nonlinear OFDM schemes. Moreover, it was shown that the nonlinearly distorted signals have information along all the subcarriers. This can be used to achieve a better detection since the receiver will have more information to compare the signals. The optimum receiver, i.e., the ML receiver, is a suitable candidate under these conditions because takes into account the overall distance between two signals, i.e., considers all the subcarriers and, consequently, takes advantage of the nonlinear distortion component. Therefore, this section is dedicated to explaining the basis principle of this type of detection.

In the scenario represented in Figure 3.1, the last block of the figure is the DFT whose output is $\mathbf{Z} = [Z_0\, Z_1 \ldots Z_{NM-1}]^T \in \mathbb{C}^{NM}$. Let us now focus in the data estimation process. This task consists in estimating the data sequence $\hat{\mathbf{X}} = [\hat{X}_0\, \hat{X}_0 \ldots \hat{X_{NM-1}}]^T \in \mathbb{C}^{NM}$ from the noisy received signal $\mathbf{Z}$ as depicted in Figure 3.5.

FIGURE 3.5: Decision input/output model

Let us consider that the decision device selects the data vector $\mathbf{X}$ that maximizes the probability of $\mathbf{X}$ given $\mathbf{Z}$, i.e., selects the data vector whose probability of having been sent, given $\mathbf{Z}$, is the largest. Note that $\mathbf{Z}$ and $\mathbf{X}$ are modelled by random variables. In addition, since the Bayes Theorem may be derived from the definition of conditional density, one can write

$$p\left(\mathbf{X}|\mathbf{Z}\right) = \frac{p\left(\mathbf{Z}|\mathbf{X}\right) p\left(\mathbf{X}\right)}{p\left(\mathbf{Z}\right)}, \tag{3.14}$$

since $p\left(\mathbf{Z}\right)$ is uniform, maximizing (3.14) is formally equivalent to the Maximum *A Posteriori* (MAP) criterion, where

$$\hat{\mathbf{X}} = \arg\max_{\mathbf{X}} \left(p\left(\mathbf{Z}|\mathbf{X}\right) p\left(\mathbf{X}\right)\right). \tag{3.15}$$

However, if we assume an uniform *a priori* distribution for $p(\mathbf{X})$, i.e., all possible transmitted data sequences are equally probable *a priori*, then the MAP criterion reduces to the ML criterion, i.e.,

$$\hat{\mathbf{X}} = \arg\max_{\mathbf{X}} \left(p\left(\mathbf{Z}|\mathbf{X}\right)\right), \tag{3.16}$$

Let us now assume that $\mathbf{Z}$ is a function of $\mathbf{X}$ and $\mathbf{N}$. In fact, the signal $\mathbf{Z}$ can be seen as the sum of the transmitted signal plus a noise factor and, thus, can be defined as

$$\mathbf{Z} = \mathbf{X} + \mathbf{N}, \tag{3.17}$$

with $[\mathbf{N}]_k \sim \mathcal{N}(0, \sigma_k^2)$, i.e,

$$p_N([\mathbf{N}]_k) = \frac{1}{\sqrt{2\pi\sigma_k^2}} \exp\left(-\frac{[\mathbf{N}]_k^2}{2\sigma_k^2}\right). \tag{3.18}$$

On the other hand, using (3.17) we can write

$$p_{Z|X}([\mathbf{Z}|\mathbf{X}]_k) = p_N([\mathbf{Z}]_k - [\mathbf{X}]_k), \tag{3.19}$$

and, consequently the PDF of each element is

$$p([\mathbf{Z}|\mathbf{X}]_k) = \frac{1}{\sqrt{2\pi\sigma_k^2}} \exp\left(-\frac{([\mathbf{Z}]_k - [\mathbf{X}]_k)^2}{2\sigma_k^2}\right). \tag{3.20}$$

Note that we are interested in maximize $p\left(\mathbf{Z}|\mathbf{X}\right)$, thus, the multivariate normal distribution $\mathbf{Z}/\mathbf{X}$ must be evaluated. Being independent the elements $[\mathbf{Z}|\mathbf{X}]_k$, the PDF of the entire vector is given by the product of the PDF of each element represented in (3.20) and we have

$$p\left(\mathbf{Z}/\mathbf{X}\right) = \prod_{k=0}^{NM-1} p\left([\mathbf{Z}|\mathbf{X}]_k\right), \tag{3.21}$$

substituting (3.20) in (3.21) we get

$$\begin{aligned} p\left(\mathbf{Z}|\mathbf{X}\right) &= \frac{1}{\left(\sqrt{2\pi}\right)^{NM-1}} \prod_{k=0}^{NM-1} \frac{1}{\sqrt{\sigma_k^2}} \prod_{k=0}^{NM-1} \exp\left(-\frac{\left([\mathbf{Z}]_k - [\mathbf{X}]_k\right)^2}{2\sigma_k^2}\right) \\ &= \frac{1}{\left(\sqrt{2\pi}\right)^{NM-1}} \left(\prod_{i=0}^{NM-1} \frac{1}{\sqrt{\sigma_k^2}}\right) \exp\left(-\sum_{k=0}^{NM-1} \frac{\left([\mathbf{Z}]_k - [\mathbf{X}]_k\right)^2}{2\sigma_k^2}\right), \end{aligned} \tag{3.22}$$

and (3.16) becomes

$$\hat{\mathbf{X}} = \arg\max_{\mathbf{X}} \left(\frac{1}{\left(\sqrt{2\pi}\right)^{NM-1}} \left(\prod_{k=0}^{NM-1} \frac{1}{\sqrt{\sigma_k^2}} \right) \exp\left(- \sum_{k=0}^{NM-1} \frac{\left([\mathbf{Z}]_k - [\mathbf{X}]_k\right)^2}{2\sigma_k^2} \right) \right). \tag{3.23}$$

Since the constant components do not affect the maximization, they can be removed from (3.23). We also note that maximize the inverse of an exponential is equivalent to minimize its argument, i.e.,

$$\hat{\mathbf{X}} = \min_{\mathbf{X}} \left(\sum_{k=0}^{NM-1} \frac{\left(|[\mathbf{Z}]|_k - |[\mathbf{X}]|_k\right)^2}{2\sigma_k^2} \right). \tag{3.24}$$

Moreover, if $\sigma_k^2 = \sigma^2 \, \forall \, k$, (3.24) reduces to the following optimization problem

$$\hat{\mathbf{X}} = \min_{\mathbf{X} \in S} \left(\sum_{k=0}^{NM-1} \left(|[\mathbf{Z}]_k| - |[\mathbf{X}]|_k\right)^2 \right) = \min_{\mathbf{X}} \left(\left|\left| \mathbf{Z} - \mathbf{X} \right|\right|^2 \right), \tag{3.25}$$

which, in fact, is formally equivalent to select the data sequence $\mathbf{X}$ that minimizes the Euclidean distance relatively to the received signal $\mathbf{Z}$ or, in other words, minimizes the Least Square (LS) error between these two data sequences. However, to minimize the differences relative to the received signal, the receiver must process the data sequence $\mathbf{X}$ as in the transmitter (see Figure 3.1 and (3.5)). Therefore, the expression (3.25) must consider the Euclidean distance between $\mathbf{Z}$ and $\mathbf{HGY}$, i.e.,

$$\begin{aligned} \hat{\mathbf{X}} &= \min_{\mathbf{X}} \left(\left|\left| \mathbf{Z} - \mathbf{HGY} \right|\right|^2 \right) \\ &= \min_{\mathbf{X}} \left(\left|\left| \mathbf{Z} - \mathbf{HGFf}(\mathbf{F^{-1}X}) \right|\right|^2 \right). \end{aligned} \tag{3.26}$$

Although optimal performance is achieved, this type of detection implies a high computational cost. Considering an OFDM signal with N in-band subcarriers and an adopted constellation with $\mathcal{M}$ points, we note that a change in one of the $N(\log_2 \mathcal{M})$ bits will lead to another possible transmitted data sequence, thus, with a full ML behaviour, the receiver must perform $2^{(\log_2 \mathcal{M})N}$ comparisons to allow the decision device to select the data estimate that has the minimum Euclidean distance relative to the received signal. This is a severe drawback for the ML detection and can jeopardize its use in some applications, namely, those that require high data rates that cannot be obtained with heavy and slow signal processing schemes.

3.3 Asymptotic Minimum Euclidean Distance

As seen before, the ML detection makes its decision based on the minimum Euclidean Distance, $\mathfrak{D}^2$, between the received signal and a possible transmitted signal that is subject to operations that were performed at the receiver. Thus, it would be desirable to characterize this distance in a theoretically way. For this purpose, this section presents an analytical method for obtaining the Euclidean distance between two nonlinearly distorted signals. Moreover, since it is expected the association of the minimum Euclidean Distance to data sequences that differ in a single bit, the considered nonlinearly sequences are associated to data sequences under these conditions. Note that this analytical method will allow to quantify the achievable asymptotic gain of the nonlinear OFDM since the ratio $\mathfrak{D}^2/E_b$ can be evaluated. In Figure 3.6 it is depicted a simplified transmission scenario of the version shown in Figure 3.1, where the frequency-domain filtering after the clipping operation is not considered (i.e., $\mathbf{G}$ is defined as in (3.12)). The frequency-domain data symbol $\mathbf{X} = [X_0\, X_1 \ldots X_{NM-1}]^T \in \mathbb{C}^{NM}$ has N useful subcarriers plus $(M-1)N$ idle subcarriers to perform the oversampling operation. The time-domain signal $\mathbf{x} = [x_0\, x_1 \ldots x_{NM-1}]^T \in \mathbb{C}^{NM}$ is obtained through an IDFT and then is submitted to a nonlinear memoryless function characterized by $\mathbf{f}(\mathbf{x})$. The channel effect is represented by (3.6). The noise is represented by $\mathbf{N} = [N_0\ N_1\ \ldots\ N_{NM-1}]^T \in \mathbb{C}^{NM}$, with $[\mathbf{N}]_k$ denoting the k^{th} frequency-domain noise component. The vector $\mathbf{Z} = [Z_0\, Z_1 \ldots Z_{NM-1}]^T \in \mathbb{C}^{NM}$ represents the received signal assuming a perfect channel estimation.

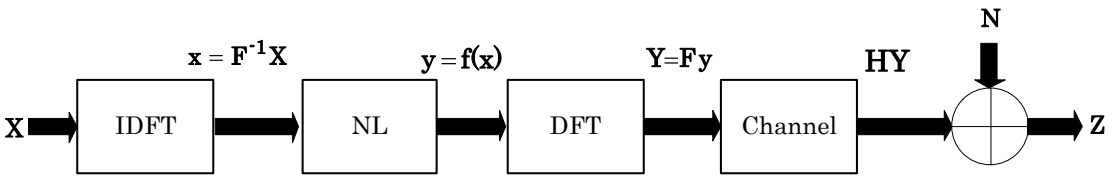

FIGURE 3.6: Signal processing scheme for the considered scenario.

In order to compute the Euclidean distance between two nonlinearly distorted signals, let us consider the frequency-domain data block, $\mathbf{X}^{(2)} = [X_0\, X_1 \ldots X_{NM-1}]^T \in \mathbb{C}^{NM}$, that differs

from $\mathbf{X}^{(1)} = [X_0\, X_1 \ldots X_{NM-1}]^T \in \mathbb{C}^{NM}$ in only $\mu = 1$ bits at the k_0^{th} subcarrier, i.e.,

$$\mathbf{X}^{(2)} = \mathbf{X}^{(1)} + \mathbf{E}, \tag{3.27}$$

where the vector $\mathbf{E} = [E_0\, E_1 \ldots E_{NM-1}]^T \in \mathbb{C}^{NM}$ can be regarded as an error array defined in the frequency-domain. Considering that the N in-band subcarriers use QPSK constellations where the complex symbols are defined as $[\mathbf{X}]_k = \pm A \pm jA$ we have

$$[\mathbf{E}]_k = \begin{cases} \pm 2A \text{ or } 2jA & k = k_0 \\ 0 & k \neq k_0. \end{cases} \tag{3.28}$$

The time-domain version of this error array $\boldsymbol{\varepsilon} \in \mathbb{C}^{NM}$ is computed through the IDFT operation, i.e., $\boldsymbol{\varepsilon} = [\varepsilon_0\, \epsilon_1 \ldots \varepsilon_{NM-1}]^T = \mathbf{F}^{-1}\mathbf{E}$ and, considering (3.2), we can write

$$[\boldsymbol{\varepsilon}]_n = \sum_{k=0}^{NM-1} [\mathbf{F}^{-1}]_{n,k}[\mathbf{E}]_k, \qquad n = 0 \ldots NM-1, \tag{3.29}$$

but, from (3.28), it is clear that $[\mathbf{E}]_k = 0$ for all subcarriers except at $k = k_0$, which allows us to write

$$\begin{aligned} [\boldsymbol{\varepsilon}]_n &= \frac{2A}{\sqrt{NM}} \exp\left(\frac{j2\pi n k_0}{NM} + j \arg([\mathbf{E}]_{k_0})\right) \\ &= \Delta \exp(j[\boldsymbol{\phi}]_n), \qquad n = 0, 1, NM-1, \end{aligned} \tag{3.30}$$

with $\Delta = 2A/\sqrt{NM}$. As mentioned before, the OFDM time-domain samples can be modelled by a complex stationary Gaussian process. Therefore, each element of $\mathbf{x}^{(1)} = \mathbf{F}^{-1}\mathbf{X}^{(1)}$ is modelled as a random variable with absolute value R and phase θ (for the sake of simplicity we drop the dependence with n). Moreover, it was seen in the Section 2.3, that the random variable $R = \sqrt{\Re(x)^2 + \Im(x)^2}$ has Rayleigh distribution, i.e., its PDF is defined by (2.52). The variable θ has uniform distribution in [0,2π], i.e.,

$$p(\theta) = \frac{1}{2\pi}, \qquad \theta \in [0, 2\pi]. \tag{3.31}$$

From (3.30), since k_0 can be any subcarrier of the N in-band subcarriers (i.e., the modified bit is anywhere along the data block), we can assume that ϕ is also modelled by a random

process where each sample is uniformly distributed in the interval $[0, 2\pi]$. Using (3.30) and focusing on the time-domain we may write

$$x^{(2)} = x^{(1)} + \varepsilon, \tag{3.32}$$

which means that

$$R' \exp(j\theta') = R \exp(j\theta) + \Delta \exp(j\phi), \tag{3.33}$$

where R' and θ' are the random variables that model the absolute value and the phase of the samples of $\mathbf{x^{(2)}}$. In Figure 3.7 is depicted the vectorial representation of $x^{(1)}$ and $x^{(2)}$.

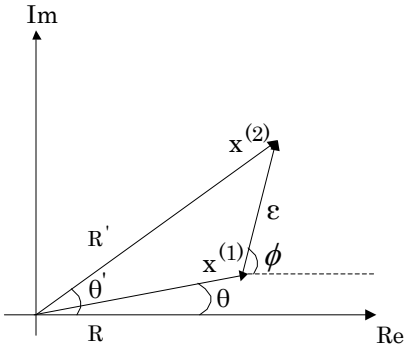

FIGURE 3.7: Vectorial representation of $x^{(1)}$ and $x^{(2)}$.

Without loss of generality, due to the circular nature of $x^{(1)}$ and $\boldsymbol{\varepsilon}$ we can assume that $\theta = 0$ as depicted in Figure 3.8.

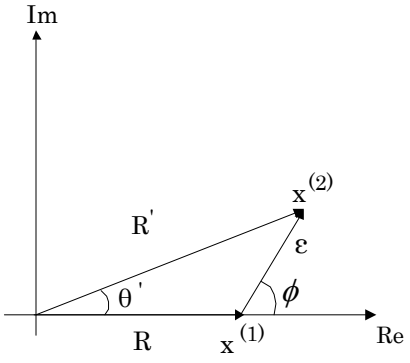

FIGURE 3.8: Vectorial representation of $x^{(1)}$ and $x^{(2)}$ when $\theta = 0$.

In this case, (3.33) can be rewritten as

$$\begin{aligned} R' \exp j\theta' &= R + \Delta \exp(j\phi) \\ &= (R + \Delta\cos(\phi)) + j\Delta\sin(\phi). \end{aligned} \tag{3.34}$$

Let us define the angle between the two time-domain sequences as $\Psi = \theta' - \theta$ (in this case $\Psi = \theta$)

$$\begin{aligned} \Psi &= \arg(R + \Delta\exp(j\phi)) \\ &= \arctan\left(\frac{\Delta\sin(\phi)}{R + \Delta\cos(\phi)}\right). \end{aligned} \tag{3.35}$$

The absolute value of $x^{(2)}$ is defined as

$$\begin{aligned} R' &= |R + \Delta\exp(j\phi)| \\ &= \sqrt{(R + \Delta\cos(\phi))^2 + (\Delta\sin(\phi))^2} \\ &= \sqrt{R^2 + 2R\Delta\cos(\phi) + \Delta^2\cos^2(\phi) + \Delta^2\sin^2(\phi)} \\ &= \sqrt{R^2 + 2R\Delta\cos(\phi) + \Delta^2\left(\cos^2(\phi) + \sin^2(\phi)\right)} \\ &= \sqrt{R^2 + 2R\Delta\cos(\phi) + \Delta^2} \\ &= R\sqrt{1 + \frac{2\Delta\cos(\phi)}{R} + \left(\frac{\Delta}{R}\right)^2}, \end{aligned} \tag{3.36}$$

which also can be written as

$$R' \overset{(a)}{\approx} R\sqrt{1 + \frac{2\Delta\cos(\phi)}{R}}, \tag{3.37}$$

where the approximation (a) is valid for $\Delta \ll R$.

With the purpose of finding more approximations for (3.37), let us now consider the Taylor Series that allows to expand a general function $f(x)$ into a power series by knowing the function and the function derivatives at a certain point $x = h$. We can express this series as

$$f(x) = f(h) + f'(h)(x-h) + f''(h)\frac{(x-h)^2}{2!} + f'''(h)\frac{(x-h)^3}{3!} + \cdots = \sum_{k=0}^{\infty}\frac{f^{(k)}(h)}{k!}(x-h)^k, \tag{3.38}$$

where $f^{(0)}(h) = f(h)$ and $f^{(k)}(h)$ is the k^{th} derivative of $f(x)$ evaluated at $x = h$ (i.e., $\frac{\mathrm{d}^k(f)}{\mathrm{d}x^k}(h)$). Let us consider only the first order approximation. In this case, only the terms corresponding to $k = 0$ and $k = 1$ are taken into account and the function $f(x)$ around h is approximated by

$$f(x) \approx f(h) + \frac{\mathrm{df}}{\mathrm{d}x}(h)\,(x - h). \tag{3.39}$$

If we apply (3.39) to the function $f(x) = \sqrt{1+2x}$, around $h = 0$, results

$$\begin{aligned} \sqrt{1+2x} &\approx \sqrt{1} + x\frac{\mathrm{d}f}{\mathrm{d}x}\left(\sqrt{1+2x}\right)\Big|_{x=0} \\ &= 1 + x\left(\frac{1}{1+2x}\right)\Big|_{x=0} \\ &= 1 + x. \end{aligned} \tag{3.40}$$

Using this result in (3.40) and considering $\frac{2\Delta\cos(\phi)}{R} \ll 1$, the definition of R' in (3.37) can be approximated by

$$\begin{aligned} R' &\approx R\left(1 + \frac{\Delta\cos(\phi)}{R}\right) \\ &= R + \Delta\cos(\phi). \end{aligned} \tag{3.41}$$

Considering again (3.39), we can approximate (3.35) (that defines the angle between $x^{(1)}$ and $x^{(2)}$) around $h = 0$, as

$$\begin{aligned} \arctan(x) &\approx \arctan(0) + x\left(\frac{\mathrm{d}f}{\mathrm{d}x}(\arctan(x))\right)\Big|_{x=0} \\ &= x\left(\frac{1}{1+x^2}\right)\Big|_{x=0} \\ &= x. \end{aligned} \tag{3.42}$$

Using (3.42) and considering $\frac{\Delta \sin(\phi)}{R+\Delta \cos(\phi)} \ll 1$ we can rewrite (3.35) as

$$\begin{aligned} \Psi &= \arctan\left(\frac{\Delta \sin(\phi)}{R+\Delta \cos(\phi)}\right) \\ &\approx \left(\frac{\Delta \sin(\phi)}{R+\Delta \cos(\phi)}\right) \\ &= \frac{\Delta \sin(\phi)}{R}\left(\frac{1}{1+\frac{\Delta}{R}\cos\phi}\right), \end{aligned} \tag{3.43}$$

but, using (3.39) to approximate $f(x) = \frac{1}{1+x}$ around $h = 0$, we get

$$\begin{aligned} \frac{1}{1+x} &\approx 1 + x\frac{\mathrm{d}f}{\mathrm{d}x}\left(\frac{1}{1+x}\right)\Big|_{x=0} \\ &= 1 + x\left(-\frac{1}{(1+x)^2}\right)\Big|_{x=0} \\ &= 1 - x, \end{aligned} \tag{3.44}$$

which makes possible to approximate (3.43) another time, resulting

$$\begin{aligned} \Psi &\approx \frac{\Delta \sin(\phi)}{R}\left(\frac{1}{1+\frac{\Delta}{R}\cos\phi}\right) \\ &\approx \frac{\Delta \sin(\phi)}{R}\left(1-\frac{\Delta}{R}\cos\phi\right) \\ &\approx \frac{\Delta \sin(\phi)}{R}. \end{aligned} \tag{3.45}$$

After all the considered approximations, we can write that

$$x^{(2)} \approx (R+\Delta\cos(\phi))\exp\left(j\frac{\Delta\sin(\phi)}{R}\right). \tag{3.46}$$

As shown in Chapter 2, in (2.45), the effect of polar memoryless nonlinearity can be written as a function of the input absolute value. Considering that the input is $x^{(2)}$, we may model the nonlinear effect as

$$f(R') = A(R')\exp\big(j\Theta(R')\big). \tag{3.47}$$

Assuming that the AM-PM characteristic is 0 (i.e., $\Theta(R') = 0$), we have,

$$f(R') = A(R'). \tag{3.48}$$

Now let us consider that $y^{(1)}$ and $y^{(2)}$ designate both the nonlinearity outputs and the random variables associated to them. For $y^{(2)}$, we have

$$\begin{aligned} y^{(2)} &= f\left(R+\Delta\cos(\phi)\right)\exp j\left(\theta'\right) \\ &= f\left(R+\Delta\cos(\phi)\right)\exp\left(j\left(\theta+\Psi\right)\right). \end{aligned} \tag{3.49}$$

Moreover, by making the first order Taylor approximation of $f(\cdot)$ around R, we can write

$$f\left(R+\Delta\cos(\phi)\right) \approx f(R)+f^{'}(R)\Delta\cos(\phi), \tag{3.50}$$

and the nonlinearity output $y^{(2)}$ can be approximated by

$$y^{(2)} \approx \left(f(R)+f^{'}(R)\Delta\cos(\phi)\right)\exp\left(j\left(\theta+\Psi\right)\right), \tag{3.51}$$

with nonlinear output for the input $x^{(1)}$ given by

$$y^{(1)} = f\left(R\right)\exp\left(j\theta\right). \tag{3.52}$$

As we are interested in computing the Euclidean distance between $y^{(1)}$ and $y^{(2)}$, we have

$$\begin{aligned} \left|y^{(2)}-y^{(1)}\right|^2 &= \left|\left(f(R)+f^{'}(R)\Delta\cos(\phi)\right)\exp\left(j\left(\theta+\Psi\right)\right)-f(R)\exp\left(j\theta\right)\right|^2 \\ &= \left|\left(\left(f(R)+f^{'}(R)\Delta\cos(\phi)\right)\exp\left(j\Psi\right)-f(R)\right)\exp\left(j\theta\right)\right|^2 \\ &= \left|\left(f(R)+f^{'}(R)\Delta\cos(\phi)\right)-f(R)\exp\left(-j\Psi\right)\right|^2 \\ &= \left(f(R)+f^{'}(R)\Delta\cos(\phi)-f(R)\cos(\Psi)\right)^2+\left(f(R)\sin(\Psi)\right)^2. \end{aligned} \tag{3.53}$$

Furthermore, knowing that $|\Psi| \ll 1$ and using (3.39) to approximate $\sin(\Psi)$ and $\cos(\Psi)$ around 0, we get

$$\begin{aligned} \sin(\Psi) &\approx \sin(0)+\Psi\left(\frac{\mathrm{d}}{\mathrm{d}\Psi}\left(\sin(\Psi)\right)\right)\Big|_{\Psi=0} \\ &= \Psi\left(\cos(\Psi)\right)\Big|_{\Psi=0} \\ &= \Psi. \end{aligned} \tag{3.54}$$

and,

$$\begin{aligned}\cos(\Psi) &\approx \cos(0) + \Psi\left(\frac{\mathrm{d}}{\mathrm{d}\Psi}\left(\cos(\Psi)\right)\right)\Big|_{\Psi=0} \\ &= 1 + \Psi\left(-\sin(\Psi)\right)\Big|_{\Psi=0} \\ &= 1.\end{aligned} \tag{3.55}$$

Applying these approximations in (3.53), we get

$$\begin{aligned}\left|y^{(2)} - y^{(1)}\right|^2 &= \left(f(R) + f^{'}(R)\Delta\cos(\phi) - f(R)\cos(\Psi)\right)^2 + \left(f(R)\sin(\Psi)\right)^2 \\ &= \left|f(R)\right|^2\left(\left(1 + \frac{f^{'}(R)}{f(R)}\Delta\cos(\phi) - \cos(\Psi)\right) + \sin^2(\Psi)\right) \\ &\approx \left|f(R)\right|^2\left(\left(\frac{f^{'}(R)}{f(R)}\Delta\cos(\phi)\right)^2 + \Psi^2\right) \\ &= \left|f(R)\right|^2\left(\left(\frac{f^{'}(R)}{f(R)}\Delta\cos(\phi)\right)^2 + \left(\frac{\Delta\sin(\phi)}{R}\right)^2\right) \\ &= \left(f^{'}(R)\Delta\cos(\phi)\right)^2 + \left(\frac{f(R)\Delta\sin(\phi)}{R}\right)^2 \\ &= \Delta^2\left(\left(f^{'}(R)\cos(\phi)\right)^2 + \left(\frac{f(R)\sin(\phi)}{R}\right)^2\right).\end{aligned} \tag{3.56}$$

Finally, using (3.10) and (2.54), the Euclidean distance between $y^{(1)}$ and $y^{(2)}$ can be written as

$$\begin{aligned}\mathfrak{D}^2 &= \left|\left|y^{(2)} - y^{(1)}\right|\right|^2 \\ &\overset{(b)}{\approx} NM\mathbb{E}\left[\left|y^{(2)} - y^{(1)}\right|^2\right] \\ &= NM\Delta^2\int_0^{\infty}\int_0^{2\pi}\left(\left(f^{'}(R)\cos(\phi)\right)^2 + \left(\frac{f(R)\sin(\phi)}{R}\right)^2\right)p(R)p(\phi)\mathrm{d}R\ \mathrm{d}\phi \\ &= NM\Delta^2\int_0^{\infty}\int_0^{2\pi}\left(\left(f^{'}(R)\cos(\phi)\right)^2 + \left(\frac{f(R)\sin(\phi)}{R}\right)^2\right)\frac{R}{\sigma^2}\exp\left(-\frac{R^2}{2\sigma^2}\right)\frac{1}{2\pi}\mathrm{d}R\ \mathrm{d}\phi,\end{aligned} \tag{3.57}$$

where the approximation (b) is valid for $N \gg 1$. From (3.57) becomes obvious that for quantifying the Euclidean Distance between two nonlinearly distorted signals we only need to know the AM/AM characteristic responsible for that distortion. If we consider a linear

transmitter (i.e., a transmitter that does not affect the signals with nonlinear effects), its AM-PM characteristic is null (i.e., $\Theta(R) = 0$) and the AM-AM characteristic is defined as

$$f(R) = R, \tag{3.58}$$

thus, the first order derivative is

$$\frac{\mathrm{d}f(R)}{\mathrm{d}R} = 1. \tag{3.59}$$

Replacing these values in equation (3.57) and considering $\sigma^2 = 1$, we get

$$\begin{aligned}
\mathfrak{D}^2 = \sum_{n=0}^{NM-1} \left| y^{(2)} - y^{(1)} \right|^2 &\approx NM\mathbb{E}\left[\left| y^{(2)} - y^{(1)} \right|^2 \right] \\
&= NM\Delta^2 \int_0^{\infty} \int_0^{2\pi} \left(\cos^2(\phi) + \sin^2(\phi)\right) \frac{R}{2\pi} \exp\left(-\frac{R^2}{2}\right) \mathrm{d}R \, \mathrm{d}\phi \\
&= NM\Delta^2 \int_0^{\infty} R \exp\left(-\frac{R^2}{2}\right) \mathrm{d}R \, \mathrm{d}\phi \\
&= NM\Delta^2 \\
&= NM\left(\frac{2A}{\sqrt{NM}}\right)^2 \\
&= 2A^2 \\
&= 4E_b.
\end{aligned} \tag{3.60}$$

This is the well-known distance between two signals for the case of a linear transmitter. Considering now a nonlinear transmitter that has a clipping device with $\Theta(R) = 0$ and AM-AM conversion characteristic defined as (3.1), we have

$$\frac{\mathrm{d}f(R)}{\mathrm{d}R} = \begin{cases} 1, & 0 \leq R \leq s_M \\ 0, & R > s_M. \end{cases} \tag{3.61}$$

Substituting these values in equation (3.57), results

$$\begin{aligned}
\mathfrak{D}^2 &= NM\Delta^2 \int_0^{s_M}\int_0^{2\pi} \left(\cos^2(\phi)+\sin^2(\phi)\right)\frac{p(R)}{2\pi}\,\mathrm{d}R\,\mathrm{d}\phi + NM\Delta^2 \int_{s_M}^{+\infty}\int_0^{2\pi} \frac{s_M^2}{R^2}\sin^2(\phi)\frac{p(R)}{2\pi}\mathrm{d}R\,\mathrm{d}\phi \\
&= NM\Delta^2\left(\int_0^{s_M} p(R)\mathrm{d}R + \int_{s_M}^{+\infty}\int_0^{2\pi} s_M^2\frac{1-\cos(2\phi)}{2}\frac{p(R)}{2\pi R^2}\mathrm{d}R\,\mathrm{d}\phi\right) \\
&= NM\Delta^2\left(\int_0^{s_M} R\exp\left(-\frac{R^2}{2\sigma^2}\right)\mathrm{d}R + \int_{s_M}^{+\infty}\frac{s_M^2}{2R\sigma^2}\exp\left(-\frac{R^2}{2\sigma^2}\right)\mathrm{d}R\right) \\
&= NM\Delta^2\left(\left[\exp\left(-\frac{R^2}{2\sigma^2}\right)\right]_0^{s_M} + \int_{s_M}^{+\infty}\frac{s_M^2}{2R\sigma^2}\exp\left(-\frac{R^2}{2\sigma^2}\right)\mathrm{d}R\right) \\
&= NM\Delta^2\left(\left(1-\exp\left(-\frac{s_M^2}{2\sigma^2}\right)\right) + \int_{s_M}^{+\infty}\frac{s_M^2}{2R\sigma^2}\exp\left(-\frac{R^2}{2\sigma^2}\right)\mathrm{d}R\right).
\end{aligned} \tag{3.62}$$

Using the definition of the asymptotic gain for nonlinear OFDM given by (3.13), (3.9) and (3.62), we have

$$\mathfrak{G} = \frac{\mathfrak{D}^2}{4E_b} \approx \frac{NM\Delta^2\left(\left(1-\exp\left(-\frac{s_M^2}{2\sigma^2}\right)\right) + \int_{s_M}^{+\infty}\frac{s_M^2}{2R\sigma^2}\exp\left(-\frac{R^2}{2\sigma^2}\right)\mathrm{d}R\right)}{4A^2\left(1-\exp\left(-\frac{s_M^2}{2\sigma^2}\right)\right)}. \tag{3.63}$$

In Figure 3.9 it is shown the Euclidean Distance between two nonlinearly sequences obtained both by simulation and analytically (considering (3.62)), with a variable number of in-band subcarriers N and different values of s_M/σ. As we can see, the analytical expression is accurate, especially for large values of N, since some approximations for obtaining this expression were made under the assumption of $N \gg 1$.

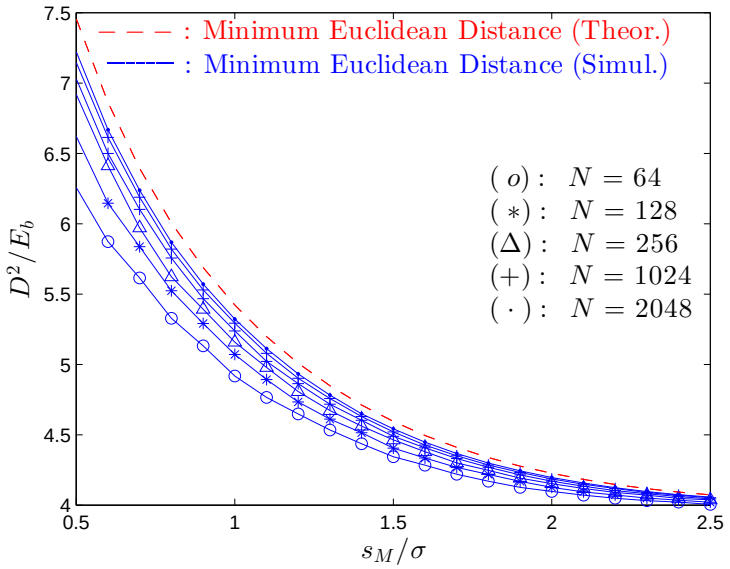

FIGURE 3.9: Evolution of the minimum Euclidean distance between two nonlinearly sequences that differ in $\mu = 1$ bits and are distorted with a normalized clipping level of s_M/σ.

3.4 Asymptotic Performance

Taking into account what has been seen, is expected that nonlinear OFDM schemes that use ML receivers can outperform conventional OFDM receivers (i.e., the ones that assume a linear transmitter), due to the higher minimum Euclidean distances between the nonlinearly distorted signals when comparing to the average bit energy E_b. It should be mentioned that the minimum Euclidean distance given by (3.62) represents a benchmark for the asymptotic performance of the optimum receiver for nonlinear OFDM schemes when its assumed an high number of in-band subcarriers. Yet, when the number of in-band subcarriers N is reduced, the expression (3.62) loses accuracy. In fact, there are fluctuations on the minimum Euclidean distance for different data sequences that this benchmark does not have into account. Moreover, the impact of an FDF after the clipping operation on the minimum Euclidean distance is not easily derived and has not been taken into account.

In this section the asymptotic performance results for nonlinear OFDM schemes with ML receivers are presented. To avoid the computational effort associated the full ML behaviour (i.e. the high number of comparisons), let us start the study of the achievable gains by obtaining the PDF associated to the minimum Euclidean distance between two nonlinearly data sequences.

The first of the considered sequences is a random data sequence represented by $\mathbf{X}^{(1)} \in \mathbb{C}^{NM}$. The second is one of the $2N$ variations of $\mathbf{X}^{(1)}$ with $\mu = 1$ bits modified, represented by $\mathbf{X}^{(2)} \in \mathbb{C}^{NM}$. The two signals are passed through a nonlinear operation as in (3.3) and the sequences $\mathbf{Y}^{(1)}$ and $\mathbf{Y}^{(2)}$ are obtained. After that, the Euclidean distance between them are computed. The minimum distance is selected from the distance set that has $2N$ distances, since there are $2N$ possible data sequences $\mathbf{X}^{(2)}$

$$\mathfrak{D}^2 = \min\left\{\mathfrak{D}^2_{1,2}\right\} \tag{3.64}$$

where, $\mathfrak{D}^2_{1,2}$ is the Euclidean distance between $\mathbf{Y}^{(1)}$ and $\mathbf{Y}^{(2)}$ defined according to (3.10).

In Figure 3.10 it is shown the PDF of the asymptotic gain of an ML receiver that is defined using (3.13) and (3.9). As expected, this is slightly higher than one, which confirms the improvement in the performance when is used a ML receiver that deals with nonlinearly distorted signals. In the same figure, we also can see that when a frequency-domain filtering operation is employed, it is less probable that the gain exceeds the unity, since a lower number of subcarriers contribute for Euclidean distance between two data sequences.

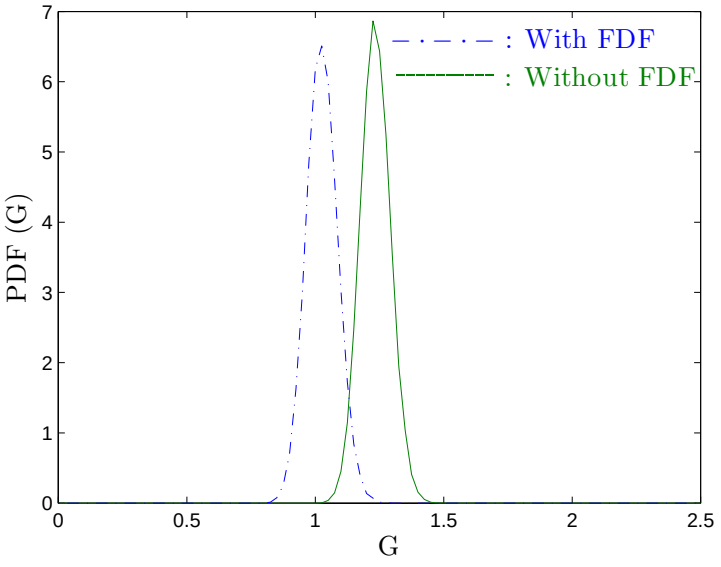

FIGURE 3.10: PDF of $\mathfrak{G} = \mathfrak{D}^2/4E_b$ for filtered and non-filtered sequences with $N = 64$ subcarriers that are submitted to a clipping device with normalized clipping level $s_M/\sigma = 1.0$.

Figure 3.11 shows the impact of the number of data subcarriers N on the PDF of $\mathfrak{G} = \mathfrak{D}^2/(4E_b)$. From the results, it is clear that the fluctuations of $\mathfrak{G}$ relative to its average value

decrease as N increases. Note that if we consider $N \to +\infty$ we are in the conditions of the expression (3.63); other lower values of N confirm the loss of accuracy of the expression due to the fluctuations on the minimum Euclidean Distance.

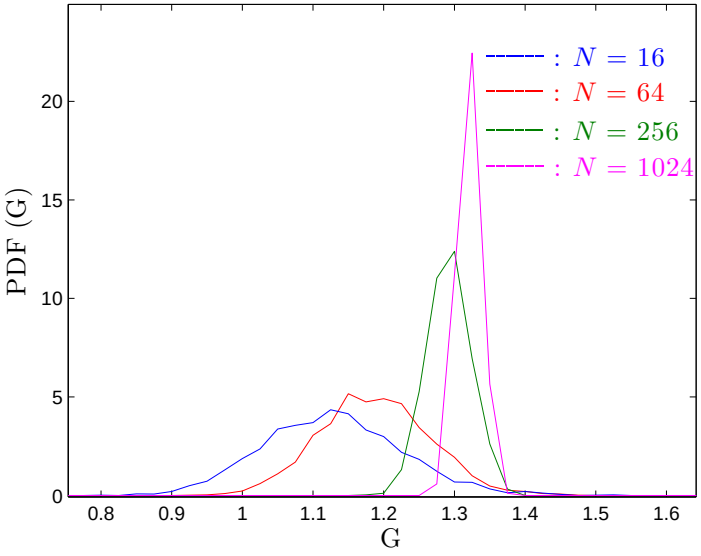

FIGURE 3.11: Impact of the number of in-band subcarriers N on the PDF of $\mathfrak{G} = \mathfrak{D}^2/(4E_b)$.

It should be stressed that when the signal has stronger nonlinear effects (for example, when the clipping device works with a small clipping level) the achievable gain is higher, as one can see in Figure 3.12. In this case, the clipping device operates with a normalized clipping level of $s_M/\sigma = 0.5$. Consequently, if we increase the number of modified bits, μ, it is expected an increase on gain, since the distance between two data sequences will be higher. In the Figure 3.13 it is shown the PDF of the gain with a variable number of modified bits. More concretely, all possible variations of $\mu = 1$, $\mu = 2$ or $\mu = 3$ relatively to each data sequence were considered in the computation of each PDF. Clearly, the minimum distance is almost associated to the sequences that differ in a single bit ($\mu = 1$) (it should be noted that with a higher μ, the distribution of the gain tends to broad). Consequently, as the area under the PDF equals unity, the PDF will have less concentrated values or, in other words, there are more fluctuations on the minimum Euclidean Distance. The achievable gains represented in the above figures, will represent an asymptotic improvement in the BER performance. Provided that the Euclidean Distance between two nonlinearly distorted signals associated to data sequences that differ in $\mu = 2$ and $\mu = 3$ is much bigger than for sequences that differ

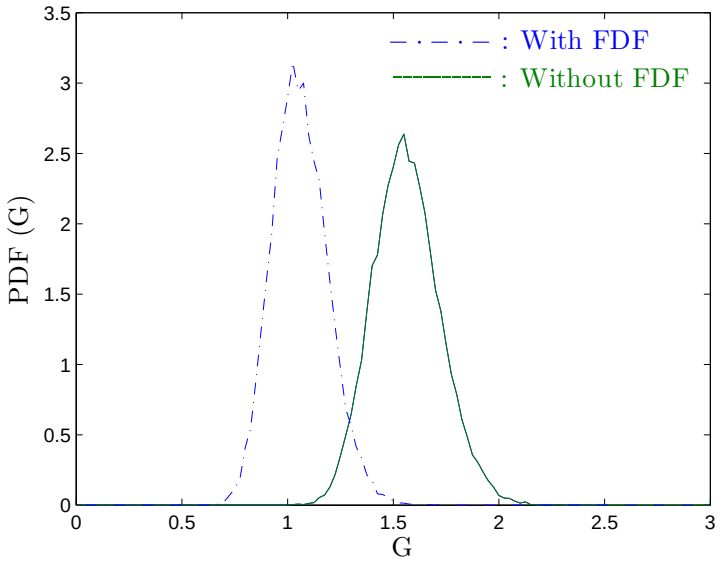

FIGURE 3.12: PDF of $\mathfrak{G} = \mathfrak{D}^2/4E_b$ for filtered and non-filtered sequences with $N = 64$ subcarriers that are submitted to a clipping device with normalized clipping level $s_M/\sigma = 0.5$.

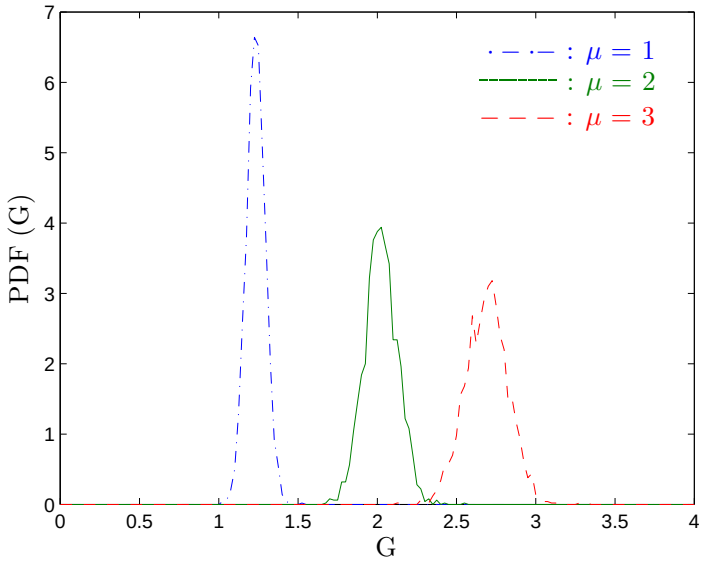

FIGURE 3.13: PDF of $\mathfrak{G} = \mathfrak{D}^2/4E_b$ for non-filtered sequences with $N = 64$ that are submitted to a clipping device with normalized clipping level $s_M/\sigma = 0.5$ considering different values of μ.

in only one bit, the BER performance (conditioned by $\mathfrak{D}^2/E_b$) for an ML receiver that deals with nonlinear OFDM signals in an AWGN channel can be approximated by

$$P_b \approx \mathbb{E}_{\{\mathbf{X}^{(1)}\}} \left[\frac{1}{2N} \sum_{\{\mathbf{X}^{(2)}\} \in \Phi_1(\{\mathbf{X}^{(1)}\})} Q\left(\sqrt{\frac{D_{1,2}^2/2}{N_0}} \right) \right], \tag{3.65}$$

where $\Phi_1(\{\mathbf{X}^{(1)}\})$ denotes the set of data sequences that differ from $\mathbf{X}^{(1)}$ in a single bit, N_0 is the PSD of the channel noise and the function $Q(b)$ is defined as

$$Q(b) = \frac{1}{2}\text{erfc}\left(\frac{b}{\sqrt{2}}\right), \tag{3.66}$$

where $\text{erfc}(a)$, the complementary error function, is expressed as

$$\text{erfc}(a) = \left(\frac{1}{\sqrt{2\pi}}\right)\int_a^\infty \exp(-t^2)\mathrm{d}t. \tag{3.67}$$

For conventional OFDM transmitters we have $\mathfrak{D}^2 = 4E_b$ for all the sequences that differ from $\mathbf{X}^{(1)}$ in only 1 bit. Thus, (3.65) reduces to the well-known result

$$P_b \approx Q\left(\sqrt{\frac{2E_b}{N_0}}\right), \tag{3.68}$$

which is the BER for a linear transmitter considering an QPSK constellation.

Let us now consider a scenario where $N = 64$, $s_M/\sigma = 0.5$ and FDF was not considered ($\mathbf{G}$ is defined as in (3.12)). In Figure 3.14 is shown the approximate ML BER under these conditions and assuming an AWGN channel. We also assume perfect synchronization and channel estimation at the receiver. In red the BER for each realization is shown, in blue it is represented the mean value of all the realizations as in (3.65). The ideal performance of conventional linear OFDM schemes was included for the sake of comparisons. As expected, due to the increased value of $\mathfrak{D}^2$ over E_b, the BER performance for OFDM dealing with nonlinearly distorted signals is improved with the use of the ML receiver. For the considered clipping level, a gain between 1 and 2 dB can be obtained. As mentioned before, the harder the nonlinear distortion effects the higher the gains as we can see in Figure 3.15 where the BER performance is depicted considering different values of s_M/σ.

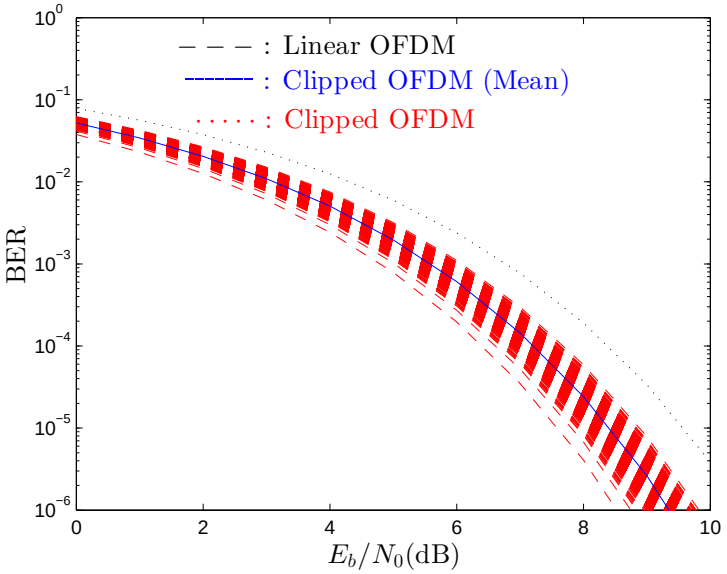

FIGURE 3.14: BER for non-filtered sequences with $N = 64$ that are submitted to a clipping device with normalized clipping level $s_M/\sigma = 1.0$ considering an ideal AWGN channel.

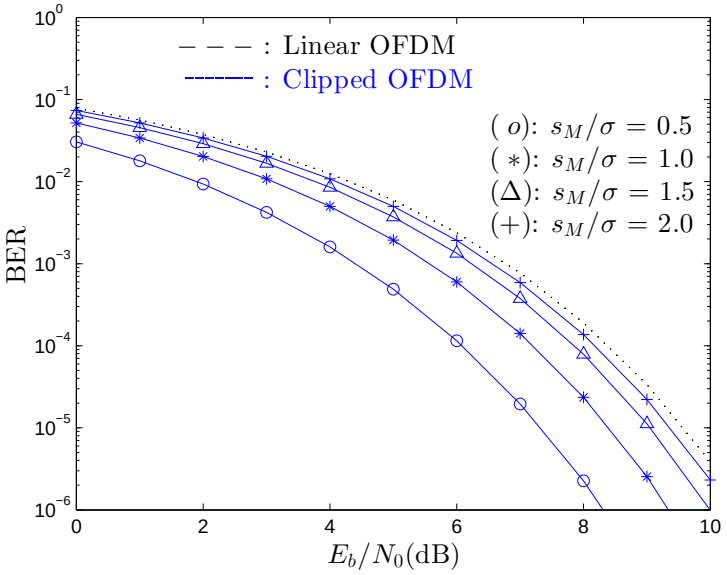

FIGURE 3.15: BER for non-filtered sequences with $N = 64$ that are submitted to a clipping device with different values of normalized clipping level s_M/σ considering an ideal AWGN channel.

From the above figure, it is clear that for higher values of normalized clipping level (say $s_M/\sigma = 2.0$), the signal presents less nonlinear distortion effects, since a lower number of amplitudes associated to the time-domain OFDM block will be clipped. Thus, there is an increased average bit energy which will make the BER performance closer to the conventional linear case. Of course, if $s_M/\sigma = \infty$ (the nonlinear distortion effect is null), the two curves will be identical.

As seen before, the use of the FDF ($\mathbf{G}$ is defined as in (3.11)) will reduce the achievable gains. We can see this effect directly on the BER performance shown in Figure 3.16. From the results, we note that for $s_M/\sigma = 0.5$, the gain is reduced in approximately 1dB. However, even with the filtering operation the gains are still considerable (especially for severe nonlinear effects). When a higher normalized clipping level is considered, the difference between the filtered and the non-filtered BER curve is smaller. This happens because for lower values of s_M/σ, there are strong nonlinear distortion effects (and, consequently, a higher $\mathfrak{D}^2/E_b$), hence, a filtering operation will be noticeable. On the other hand, when s_M/σ assumes higher values, the distortion component of the nonlinear signal will have less amplitude along the subcarriers the OFDM block. Therefore, the filtering operation employed by the transmitter can be almost neglected as is depicted in Figure 3.16. When the FDF is employed after the clipping operation, the resultant time-domain signal has some regrowth in the envelope fluctuations, which goes against the purpose of this technique. A simple way to overcome this problem is by repeating the clipping and filtering procedures L times [11]. In fact, by repeating the clipping and filtering just 2 to 4 times the regrowth in the envelope fluctuations can be reduced significantly despite of maintaining the bandwidth of conventional, linear OFDM signals. In Figure 3.17 it is shown the complementary cumulative density function (CCDF) for the absolute values of the transmitted signal.

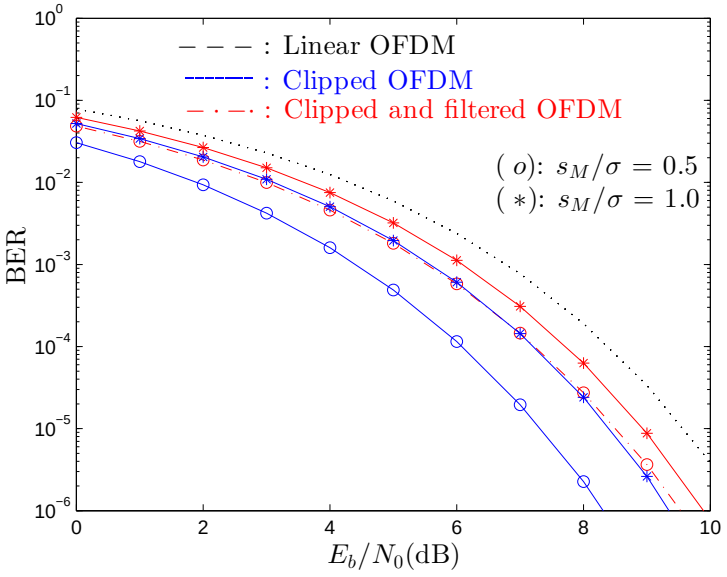

FIGURE 3.16: BER for an OFDM signal with $N = 64$ with and without frequency-domain filtering, considering different values of s_M/σ and an ideal AWGN channel.

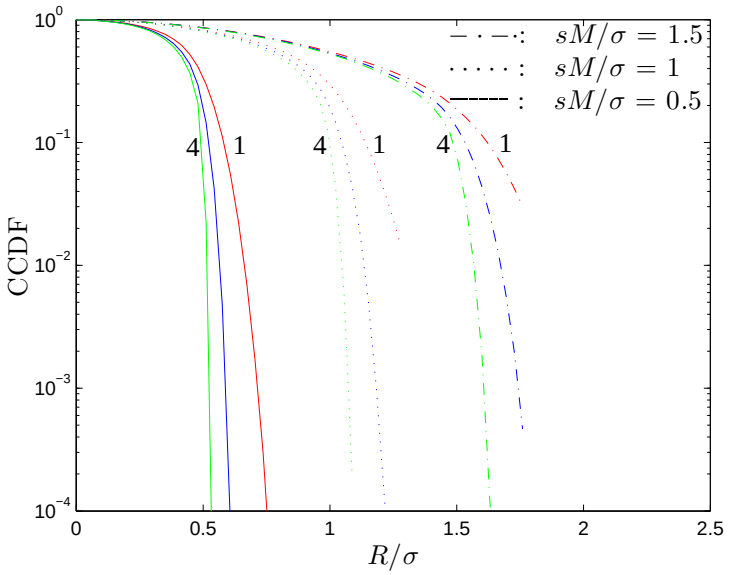

FIGURE 3.17: CCDF for the absolute value of the transmitted OFDM signal for different values of s_M/σ.

Clearly, the higher the number of the clipping and filtering iterations L, the smaller the probability of exceeding the clipping level. From the figure, we can see that when $L = 1$ (i.e., the signal is filtered only one time) the regrowth of the complex envelope is very high and, in fact, the time-domain filtered signal is not limited by s_M/σ but approximately by $s_M/\sigma + 0.5$. On the other hand, with $L = 4$ the complex envelope is practically limited by the adopted s_M/σ. It should be pointed out that the overall nonlinear distortion effects increase with the number of clipping and filtering iterations and, consequently, the gains will be affected. The BER for signals with L clipping and filtering iterations is depicted in Figure 3.18. It is clear that for high values of L, the performance is better. This was an expected result since the signal is clipped and filtered several times, which leads to the existence of higher nonlinear distortion effects and, consequently, higher gains.

In all BER curves presented before, we consider an ideal AWGN channel. Let us now focus in another scenario, where the transmission is made under a frequency-selective channel characterized by the channel frequency response $\mathbf{H} = \text{diag}\left([H_0\, H_1 \ldots H_{NM-1}]^T\right)$. In this case, we need to define the equivalent Euclidean Distance between two received signals associated to the data sequences $\mathbf{X}^{(1)}$ and $\mathbf{X}^{(2)}$ as

$$D^2_{Eq_{1,2}}(\mathbf{H}) = \sum_{k=0}^{NM-1} \left|[\mathbf{H}]_k\right|^2 \left|\alpha[\mathbf{X}]_k^{(1)} + [\mathbf{D}]_k^{(k)} - \alpha[\mathbf{X}]_k^{(2)} - [\mathbf{D}]_k^{(2)}\right|^2. \tag{3.69}$$

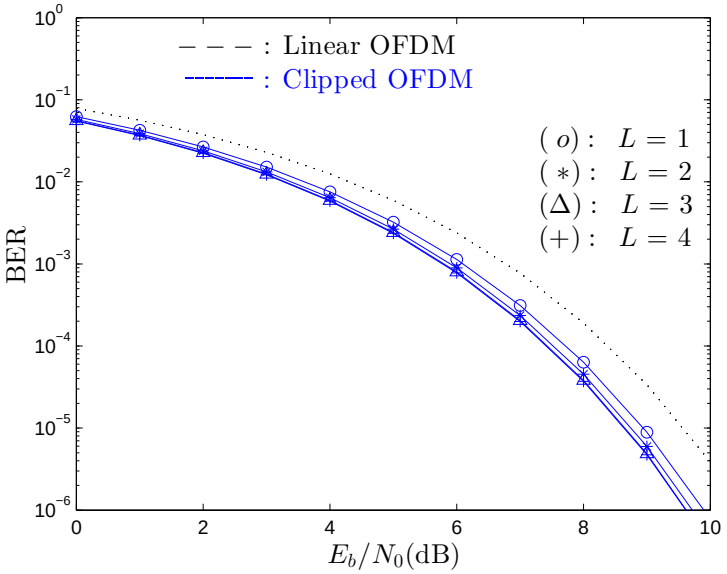

FIGURE 3.18: BER for an OFDM signal with $N = 64$ and L clipping and filtering iterations considering $s_M/\sigma = 1.0$ and an ideal AWGN channel.

The BER associated to the channel realization $\mathbf{H}$ will be given by

$$P_b(\mathbf{H}) \approx \frac{1}{2N} \sum_{\mathbf{X}^{(2)} \in \Phi_1(\mathbf{X}^{(1)})} Q\left(\sqrt{\frac{D^2_{Eq_{1,2}}(\mathbf{H})/2}{N_0}}\right), \tag{3.70}$$

and the average BER can be defined through the following multiple integral

$$P_b \approx \int P_b(\mathbf{H}) p(\mathbf{H}) d\mathbf{H}, \tag{3.71}$$

where $p(\mathbf{H})$ denotes the joint probability density function of the overall channel frequency response $\mathbf{H}$. Note that this integral is difficult to evaluate. Its value can be estimated by averaging over a large number of independent channel realizations. Let us now consider an XTAP channel that has 32 symbol-spaced multipath components with uncorrelated Rayleigh fading. In Figure 3.19 are shown the BER results for nonlinearly distorted OFDM signals under these conditions. It is clear that the achievable gains of an ideal ML receiver are even higher for frequency-selective channels than the ones with an ideal AWGN channel. This additional gain is associated to the diversity effects in the transmitted signals that are inherent to the nonlinear distortion. It is important to remark that the results that are presented in this section consider the transmission of "typical" sequences. The conclusions can be substantially different, for instance, for sequences where all the subcarriers carry the same symbol. However,

these sequences are very rare. In fact, they can be avoided in practice through the use of scrambling procedures and, thus, its effect on the overall performance can be neglected.

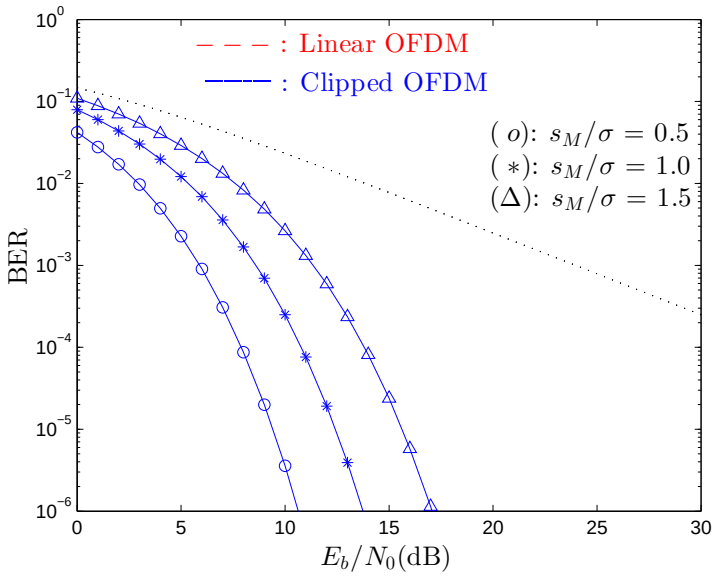

FIGURE 3.19: BER for a non-filtered OFDM signal with $N = 64$ subcarriers considering an frequency-selective channel.

Chapter 4

Maximum-Likelihood Based Receivers

In the previous chapter it was shown that using an optimum receiver, the nonlinear OFDM has better performance than the conventional linear scheme. However, it is well known that the main drawback of the ML detection is the corresponding complexity. As mentioned before, given an OFDM signal with N subcarriers and a $\mathcal{M}$-QAM constellation, the ML receiver must select the data sequence that has minimum Euclidean Distance relative to the received signal, which implies testing over $2^{(\log_2 \mathcal{M})N}$ possible data sequences. Therefore, the complexity of this type of receivers can be prohibitively high, even considering a small number of subcarriers. To avoid this problem, several ML based receivers are presented and evaluated in this chapter. These sub-optimal receivers allow notable performance improvements, being able to reduce significantly the gap between the optimum performance and the performance of conventional OFDM receivers. The motivation behind these techniques is that usually the optimal sequence differs from the *hard decision sequence* in a small number of bits. Therefore, only a small fraction of all possible sequences must be tested, while still having high chances that the optimal sequence is among them and, consequently, achieve both a close-to-optimum performance and a reduction in the computational load.

All presented sub-optimal receivers work similarly for an ideal AWGN channel as well as for a frequency-selective channel. The only required modification in the second scenario is that in the Euclidean distances between candidate signals, the channel frequency response should be

taken into account (i.e., the set $\mathbf{H}$) as in (3.69).

This chapter is organized as follows: in Section 4.1 several sub-optimal receivers are described and their algorithms are presented. Section 4.2 presents a method to obtain the approximated performance of the optimum receivers. Finally, in Section 4.3, some BER performance results of the previously described sub-optimal receivers are presented and discussed. The impact of using clipping and filtering, diversity schemes and higher constellations is also studied in this section.

4.1 Sub-Optimal receivers

As seen before, in typical OFDM implementations, the receiver does not take advantage of the information that is present in the nonlinear distortion component. Therefore, the performance drops with the increase of distortion level as depicted in Figure 4.1. From the BER results, becomes clear that for very high values of s_M/σ the BER curve tends to be flat, assuming a fixed value even for high values of E_b/N_0.

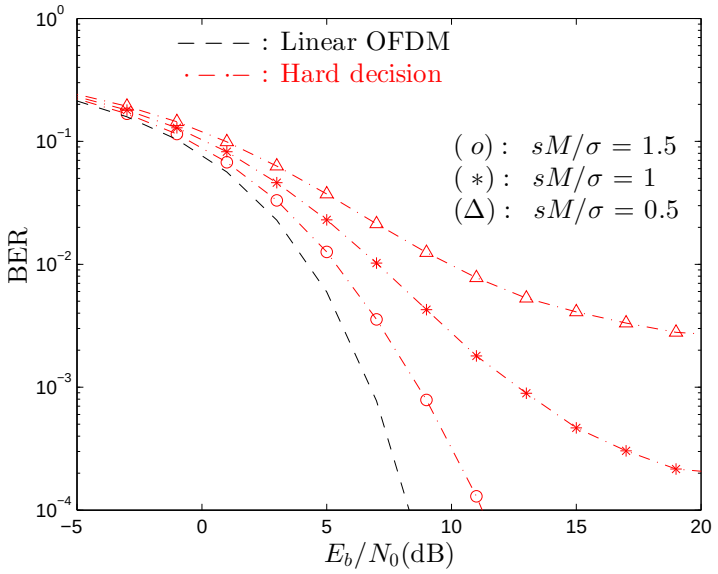

FIGURE 4.1: BER for nonlinear OFDM signal with $N = 64$ data subcarriers, considering typical receivers.

In this section, four sub optimum receivers are presented. Each sub-optimal receiver starts with the acquisition of the estimated signal associated to a conventional OFDM receiver (which will be denoted "*hard decision sequence*" in the remaining of this work). After that, each

receiver performs variations in the bits of this sequence, obtains the corresponding nonlinear signal to be transmitted (i.e., the modified *hard decision sequence* is submitted to the clipping operation and subsequent frequency-domain filtering that were employed in the transmitter), then computes the corresponding Euclidean distance relative to the received sequence and chooses the sequence among the original *hard decision sequence* and all variations of it that were tested that have smaller Euclidean distance to the received signal. If the *hard decision sequence* modification is denoted as $\mathbf{X^{mod}}$, the sub-optimal receiver will make its decision according to (3.26), i.e.,

$$\hat{\mathbf{X}} = \min_{\mathbf{X^{mod}}} \left(\left|\left| \mathbf{Z} - \mathbf{HGFf}(\mathbf{F^{-1}X^{mod}}) \right|\right|^2 \right). \tag{4.1}$$

Of course, due to the noise in the transmission path, the sequence $\mathbf{X^{mod}}$ that has the minimum Euclidean Distance relative to $\mathbf{Z}$, can still have errors when compared to the transmitted data sequence $\mathbf{X}$, that will vary according to the SNR. Let us now consider the sub-optimal methods that were developed.

Starting with the *hard decision sequence* the sub-optimal receiver I selects the L_b bits with smaller reliability (i.e., the bits where the corresponding signal is closer to the decision threshold) and performs all 2^{L_b} possible variations among those bits, saving the euclidean distance between each variation and the hard decision sequence. After this process, selects the variation of the *hard decision sequence* that has smaller Euclidean Distance relative to the received signal. The corresponding algorithm can be resumed as follows:

Sub-Optimal Receiver I

$\mathbf{Z} \leftarrow$ received signal {the nonlinearly signal given by (3.5)}

$\mathbf{Z_{bits}} \leftarrow$ get hard decision bits ($\mathbf{Z}$) {$1 \times \log_2(\mathcal{M})N$ row matrix with hard decision}

$\mathbf{J} \leftarrow$ get less reliable bits ($\mathbf{Z_{bits}}$) {$1 \times L_b$ row matrix with weaker bits indexes}

$\mathbf{T} \leftarrow \mathbf{0}_{\log_2(\mathcal{M})N \times 2^{L_b}}$ {$\log_2(\mathcal{M})N \times 2^{L_b}$ matrix with all tested sequences}

$\mathbf{D^2_{Array}} \leftarrow \mathbf{0}_{1 \times 2^{L_b}}$ {1×2^{L_b} matrix with Euclidean Distances}

$\mathbf{C} \leftarrow$ get binary combinations(L_b) {$L_b \times 2^{L_b}$ matrix with all 2^{L_b} bit combinations}

for $k = 1 \rightarrow 2^{L_b}$ **do**

  $\mathbf{Z^{mod}_{bits}} \leftarrow \mathbf{Z_{bits}}$

  for $i = 1 \rightarrow L_b$ **do**

    $[\mathbf{Z^{mod}_{bits}}]_{[\mathbf{J}]_i} \leftarrow [\mathbf{C}]_{k,i}$

  end for

  $[\mathbf{D^2_{Array}}]_k \leftarrow$ get euclidean distance ($\mathbf{Z^{mod}_{bits}}, \mathbf{Z_{bits}}$)

  $[\mathbf{T}]_{;k} \leftarrow \mathbf{Z^{mod}_{bits}}$

end for

$D^2 \leftarrow \min(\mathbf{D^2_{Array}})$ {index for the minimum euclidean distance}

$\hat{\mathbf{X}} \leftarrow [\mathbf{T}]_{;D^2}$ {sequence with the minimum euclidean distance}

Total of sequences analysed by the method : 2^{L_b}.

On the other hand, the sub-optimal receiver II switches each one of the $2N$ bits of the *hard decision sequence* to obtain $2N$ variations of it and then chooses the closer variation in terms of Euclidean distance relative to the received signal.

Sub-Optimal Receiver II

$\mathbf{Z} \leftarrow$ received signal {the nonlinearly signal given by (3.5)}

$\mathbf{Z_{bits}} \leftarrow$ get hard decision bits ($\mathbf{Z}$) {$1 \times \log_2(\mathcal{M})NN$ row matrix with hard decision}

$\mathbf{D^2_{Array}} \leftarrow \mathbf{0}_{1\times\log_2(\mathcal{M})N}$ {$1 \times \log_2(\mathcal{M})N$ matrix with Euclidean Distances}

for $k = 1 \rightarrow \log_2(\mathcal{M})N$ **do**

$\mathbf{Z^{mod}_{bits}} \leftarrow \mathbf{Z_{bits}}$

$[\mathbf{Z^{mod}_{bits}}]_k \leftarrow$ not $[\mathbf{Z_{bits}}]_k$

end for

$[\mathbf{D^2_{Array}}]_k \leftarrow$ get euclidean distance ($\mathbf{Z^{mod}_{bits}}, \mathbf{Z_{bits}}$)

$D^2 \leftarrow \min(\mathbf{D^2_{Array}})$ {index for the minimum euclidean distance}

$[\mathbf{Z_{bits}}]_{D^2} \leftarrow$ not $[\mathbf{Z_{bits}}]_{D^2}$

$\hat{\mathbf{X}} \leftarrow [\mathbf{Z_{bits}}]$ {sequence with the minimum euclidean distance}

Total of sequences analysed by the method : $\log_2(\mathcal{M})N$.

The sub-optimal receiver III starts with the *hard decision sequence* and switches the first bit. If the Euclidean distance relative to the received sequence improves the bit remains changed, if not we return to the original bit. After that, switch to the second bit and does the same. This procedure is repeated until the last bit is reached. At this time, the receiver has a sequence whose Euclidean distance relative to the received sequence is smaller (or at least equal) to the distance from the *hard decision sequence* to the received signal. In addition, since some of the bits might be changed with this procedure, the receiver can restart changing the first bit and repeat the procedure K times. Therefore, in a schematic way, the algorithm has the following steps:

Sub-Optimal Receiver III

$\mathbf{Z} \leftarrow$ received signal {the nonlinearly signal given by (3.5)}

$\mathbf{Z_{bits}} \leftarrow$ get hard decision bits ($\mathbf{Z}$) {$1 \times \log_2(\mathcal{M})NN$ row matrix with hard decision}

$D^2_{min} \leftarrow$ get euclidean distance ($\mathbf{Z_{bits}}$) {save the starting euclidean distance}

$\mathbf{Z^{actual}_{bits}} \leftarrow \mathbf{Z_{bits}}$ {save the starting sequence}

for $n = 1 \rightarrow K$ **do**

  for $i = 1 \rightarrow \log_2(\mathcal{M})N$ **do**

    $[\mathbf{Z^{actual}_{bits}}]_k \leftarrow$ not $[\mathbf{Z^{actual}_{bits}}]_k$

    $D^2 \leftarrow$ get euclidean distance ($\mathbf{Z^{actual}_{bits}}, \mathbf{Z_{bits}}$)

    if $D^2 \leq D^2_{min}$) **then**

      $D^2_{min} \leftarrow D^2$

    else

      $[\mathbf{Z^{actual}_{bits}}]_k \leftarrow$ not $[\mathbf{Z^{actual}_{bits}}]_k$

    end if

  end for

end for

$\hat{\mathbf{X}} \leftarrow \mathbf{Z^{actual}_{bits}}$ {sequence with the minimum euclidean distance}

Total of sequences analysed by the method : $\log_2(\mathcal{M})NK$.

The sub-optimal receiver IV is a variant of the sub-optimal receiver III where, instead of modifying all transmitted bits, only the P bits with smaller reliability are modified. This reduces the receiver complexity, since the number of bit modifications per iteration is reduced from $2N$ to P. As with sub optimal receiver III, this receiver can repeat the procedure K times, since the bit modifications are maintained if they lead to improved Euclidean distances. The steps for this algorithm are:

Sub-Optimal Receiver IV

$\mathbf{Z} \leftarrow$ received signal {the nonlinearly signal given by (3.5)}

$\mathbf{Z_{bits}} \leftarrow$ get hard decision bits ($\mathbf{Z}$) {$1 \times \log_2(\mathcal{M})NN$ row matrix with hard decision}

$\mathbf{J} \leftarrow$ get P less reliable bits ($\mathbf{Z_{bits}}$) {$1 \times P$ row matrix with weaker bits indexes}

$D^2_{min} \leftarrow$ get euclidean distance ($\mathbf{Z_{bits}}$) {save the starting euclidean distance}

$\mathbf{Z^{actual}_{bits}} \leftarrow \mathbf{Z_{bits}}$ {save the starting sequence}

for $n = 1 \rightarrow K$ **do**

  for $i = 1 \rightarrow P$ **do**

    $[\mathbf{Z^{actual}_{bits}}]_{[\mathbf{J}]_k} \leftarrow$ not $[\mathbf{Z^{actual}_{bits}}]_{[\mathbf{J}]_k}$

    $D^2 \leftarrow$ get euclidean distance ($\mathbf{Z^{actual}_{bits}}, \mathbf{Z_{bits}}$)

    if $D^2 \leq D^2_{min}$) **then**

      $D^2_{min} \leftarrow D^2$

    else

      $[\mathbf{Z^{actual}_{bits}}]_k \leftarrow$ not $[\mathbf{Z^{actual}_{bits}}]_k$

    end if

  end for

end for

$\hat{\mathbf{X}} \leftarrow \mathbf{Z^{actual}_{bits}}$ {sequence with the minimum euclidean distance}

Total of sequences analysed by the method : PK.

It should be pointed out that these receivers allow a severe reduction of the complexity when compared with the optimum receiver. In the Table 4.1 are presented the number of comparisons that each receiver does before take a decision, considering a QPSK constellation (i.e. $\mathcal{M} = 4$).

	Opt Receiver	**Sub-Opt I** $L_b = N/8$	**Sub-Opt II**	**Sub-Opt III** $K = 2$	**Sub-Opt IV** $K = 2,\ P = N/2$
Iterations	$2^{\log_2(\mathcal{M})N}$	2^{L_b}	$\log_2(\mathcal{M})N$	$\log_2(\mathcal{M})NK$	PK
$N = 16$	4,2950E+09	4	32	64	16
$N = 64$	3,4028E+38	256	128	256	64
$N = 128$	1,1579E+77	65536	256	512	128
$N = 256$	1,3408E+154	4,2950e+09	512	1024	256

TABLE 4.1: Complexity comparison

From the values shown in Table 4.1, it becomes obvious that the complexity of the optimum receiver is prohibitively high, even considering a small number of subcarriers, which compromises its practical implementation. Let us now focus on the proposed sub-optimal receivers. For example, considering an OFDM signal with $N = 64$ in-band subcarriers and the sub-optimal method II, it is possible to analyse only 256 of 3,4028E+38 distances, i.e., only 7,5232E-35% of the distances when comparing with the full ML behaviour, which represents a substantial reduction in the computational load. Moreover, contrary to the optimum receiver, it is clear that the computational complexities associated to the sub-optimal methods II, III and IV, do not grow exponentially with the number of the in-band subcarriers. Instead of this, they present a linear behaviour, having a slope that depends on $\mathcal{M}$, K and P.

4.2 Approximate Optimum Performance

To evaluate the developed sub-optimal receivers, it would be desirable to compare their performance with the real performance of an optimum receiver. Unfortunately, as seen in the last section, such receiver has large computational requirements which make its simulation inviable, unless the number of subcarriers is very low. In addition, although the BER computation method defined in (3.65) is suitable for obtaining the asymptotic BER performance, it looses accuracy in the working regions of common wireless communication systems where moderate BER values predominate. However, it is possible to obtain an approximation of the optimum performance by assuming that the optimum estimate is likely to be one of the following sequences:

- The *hard decision sequence* or one of its variations (that could be obtained as described in the previous section).
- The transmitted sequence or one of its variations. Note that these variations can also be calculated using a procedure similar to the one described in Section 4.1, but instead of considering the starting sequence as the *hard decision sequence*, it should be considered the transmitted sequence (that under the simulation environment is known at the receiver side).

In that sense, the optimum estimate is defined as the sequence that has the minimum euclidean distance relative to the received signal, among the sequences presented in these two previous items. In Figure 4.2 it is shown the approximate optimum performance when is adopted the sub-optimal receiver III to make the variations of the two starting sequences. It was also considered an OFDM signal with $N = 64$ subcarriers, a normalized clipping level of $s_M/\sigma = 1.0$ and an ideal AWGN channel. From the results, we note that the approximate optimum performance is better than the one obtained by the conventional and linear OFDM schemes even for only $K = 1$ iterations. As expected this performance presents a very high improvement when compared to the hard-decision that does not take into account the nonlinear distortion effects for detection purposes. Moreover, it is expected that this performance is a bound for the performance of the proposed sub-optimal receivers.

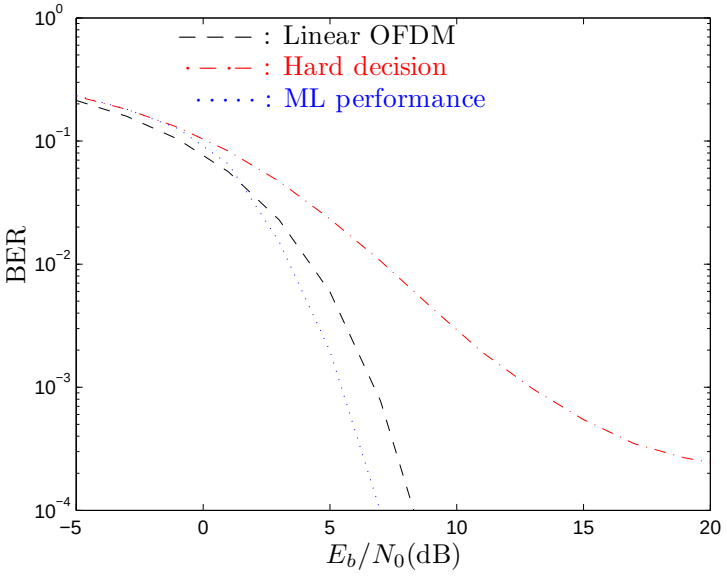

FIGURE 4.2: BER for the approximate ML receiver considering $N = 64$ subcarriers, a normalized clipping level of $s_M/\sigma = 1.0$ and an ideal AWGN channel

The approximate optimum performance under the same conditions but considering a transmission over a XTAP channel is presented in Figure 4.3. Again, we have substantial improvements relative to the linear case and the hard detection, with gains even higher than in the case where an ideal AWGN is considered. The cause for that relies in the diversity associated to the nonlinear distortion component.

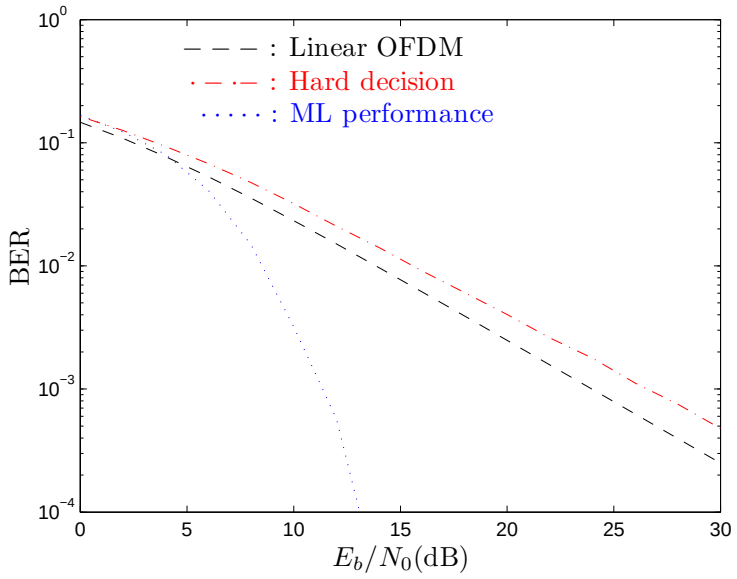

FIGURE 4.3: BER for the approximate ML receiver considering $N = 64$ subcarriers, a normalized clipping level of $sM/\sigma = 1.0$ and an frequency- selective channel

4.3 Performance results

In this section, several BER performance results for the sub-optimal receivers described in Section 4.1 are presented and discussed. In the subsection 4.3.2, the impact of iterative clipping and filtering procedures in the BER performance of these receivers is shown. The impact of using diversity schemes is analysed in subsection 4.3.3. Lastly, in subsection 4.3.4, it is studied the performance of the proposed receivers considering high order constellations.

4.3.1 Sub-optimal receivers performance

To quantify the improvements of the proposed sub-optimal receivers, we consider OFDM signal that, unless otherwise stated, have $N = 64$ useful subcarriers with QPSK constellations (i.e., $\mathcal{M} = 4$) and an oversampling factor $M = 4$. The QPSK symbols are selected from the data signal using a Gray mapping rule. The nonlinear device corresponds to an ideal envelope clipping with a normalized clipping level s_M/σ (unless otherwise stated, we assume $s_M/\sigma = 1.0$). We consider both an ideal AWGN channel and a frequency-selective channel that has 32 symbol-spaced multipath components with uncorrelated Rayleigh fading. In both cases, it is assumed perfect synchronization and channel estimation at the receiver. For the sake of

comparisons, some figures include the approximate optimum performance (being denoted as "ML performance"), which was obtained as described in the previous section. In addition, all the figures contain the BER for linear OFDM schemes that, considering QPSK constellations, can be approximated by (3.68). The BER for linear OFDM schemes considering a Rayleigh fading channel is given by (see [38], Equation(14-3-7)),

$$P_b \approx \frac{1}{2}\left(1 - \sqrt{\frac{E_b/N_0}{1 + E_b/N_0}}\right). \tag{4.2}$$

Let us start by considering an ideal AWGN channel. Figure 4.4 shows the BER for sub-optimal receiver I with different values of L_b. From this figure, it is clear that the performance relative to conventional OFDM schemes can be improved substantially, especially for larger values of L_b (i.e., when a larger number of weaker bits are selected to be changed). For example, when $L_b = 2$, this method achieves a BER of 10^{-3} with an E_b/N_0 of 9.2 dB, which means that there is a gain of 3.2 dB when comparing with the hard decision (that needs an E_b/N_0 of 12.5 dB for the same BER value). For a higher value of L_b, let us say $L_b = 8$, we can expect a gain around 5.3 dB. However, it is important to note that for small values of L_b that lead to practical implementations, the performance of this receiver is always worse than the performance with a linear transmitter. Therefore, although this sub-optimal receiver has significant gains with a relative small value of L_b, its performance degrades substantially for a larger number of subcarriers N, i.e., it is conditioned by the relation $L_b/2N$.

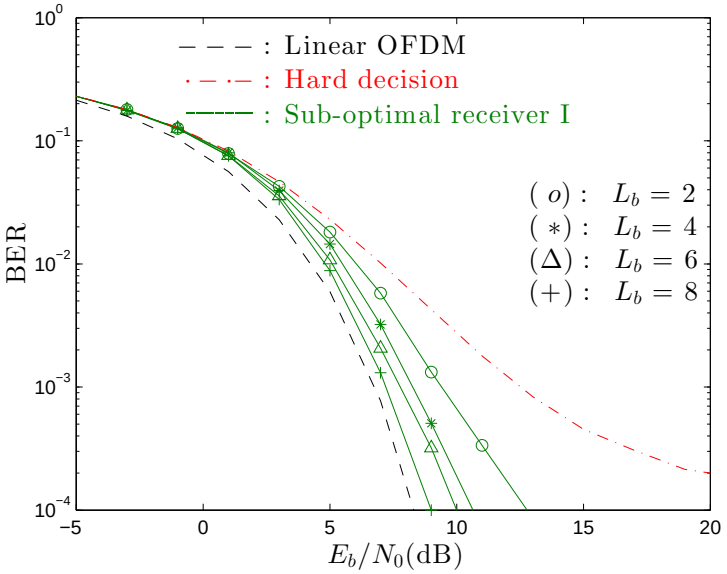

FIGURE 4.4: BER of Sub-optimal receiver I for an OFDM signal with $N = 64$ data subcarriers, considering different values of L_b and an ideal AWGN channel.

To illustrate this dependence, let us look at Figure 4.5 where the OFDM have $N = 256$ subcarriers and the same values of L_b were considered. From the figure, when considering $L_b = 8$, we note that this method needs 9.2 dB to achieve a BER value of 10^{-3} (more 2 dB than with $N = 64$). Consequently, when the number of subcarriers is very high the only way to maintain the performance is increasing the value of L_b.

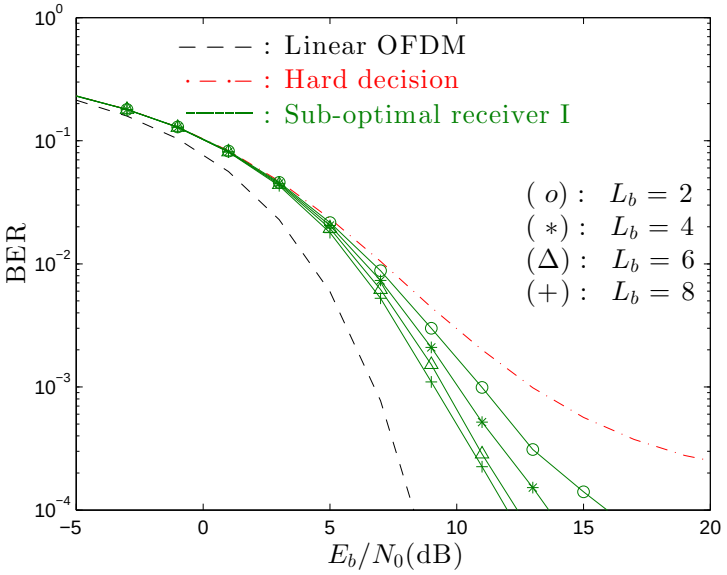

FIGURE 4.5: BER of Sub-optimal receiver I for an OFDM signal with $N = 256$ data subcarriers, considering different values of L_b and an ideal AWGN channel.

Let us now change the simulation environment and consider a more realistic OFDM scenario where the channel presents frequency selective fading. The considered channel has 32 symbol-spaced rays. Figure 4.6 presents the BER of the sub-optimal receiver I for different values of L_b and a normalized clipping level $s_M/\sigma = 1$. As expected, the gains of this sub-optimal receiver are higher than the ones in an ideal AWGN channel. This is a consequence of the fact that the sub-optimal receivers take advantage of the implicit diversity effects inherent to the nonlinear distortion. Namely, for every value of L_b that was considered in the simulation, the performance of this sub-optimal receiver is always better than the performance of the conventional OFDM schemes (which does not happen even for $L_b = 8$ in the AWGN case). For instance, even when only two bits are modified in the OFDM block and, consequently, only $2/64$ $(3,13\%)$ of the total number of bits are changed, the performance is still better when compared with the linear OFDM. Therefore, lower values of L_b (i.e., lower value of the relation $L_b/2N$) can be used, which means low complexity, despite of maintaining excellent performances.

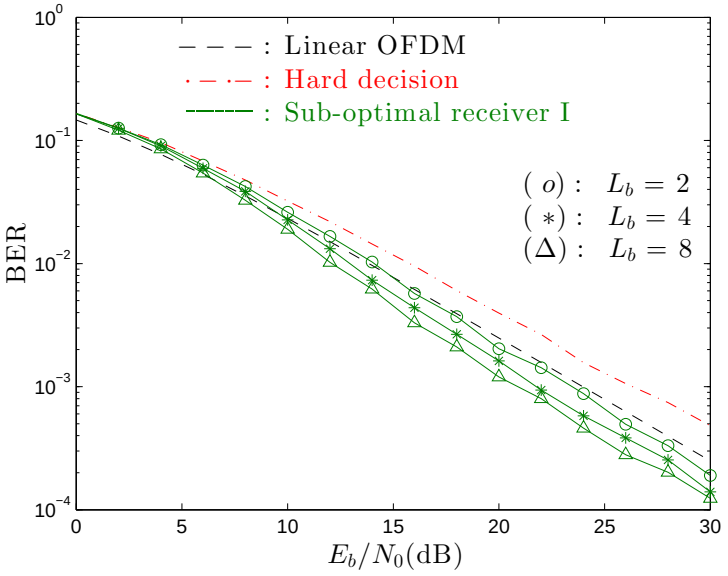

FIGURE 4.6: BER of Sub-optimal receiver I for an OFDM signal with $N = 64$ data subcarriers, considering different values of L_b and an frequency selective channel.

Let us consider now the sub-optimal receiver II. In Figure 4.7, it is shown the BER for this receiver considering an ideal AWGN channel. From the results, it is clear that this method has improvements when compared to the hard-decision performance. However, the gains are lower relatively to those obtained by the sub-optimal receiver I (when higher values of L_b are

considered.). The main reason of these lower gains is that this method does not has an high capacity of modifying the *hard decision sequence*, since it only can modify one bit in the entire data block. Thus, if the optimum estimate differs from the *hard decision sequence* in a higher number of bits, it can not be found by this receiver. However, the complexity is reduced by half relative to I (considering $L_b = 8$ as in Table 4.1). Another important property is that since this method modifies all the bits in the OFDM signal, its complexity is only related with the number of in-band subcarriers and the number of points in the adopted constellation, thus, there are not any parameters to be adjusted as in the other proposed sub-optimal receivers.

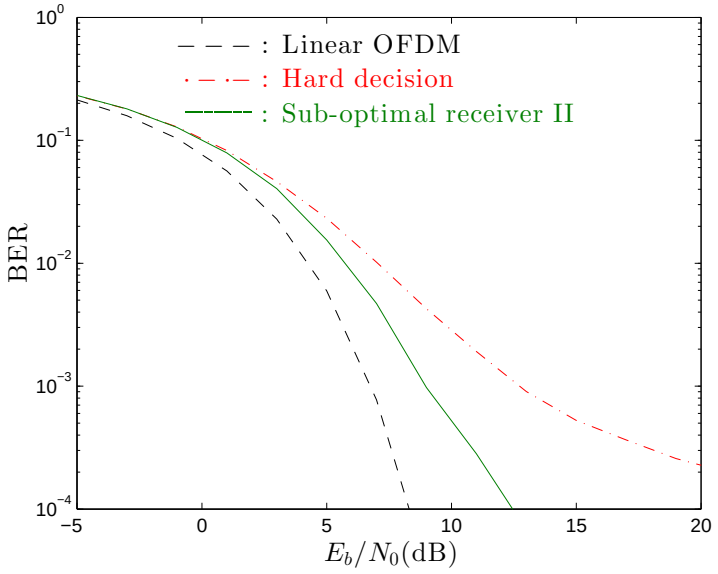

FIGURE 4.7: BER of Sub-optimal receiver II for an OFDM signal with $N = 64$ data subcarriers, considering an ideal AWGN channel

Let us now consider the performance of the sub-optimal receiver II when the transmission is made in a frequency-selective channel. Figure 4.8, refers the BER under these conditions. Again, the gains are higher when the channel has selectivity in frequency. The performance of this method is considerably better than conventional linear OFDM schemes. For example, to achieve a BER of 10^{-3} it needs an E_b/N_0 around 20 dB which means a power gain of 7 dB relative to the linear case and 4 dB relative to hard-decision.

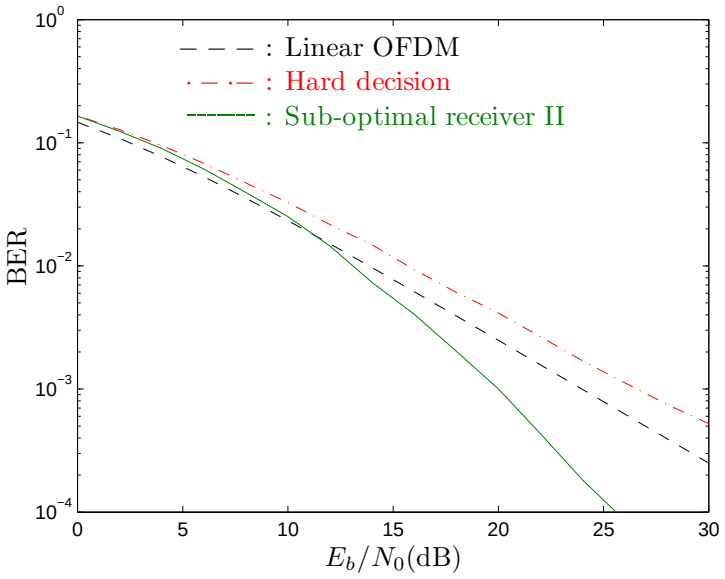

FIGURE 4.8: BER of Sub-optimal receiver II for an OFDM signal with $N = 64$ data subcarriers, considering a frequency-selective channel

Let us focus now on the sub-optimal receiver III. This receiver has one parameter that can be adjusted: the number of times K that main cycle of bit modifications is repeated. In Figure 4.9, it is shown the BER when the parameter K assumes different values. For the sake of comparisons, the approximate optimum performance was also included. This method also allows remarkable gains when comparing to linear OFDM. From the figure, we note that for $K = 2$ cycles the achievable performance is better than for $K = 1$, with gains around 1 dB and close to the approximate optimum performance. However, larger values of K (i.e. $K \geq 2$) should not be considered, since the complexity increases and only marginal gains can be achieved.

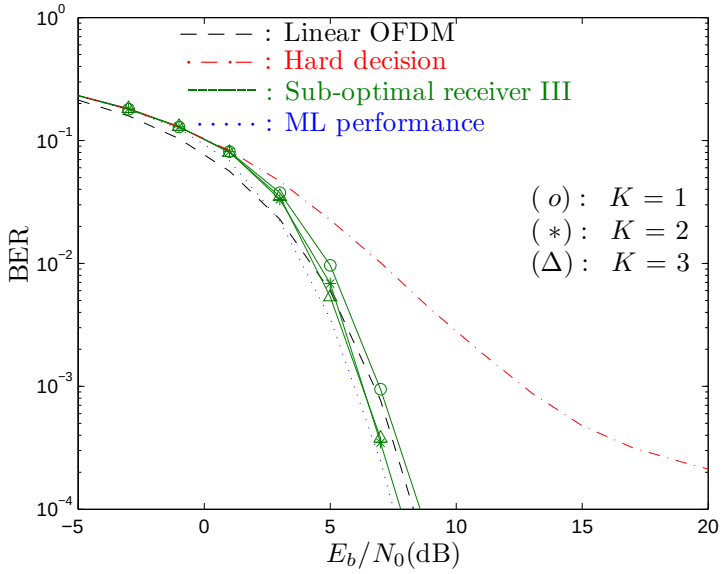

FIGURE 4.9: BER of Sub-optimal receiver III for an OFDM signal with $N = 64$ data subcarriers, with different values of K and considering an ideal AWGN channel

Let us now see what happens when the channel presents frequency selective fading. For the mentioned reasons, the receiver works with $K = 2$. In Figure 4.10 it is shown the BER under these conditions.

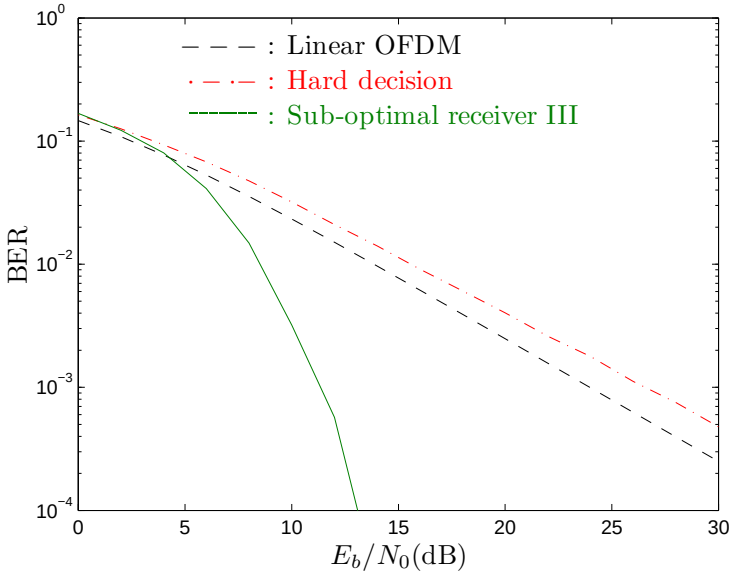

FIGURE 4.10: BER of Sub-optimal receiver III for an OFDM signal with $N = 64$ data subcarriers, considering $K = 2$ and a frequency selective channel

Despite being the most complex sub-optimal method, is the best in terms of performance.

From the analysis of previous figure, it is clear that this receiver provides substantial gains. These very high gains are supported by its behaviour but also due to the diversity that is inherent to the nonlinear distortion effect which can be utilized in fading channels. To achieve a BER of 10^{-3} this receiver needs an E_b/N_0 equal to 11.3 dB, i.e., less than a half of the required on conventional OFDM schemes.

Let us now take into account the sub-optimal receiver IV. As seen before, the complexity using this receiver can be reduced when comparing to the sub-optimal receiver III since only $P \leq 2N$ weaker bits are modified. In Figure 4.11 it is shown the BER considering different values of P. As we can see the higher the P better will be the performance. Since the complexity is reduced by a factor of 4, a value of $N/2$ practically yields the same performance of the one achieved with the sub-optimal receiver III (i.e., when $P = N/2$).

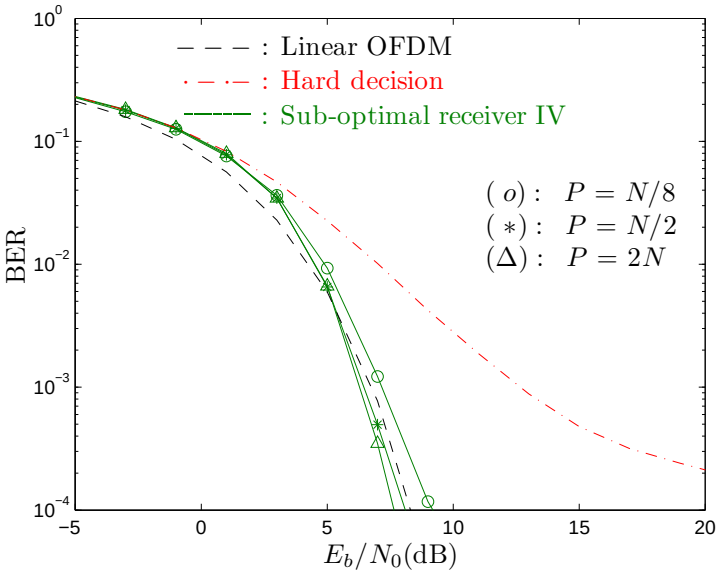

FIGURE 4.11: BER of Sub-optimal receiver IV for an OFDM signal with $N = 64$ data subcarriers, with different values of P and considering an ideal AWGN channel

Let us now consider the BER for these values of P but, considering a frequency selective channel as the one represented in the Figure 4.12. Again, the larger the P the better the performance. However, it is important to note that in the case of a frequency selective channel, the receiver must perform the $P = 2N$ modifications since, contrarily to the ideal AWGN case, there is a significant difference relative to $P = N/2$. It is also important to point out that when $P = 2N$ the performance is very close to the approximate ML performance obtained as was explained

in Section 4.2. This is a remarkable result since, even with an accentuated reduction on the complexity, is still possible a performance that is close to the one of the optimum receiver.

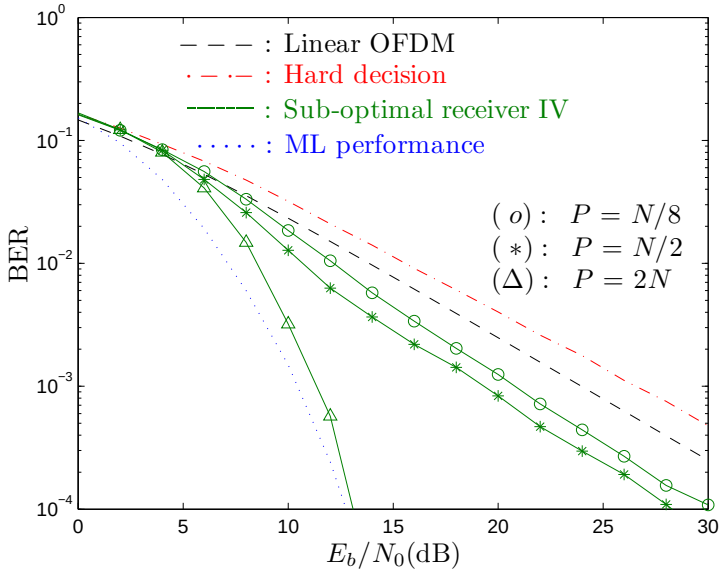

FIGURE 4.12: BER of Sub-optimal receiver IV for an OFDM signal with $N = 64$ data subcarriers, with different values of P and considering a frequency selective channel

In Figure 4.13 and Figure 4.14 the performance of all suboptimum receivers were included for the sake of comparisons.

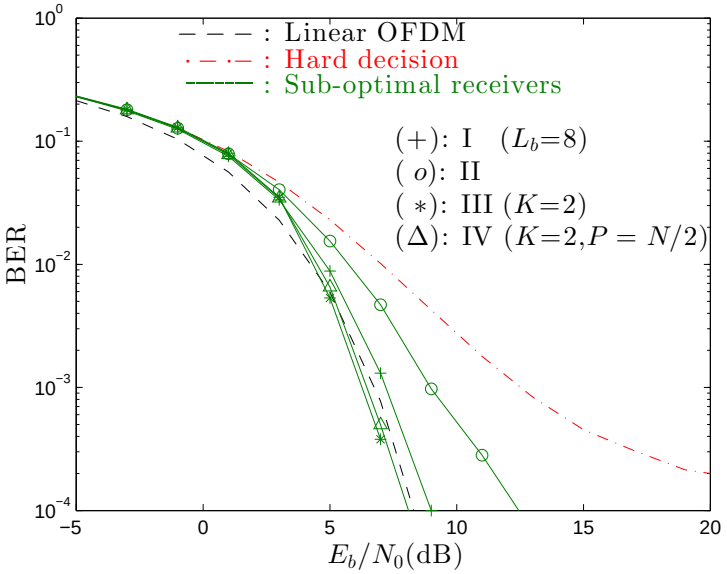

FIGURE 4.13: BER of all Suboptimal receivers for an OFDM signal with $N = 64$ data subcarriers considering an ideal AWGN channel

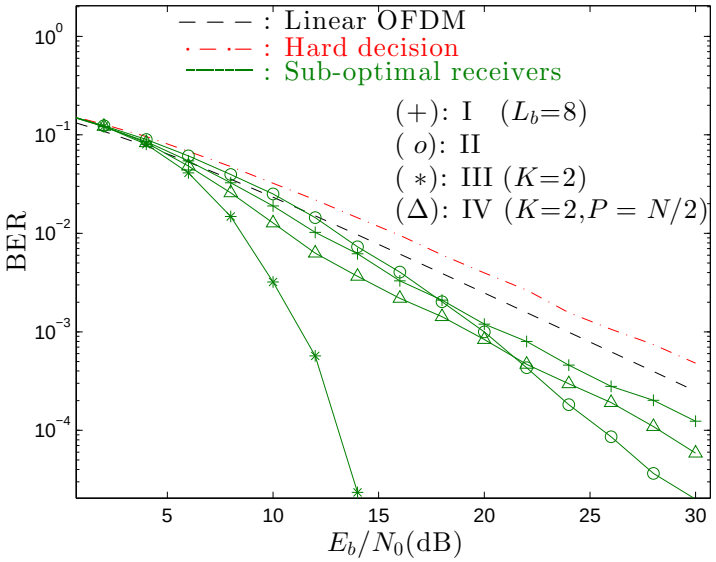

FIGURE 4.14: BER of all Suboptimal receivers for an OFDM signal with $N = 64$ data subcarriers considering a frequency selective channel

4.3.2 Impact of iterative clipping and filtering

As seen in Section 3.1 the use of the iterative clipping and filtering procedures can reduce significantly the envelope fluctuations of the OFDM signals while maintain the bandwidth of the conventional schemes. It must be recalled that a second clipping procedure is realised to suppress the regrowth in the envelope fluctuations due to the filtering procedure and so forth. It is also important to remark that clipping and filtering operations are done in different domains. While the clipping is realised in time-domain, the filtering is realised in frequency-domain to eliminate the out-of-band radiation.

Another interesting analysis done in this subsection concerns how these techniques affect the BER performance Fof the proposed sub-optimal receivers. Since the best receiver in terms of performance is the sub-optimal receiver III, it is the chosen for these simulations. In Figure 4.15 it is shown the BER considering L number of clipping and filtering iterations and a frequency selective channel. From the figure and taking into account the hard decision, it is clear that the larger the value of L, the higher the nonlinear distortion effects and, consequently, the lower the performance. If we focus on the performance of the sub-optimal receiver, we have the same behaviour. The larger the L, the lower the performance. However, this is not expected since, higher nonlinear distortion effects should provide bigger gains due to the increased minimum

euclidean distances over the average bit energy. The reason for this is mainly in the sub-optimal receiver nature, i.e., it does not test all the possible data sequences but only the most likely candidates. As expected, if we consider the approximate optimum performance (that is closer to the optimum receiver behaviour), the performance increases with the enhancement of nonlinear effects.

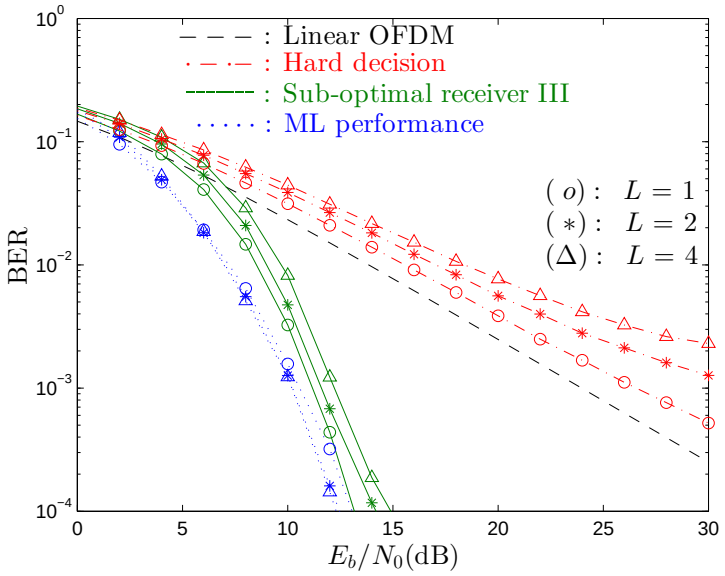

FIGURE 4.15: BER of Sub-optimal receiver III for an OFDM signal with $N = 64$ data subcarriers, with different values of L and considering a frequency selective channel

In Figure 4.16 it is shown the impact in the suboptimal receiver III considering a ideal AWGN. From the depicted results, it is clear the worse performance for higher values of P the worse the performance as in the frequency selective channel. Again, the cause for this relies on the semi-optimum behaviour of the receiver that does not test all the possible transmitted sequences. Consequently, higher nonlinear distortion effects do not mean better performances.

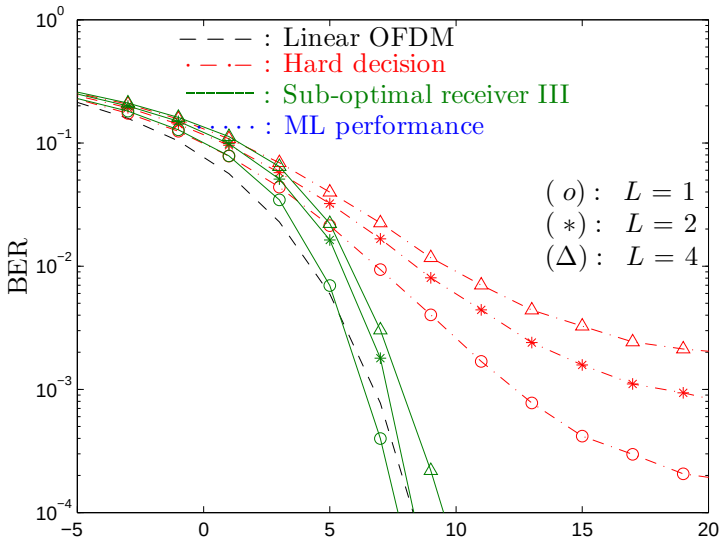

FIGURE 4.16: BER of Sub-optimal receiver III for an OFDM signal with $N = 64$ data subcarriers, with different values of L and considering a ideal AWGN channel

4.3.3 Impact of diversity

It is well known that diversity schemes can be used to increase the capacity of the wireless communication systems both in terms of the radio link quality and data rates. The main reason behind these improvements is that the errors typically occur when the channel is in a deep fade. Therefore, if the receiver is supplied by several replicas of the data signal transmitted over independent fading channels, the probability of occurring a deep fade simultaneously in all replicas becomes substantially reduced. In this subsection is considered a single input multiple output (SIMO) scheme of N_{R_x} order (i.e., N_{Rx} represents the number of receiver antennas) and it is evaluated the respective impact in performance. Note that, with diversity, the BER for the linear OFDM considering an ideal AWGN can be approximated by

$$P_b \approx Q\left(\sqrt{\frac{2N_{Rx}E_b}{N_0}}\right), \tag{4.3}$$

where it is clear that the asymptotic behaviour is conditioned by the number of antennas. Therefore, it can be expected a performance improvement for larger values of N_{R_x}. This behaviour is confirmed with the results of Figure 4.17, where is represented the BER for the

sub-optimal receiver II considering different values for N_{Rx} and a subsequent frequency-domain filtering operation.

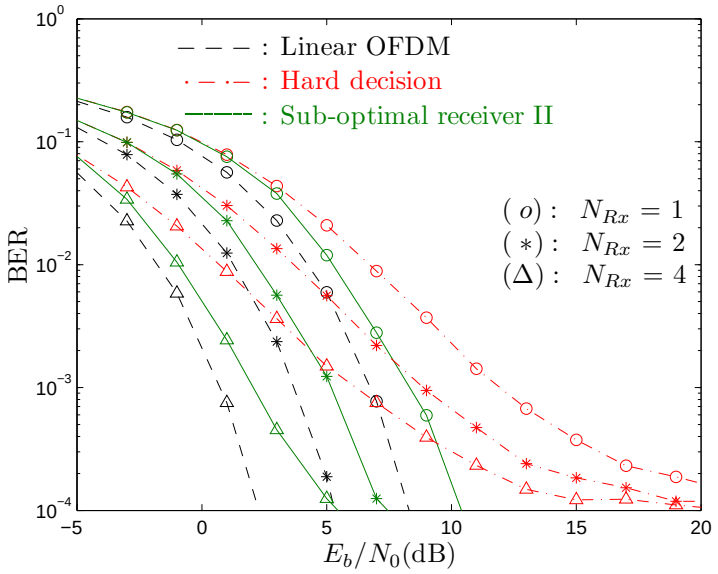

FIGURE 4.17: BER of Sub-optimal receiver II for an filtered OFDM signal with $N = 64$ data subcarriers, with different values of N_{Rx} and considering an ideal AWGN channel

Clearly, for larger values of N_{Rx} the performance of the sub-optimal receiver II is better. However, since there are gains in all performances, the relative gains (i.e., the proposed receiver versus the linear OFDM) are approximately constant for all considered values of N_{Rx}.

When a frequency-selective channel is considered the BER for linear OFDM is approximated by (see [38], Equation(14-4-15))

$$P_b \approx \left(\frac{1}{2}\left(1-\sqrt{\frac{E_b/N_0}{1+E_b/N_0}}\right)\right)^{N_{Rx}} \left[\sum_{l=0}^{N_{Rx}-1}\binom{N_{Rx}-1+l}{l}\left(\frac{1}{2}\left(1+\sqrt{\frac{E_b/N_0}{1+E_b/N_0}}\right)\right)^{l}\right]. \tag{4.4}$$

In Figure 4.18 is represented the BER for the sub-optimal receiver IV considering different values of P, two antennas at the receiver (i.e., $N_{Rx} = 2$) and a frequency-selective channel. As we can see, this diversity scheme provide substantial improvements in the performance. For instance, considering $P = 2N$, this sub-optimal receiver only needs $E_b/N_0 = 8.4$ dB to achieve BER of 10^{-4}. However, when the hard decision is considered, it should be pointed out that this BER value is unachievable even with very high values of E_b/N_0, since the BER has

a lower limit smaller than 10^{-4}. From the comparison with the conventional linear OFDM schemes, this receiver achieves a gain near 7.8 dB.

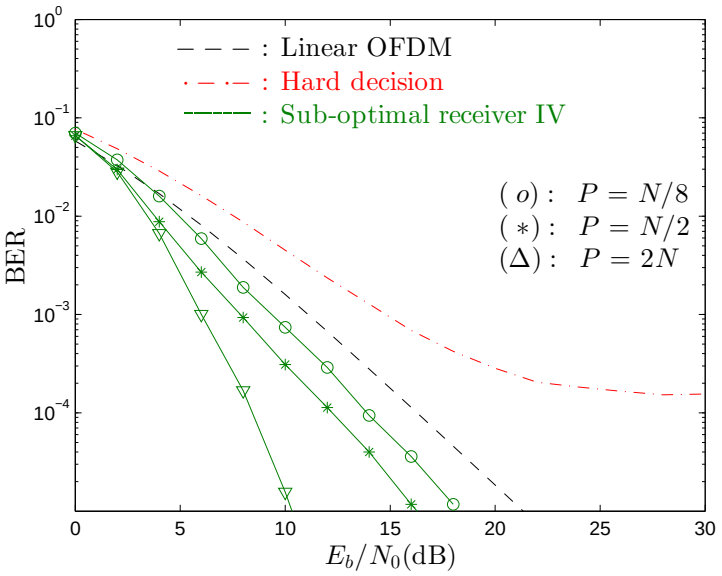

FIGURE 4.18: BER of Sub-optimal receiver IV for an OFDM signal with $N = 64$ data subcarriers, with $N_{Rx} = 2$ and considering a frequency selective channel.

We shall now consider the Figure 4.19 where is shown the BER for the sub-optimal receiver IV considering a SIMO scheme of fourth order and different values of P. As expected, when the number of receiver antennas N_{Rx} increase, the performance also increase. For achieving a BER of 10^{-4} only an E_b/N_0 around 3.5 dB is required, which is a very low value. Althoug, from the same figure can be seen that the BER does not have a threshold value due to the nonlinear distortion.

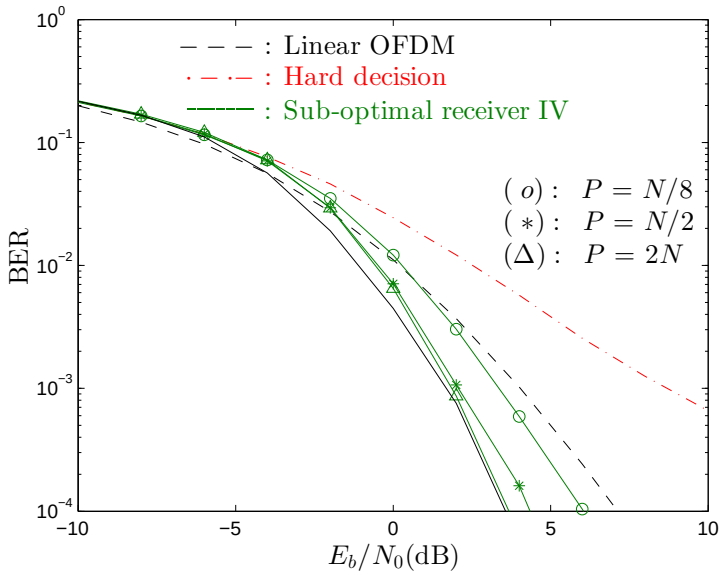

FIGURE 4.19: BER of Sub-optimal receiver IV for an OFDM signal with $N = 64$ data subcarriers, with $N_{R_x} = 4$ and considering a frequency selective channel.

4.3.4 Impact of higher constellations

Here in it is analysed the impact of higher constellations (i.e., $\mathcal{M} > 2$) in the BER performance of the proposed sub-optimal receivers. More concretely, it is adopted an 16-QAM constellation. In this case, $\mathcal{M} = 4$, leading to the existence $4N$ bits per transmitted data block. Note that with bigger constellations the adopted clipping level must be higher since, the amplitude of the complex data symbols is also higher. In addition, the performance of conventional linear OFDM is worse since more bits are transmitted for the same power levels.

In Figure 4.20 is depicted the BER for the sub-optimal receiver IV considering different values of P and $s_M/\sigma = 1.6$ in an frequency selective channel. It is obvious that the gains obtained with QPSK constellations can also be obtained with bigger constellations. However, contrary to the QPSK case, only considering values of $P > 2N$, i.e., when at least half of the bits in the block are modified, make the performance of this sub-optimal receiver better than the hard decision.

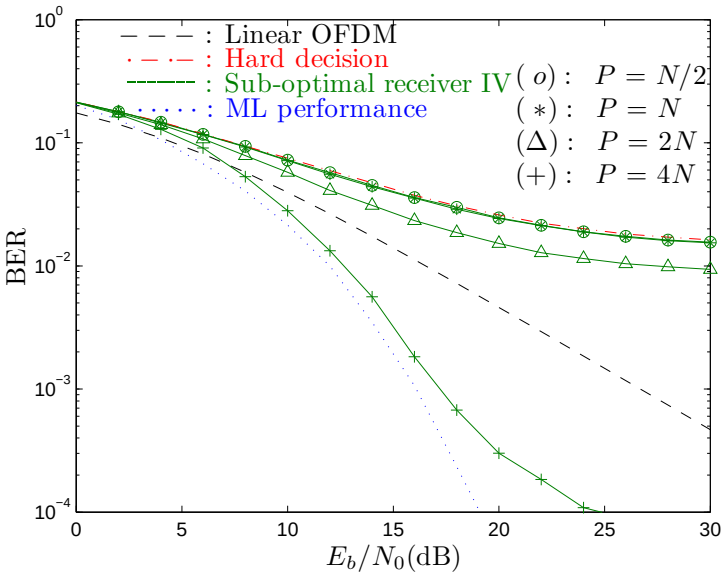

FIGURE 4.20: BER of Sub-optimal receiver IV for an OFDM signal with $N = 64$ data subcarriers, considering a 16-QAM constellation and a frequency selective channel.

Note also that the complexity reduction is also assured since the performance is almost the same for $P = N/2$ or $P = N$. When $P = 4N$, which means that all the bits are modified, the performance is better than in the linear OFDM case and, in addition, the performance is very close to the one obtained by the approximated optimum receiver. Let us now see what happens when an ideal AWGN channel is considered. Note that the BER for the linear OFDM case in an ideal AWGN is, considering (3.65), approximated by

$$P_b \approx \frac{3}{4} Q\left(\sqrt{\frac{4E_b}{5N_0}}\right). \tag{4.5}$$

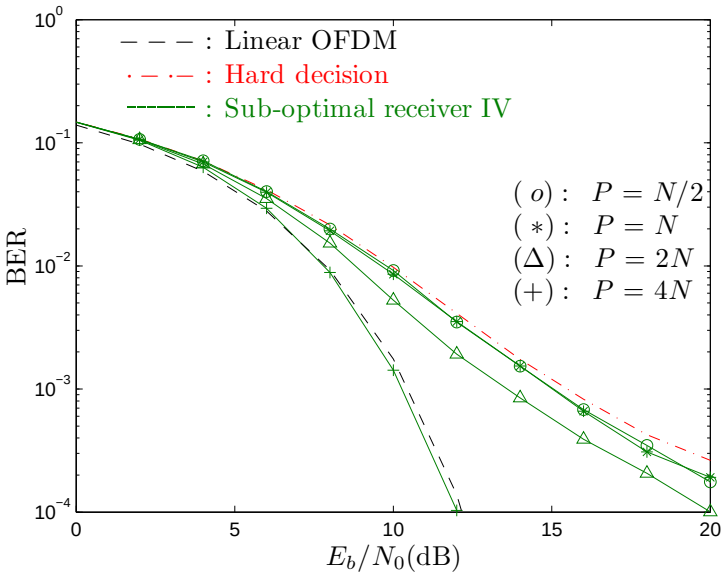

FIGURE 4.21: BER of Sub-optimal receiver IV for an OFDM signal with $N = 64$ data subcarriers, considering a 16-QAM constellation and an ideal AWGN channel

Although the gains are lower when comparing to the ones obtained with QPSK they continue to be substantial. As in the fading channel, the performance of the sub-optimal receiver is only better than the linear OFDM for $P = 4N$ (which, in fact, corresponds to the behaviour of the sub-optimal receiver III).

Chapter 5

Conclusions and future work

5.1 Conclusions

This work was intended to demonstrate the achievable performance of maximum likelihood detection for OFDM signals with strong nonlinear effects that are traditionally regarded as undesirable distortion.

In Chapter 2 is presented a brief introduction to OFDM signals, being identified that the reasons besides the adoption of this multicarrier scheme in several broadband communication systems are the high spectral efficiency, which is very important since the frequency spectrum is expensive and limited, and the facility to deal with frequency-selective channels through the use of simple frequency-domain equalizers. It has been also verified that due to its multicarrier nature, the OFDM signals present high sensitivity to nonlinear distortion effects. The most promising technique to reduce the envelope fluctuations is based on a clipping in the time-domain followed by a filtering operation in the frequency-domain. This operation causes the transmitted signals to have nonlinear distortion effects. To study this effects, it was shown that the OFDM complex envelope can be modelled by a Gaussian random process, which allow the theoretical characterization of the nonlinearly distorted signals. In this analysis it was presented the expression for the PSD of the nonlinearly signal and as expected, it was verified that nonlinear effect brings a spectral broadening due to the existence of intermodulation products.

In Chapter 3 it was studied the main reason behind the performances of ML detection for OFDM signals with nonlinear effects and it was shown that contrary to what one could expect, the performance of nonlinear OFDM can be better than the linear case. It is shown that when in the presence of this distortion, the Euclidean Distance between two signals have energy in the entire transmission bandwidth which, together with reduction in the average bit energy, i.e., higher D^2/E_b, can explain the asymptotic gain of this scenario. In the third chapter it is also verified that the optimum performance is obtained with an ML receiver, being analysed the basis of its behaviour. Since the achievable performance of nonlinear OFDM is conditioned by the ratio D^2/E_b, an closed-expression for the minimum Euclidean distance between two nonlinear distorted signals was presented. This expression allows a quantification of the gains with an accuracy that are dependent on the number of the in-band subcarriers which can be explained due to the approximations that were made based on the assumption of $N \gg 1$.

Although the ML detection brings the optimal performance its complexity is too high. In the Chapter 4 were presented four sub-optimal methods that have substantially low complexity when compared to the full ML receiver. Despite of that, they present excellent performances which can be explained mainly since the optimal sequence differs in a small amount of bits when compared to the hard-decision sequence. Still in this chapter, the BER performance of the sub-optimum receivers were presented and compared to an approximate optimum performance. It was seen that the achievable gains can reach values around 5 dB but are higher when frequency-selective channels are considered, which can be explained due to the inherent diversity effects of the nonlinearly distorted signals. It was verified that when are employed iterative clipping and filtering operations the achievable performances can be even better since there are higher nonlinear distortion effects. It was also shown that use of diversity schemes also improves the performance of the proposed sub-optimal receivers. The impact of use bigger constellations, namely a 16-QAM constellation, is studied and it is shown that substantial gains are also achieved.

5.2 Future work

In this thesis it was studied the performance of OFDM signals that are passed trough a clipping operation. However, other type of nonlinearities can be studied in future research activities.

The theoretical expression that evaluates the minimum Euclidean Distance between to non-linearly signals was developed under some approximations. An extensive theoretical analysis can be made to achieve more accuracy. In addition, considering a more realistic scenario, a subsequent filtering operation can be used to remove the out-of-band radiation. A theoretical expression that takes into account this filtering operation can be developed as well as one that covers the iterative clipping and filtering case, which will allow a theoretical quantification of the filtered nonlinear OFDM signal.

The sub-optimal methods presented here approach the optimum performance. However they still are complex to be applied in a realistic scenario. For this reason, less complex methods can be developed and evaluated in future works.

Bibliography

[1] L. Cimini Jr., "Analysis and Simulation of a Digital Mobile Channel Using Orthogonal Frequency Division Multiplexing", *IEEE Trans. on Comm.*, Vol. 33, No. 7, pp. 665–675, Jul. 1985.

[2] R. Nee and R. Prasad, "OFDM for Wireless Multimedia Communications", Artech House, 2000.

[3] A. Jones and T. Wilkinson, "Combined Coding for Error Control and Increased Robustness to System Nonlinearities in OFDM", *IEEE VTC'96*, Atlanta, May 1996.

[4] S. Müller, R. Bräuml, R. Fischer and J. Huber, "OFDM with Reduced Peak-to-Average Power Ratio by Multiple Signal Representation", *Annales of Telecommunications*, Vol. 52, Feb. 1997.

[5] S. Müller and J. Huber, "A Comparison of Peak Reduction Schemes for OFDM", *IEEE GLOBECOM'97*, Phoenix, USA, May 1997.

[6] R. O'Neill and L. Lopes, "Envelope Variations and Spectral Splatter in Clipped Multicarrier Signals", *IEEE PIMRC'95*, Sep. 1995.

[7] X. Li and L.J. Cimini, Jr., "Effects of Clipping and Filtering on the Performance of OFDM", *IEEE Comm. Let.*, May 1998.

[8] R. Dinis and A. Gusmão, "A Class of Signal Processing Algorithms for Good Power/Bandwidth Tradeoffs with OFDM Transmission", *IEEE ISIT'2000*, Sorrento, Italy, June 2000

[9] H. Ochiai and H. Imai, "Performance of Deliberate Clipping with Adaptive Symbol Selection for Strictly Band-Limited OFDM Systems", *IEEE JSAC*, Vol. 18, No. 11, Nov. 2000.

[10] H. Ochiai and H. Imai, "Performance Analysis of Deliberately Clipped OFDM Signals", *IEEE Trans. on Comm.*Vol. 50, No. 1, Jan. 2002.

[11] R. Dinis and A. Gusmão, "A Class of Nonlinear Signal Processing Schemes for Bandwidth-Efficient OFDM Transmission with Low Envelope Fluctuation", *IEEE Trans. on Comm.*, Vol. 52, No. 11, pp. 2009–2018, Nov. 2004.

[12] R. Dinis and A. Gusmão, "Performance Evaluation of OFDM Transmission with Conventional and Two-Branch Combining Power Amplification Schemes", *IEEE GLOBECOM'96*, London, Vol. 1, pp. 734–739, Nov. 1996.

[13] R. Dinis and A. Gusmão, "Signal Processing Schemes for Power/Bandwidth Efficient OFDM Transmission with Conventional or LINC Transmitter Structures", *IEEE ICC'2001*, Helsinki, Vol. 4, pp. 1021–1027, June 2001.

[14] R. Dinis and A. Gusmão, "Nonlinear Signal Processing Schemes for OFDM Modulations within Conventional or LINC Transmitter Structures", *European Trans. on Telecomm.*, 2008.

[15] R. Dinis and P. Silva, "Analytical Evaluation of Nonlinear Effects in MC-CDMA Signals", *IEEE Trans. on Wireless Comm.*, Ago. 2006.

[16] T. Araújo and R. Dinis, "Performance Evaluation of Quantization Effects on Multicarrier Modulated Signals", *IEEE Trans. on Vehicular Technology*, Vol. 56, No. 5, parte 2, pp. 2922-2930, Set. 2007.

[17] T. Araújo and R. Dinis, "On the Accuracy of the Gaussian Approximation for the Evaluation of Nonlinear Effects in OFDM Signals", *IEEE Trans. on Wireless Comm.*, Vol.9, No.11, pp. 3472-3479, Nov. 2010.

[18] T. Araújo and R. Dinis, "Loading Techniques for OFDM Systems with Nonlinear Distortion Effects", *European Trans. on Telecommunications*, 2012.

[19] A. Papoulis, "Probability, Random Variables and Stochastic Process, 3rd", ed. New York: McGraw-Hill, 1991.

[20] Yuanbin Guo and Joseph R. Cavallaro , " A novel adaptive pre-distorter using LG estimation of SSPA non-linearity in mobile OFDM systems", 2002.

[21] H. Rowe, "Memoryless Nonlinearities with Gaussian Input: Elementary Results", *Bell System Tech. Journal*, Vol. 61, Sep. 1982.

[22] J. Tellado, L. Hoo and J. Cioffi, "Maximum Likelihood Detection of Nonlinearly Distorted Multicarrier Symbols by Iterative Decoding", *IEEE Trans. on Comm.*, Vol. 51, Feb. 2003.

[23] A. Gusmão, R. Dinis and P. Torres, "Low-PMEPR OFDM Transmission with an Iterative Receiver Technique for Cancelation of Nonlinear Distortion", *IEEE VTC'05(Fall)*, Vol. 4, pp. 2367–2371, Sep. 2005.

[24] P.Carvalho, R.Dinis and M.Luzio, "Analytical Characterization of Nonlinearly Distorted TC-OQAM Signals", *IEEE ICSPCS*, Omaha, USA, Sep. 2009.

[25] J. Guerreiro, R. Dinis and P. Montezuma, "Approaching the Maximum Likelihood Performance with Nonlinearly Distorted OFDM Signals", *IEEE VTC'2012 (Spring)*, Yokohama, Japan, May 2012.

[26] J. Guerreiro, R. Dinis and P. Montezuma, "Optimum and Sub-Optimum Receivers for OFDM Signals with Iterative Clipping and filtering", *IEEE VTC'2012 (Fall)*, Qubec City, Canada, Sep.

2012.

[27] J. Guerreiro, R. Dinis and P. Montezuma, "ML-Based Receivers for Underwater Networks Using OFDM Signals with Strong Nonlinear Distortion Effects" *MILCOM 2012*, Florida, USA, Oct. 2012.

[28] *Digital Video Broadcasting (DVB); Framing structure, channel coding and modulation for digital terrestrial television*, ETSI Standard: EN 300 744 V1.6.1, Jan. 2009.

[29] *IEEE Standard for Local and Metropolitan Area Networks - Part 16: Air Interface for Fixed Broadband Wireless Access Systems*, IEEE 802.16-2004, Oct. 2004.

[30] *Part 16: Air Interface for Fixed and Mobile Broadband Wireless Access Systems Amendment 2: Physical and Medium Access Control Layers for Combined Fixed and Mobile Operation in Licensed Bands and Corrigendum 1*, IEEE 802.16-2005, Feb. 2006.

[31] *3rd Generation Partnership Project: Technical Specification Group Radio Access Network; Physical Layers Aspects for Evolved UTRA*, 3GPPP TR 25.814, 2006.

[32] J. W. Cooley and J. W. Tukey., "An algorithm for the machine calculation of complex fourier series", *Mathematics of Computation*, 19(90):297-301, April 1965.

[33] Price, R. "A Useful Theorem for Non-Linear Devices Having Gaussian Inputs", *IEEE Trans. Inform.* Th. 4, 69-72, 1958.

[34] A.van den Bos." The multivariate complex normal distribution - a generalization.", *IEEE Trans. Inform.*, 41(2):537-539, March 1995.

[35] N. M. Blachman. " The uncorrelated output components of a nonlinearity.", *IEEE Trans. Inform.*, 14(2):250-255, March 1968.

[36] M. Abramowitz and I. Stegun, *Handbook of Mathematical Functions"*, New York, Dover Publications, 1972.

[37] A. P. Prudnikov,Y. A. Brychkov and O. I. Marichev. "Integrals and Series, Volume 2 - Special Functions.", Gordon and Breach Science Publishers , 1986.

[38] J. G. Proakis, "Digital Communications - 4th Edition", McGraw-Hill,2001.

Appendix A - Output Autocorrelation for Polar Memoryless Non-linearities with Gaussian Inputs

Let us consider a bandpass signal with real part (2.32), where its complex envelope is given by

$$x(t) = R(t)e^{j\varphi(t)} = x_I(t) + jx_Q(t), \tag{A.1}$$

where $R = R(t) = |x(t)|$ is assumed to be a complex Gaussian process with equally distributed, zero mean real and imaginary components. The autocorrelation of $x(t)$ is given by

$$R_x(\tau) = E[x(t)x^*(t-\tau)] = E\left[\left(x_I(t) + jx_Q(t)\right)\left(x_I(t) - jx_Q(t)\right)\right], \tag{A.2}$$

but, recalling that, $E[A(t) \pm B(t)] = E[A(t)] \pm E[B(t)]$, we can write

$$R_x(\tau) = R_{II}(\tau) + R_{QQ}(\tau) + j\left(R_{QI}(\tau) - R_{IQ}(\tau)\right), \tag{A.3}$$

with

$$R_{II}(\tau) = E[x_I(t)x_I(t-\tau)] \tag{A.4}$$

$$R_{QQ}(\tau) = E[x_Q(t)x_Q(t-\tau)] = R_{II}(\tau) \tag{A.5}$$

$$R_{QI}(\tau) = E[x_Q(t)x_I(t-\tau)] \tag{A.6}$$

$$R_{IQ}(\tau) = E[x_I(t)x_Q(t-\tau)] - R_{QI}(\tau) \tag{A.7}$$

Noting that $R_x(0) = E[x^2(t)] = 2R_{II}(0) = 2\sigma^2$, since $R_{II}(0) = R_{QQ}(0) = \sigma$ and $R_{IQ}(0) = R_{QI}(0) = 0$, we also may write

$$R_x(\tau) = 2(R_{II}(\tau) + jR_{QI}(\tau)), \tag{A.8}$$

In the section 2.3 we saw that the complex envelope of the non-linearity output can be written as

$$y(t) = g\left(x(t)\right) = g\left(R(t)e^{j\varphi(t)}\right) = f(R)e^{j\varphi}, \tag{A.9}$$

with $f(R) = A(R)e^{j\Theta(R)}$ representing the function that characterizes the polar memoryless non-linearity. The autocorrelation of the output is

$$\begin{aligned} R_y(\tau) &= E[y(t)y^*(t-\tau)] \\ &= E[g(x_1)g^*(x_2)] \\ &= E[g(x_{1I} + jx_{1Q})g(x_{2I} - jx_{2Q})] \\ &= \int_{-\infty}^{+\infty}\int_{-\infty}^{+\infty}\int_{-\infty}^{+\infty}\int_{-\infty}^{+\infty} g(x_{1I} + jx_{1Q})g(x_{2I} - jx_{2Q})p(x_{1I}, x_{1Q}, x_{2I}, x_{2Q})\mathrm{d}x_{1I}\mathrm{d}x_{1Q}\mathrm{d}x_{2I}\mathrm{d}x_{2Q}, \end{aligned} \tag{A.10}$$

with $x_1 = x(t) = x_{1I} + jx_{1Q}$ and $x_2 = x(t-\tau) = x_{2I} + jx_{2Q}$. Let us consider the vector $\mathbf{w} = [x_{1I}\, x_{1Q}\, x_{2I}\, x_{2Q}]^T$, where the superscript T denotes transposition. Since we are assuming that $E[x_{1I}] = E[x_{1Q}] = E[x_{2I}] = E[x_{2Q}] = 0$, the covariance of $\mathbf{w}$ is the matrix $\mathbf{W}$ that is

written as

$$\begin{aligned}\mathbf{W} &= E[\mathbf{w}\mathbf{w}^T] \\ &= \begin{bmatrix} E[x_{1I}x_{1I}] & E[x_{1I}x_{1Q}] & E[x_{1I}x_{2I}] & E[x_{1I}x_{2Q}] \\ E[x_{1Q}x_{1I}] & E[x_{1Q}x_{1Q}] & E[x_{1Q}x_{2I}] & E[x_{1Q}x_{2Q}] \\ E[x_{2I}x_{1I}] & E[x_{2I}x_{1Q}] & E[x_{2I}x_{2I}] & E[x_{2I}x_{2Q}] \\ E[x_{2Q}x_{1I}] & E[x_{2Q}x_{1Q}] & E[x_{2Q}x_{2I}] & E[x_{2Q}x_{2Q}] \end{bmatrix} \\ &= \begin{bmatrix} \sigma^2 & 0 & R_{II}(\tau) & -R_{QI}(\tau) \\ 0 & \sigma^2 & R_{QI}(\tau) & R_{II}(\tau) \\ R_{II}(\tau) & -R_{QI}(\tau) & \sigma^2 & 0 \\ R_{QI}(\tau) & R_{II}(\tau) & 0 & \sigma^2 \end{bmatrix}\end{aligned} \tag{A.11}$$

with its determinant defined as

$$\det(\mathbf{W}) = \sigma^8 \left(1 - \frac{R_{II}^2(\tau) + R_{QI}^2(\tau)}{\sigma^4}\right)^2 = \sigma^8 \left(1 - \frac{|R_x(\tau)|^2}{4\sigma^4}\right)^2 = \sigma^8 \left(1 - \rho^2\right)^2, \tag{A.12}$$

where ρ denotes the correlation coefficient (i.e., the normalized autocorrelation of the output) defined as

$$\rho = \frac{|R_x(\tau)|}{R_x(0)} = \frac{|R_x(\tau)|}{2\sigma^2} \tag{A.13}$$

Since $\det(\mathbf{W})$ is non-zero, we can compute the inverse of $\mathbf{W}$, resulting

$$\mathbf{W}^{-1} = \begin{bmatrix} \sigma^2 & 0 & -R_{II}(\tau) & R_{QI}(\tau) \\ 0 & \sigma^2 & -R_{QI}(\tau) & -R_{II}(\tau) \\ -R_{II}(\tau) & R_{QI}(\tau) & \sigma^2 & 0 \\ -R_{QI}(\tau) & -R_{II}(\tau) & 0 & \sigma^2 \end{bmatrix} \tag{A.14}$$

The joint PDF of the vector $\mathbf{w}$ is given by [34]

$$p(w) = \frac{1}{(2\pi)^2 \sqrt{\det(\mathbf{W})}} e^{-\frac{1}{2} w^T \mathbf{W}^{-1} w} = \frac{1}{4\pi^2 \sigma^4 \left(1 - \rho^2\right)^2} e^A \tag{A.15}$$

with

$$A = -\frac{\sigma^2\left(x_{1I}^2 + x_{2I}^2 + x_{1Q}^2 + x_{2Q}^2\right) - 2R_{II}(\tau)\left(x_{1I}x_{2I} + x_{1Q}x_{2Q}\right) - 2R_{Q_I}(\tau)\left(x_{1I}x_{2Q} - x_{1Q}x_{2I}\right)}{2\sqrt{\det(\mathbf{W})}}$$
$$= -\frac{\sigma^2\left(|x_1|^2 + |x_2|^2\right) - \mathrm{Re}\left\{R_x(\tau)x_1x_2^*\right\}}{2\sigma^4(1-\rho^2)} \tag{A.16}$$

Let us now consider polar coordinates, i.e., $x_1 = R_1e^{j\varphi_1}$ and $x_2 = R_2e^{j\varphi_2}$. In this case, we can write (A.16) as [35]

$$A = -\frac{\sigma^2\left(R_1^2 + R_2^2\right) - |R_x(\tau)|R_1R_2\cos\left(\varphi_1 - \varphi_2 + \arg\left\{R_x(\tau)\right\}\right)}{2\sigma^4(1-\rho^2)}$$
$$= -\frac{R_1^2 + R_2^2 - 2\rho R_1R_2\cos\left(\varphi_1 - \varphi_2 + \phi\right)}{\rho_0}, \tag{A.17}$$

with $\phi = \arg\left\{R_x(\tau)\right\}$ and $\rho_0 = 2\sigma^2(1-\rho^2)$. Using (A.15) and (A.17) in (A.10) and applying the considered polar coordinate transform, we have

$$R_y(\tau) = \frac{1}{2\pi^2\sigma^2\rho_0}\int_0^{+\infty}\int_0^{+\infty}\int_0^{2\pi}\int_0^{2\pi} f(R_1)f^*(R_2)e^{j(\varphi_1-\varphi_2)}e^{-\frac{R_1^2+R_2^2-2\rho R_1R_2\cos(\varphi_1-\varphi_2+\phi)}{\rho_0}}$$
$$R_1R_2\mathrm{d}R_1\mathrm{d}R_2\mathrm{d}\varphi_1\mathrm{d}\varphi_2 \tag{A.18}$$

And, with some manipulations, we may write

$$R_y(\tau) = \frac{1}{2\pi^2\sigma^2\rho_0}\int_0^{+\infty}\int_0^{+\infty}\int_0^{2\pi}\int_0^{2\pi} f(R_1)f^*(R_2)R_1R_2e^{-\frac{R_1^2+R_2^2}{\rho_0}}$$
$$\left(\int_0^{2\pi}\int_0^{2\pi} e^{j(\varphi_1-\varphi_2+\phi-\phi)}e^{\frac{2\rho R_1R_2\cos(\varphi_1-\varphi_2+\phi)}{\rho_0}}\mathrm{d}\varphi_1\mathrm{d}\varphi_2\right)\mathrm{d}R_1\mathrm{d}R_2$$
$$= \frac{e^{-j\phi}}{2\pi^2\sigma^2\rho_0}\int_0^{+\infty}\int_0^{+\infty}\int_0^{2\pi}\int_0^{2\pi} f(R_1)f^*(R_2)R_1R_2e^{-\frac{R_1^2+R_2^2}{\rho_0}}$$
$$\left(\int_0^{2\pi}\int_0^{2\pi} e^{j(\varphi_1-\varphi_2+\phi)}e^{\frac{2\rho R_1R_2\cos(\varphi_1-\varphi_2+\phi)}{\rho_0}}\mathrm{d}\varphi_1\mathrm{d}\varphi_2\right)\mathrm{d}R_1\mathrm{d}R_2 \tag{A.19}$$

Let us now consider the modified Bessel function of first kind , $I_n(z)$, that can be written as (see [36], Equation(9.6.19))

$$I_n(z) = \frac{1}{\pi}\int_0^{\pi} \cos(n\theta)e^{z\cos(\theta)}\mathrm{d}\theta \tag{A.20}$$

considering $n = 1$, $z = \frac{2\rho R_1 R_2}{\rho_0}$ and $\theta = \varphi_1 - \varphi_2 + \phi$ we have

$$I_1\left(\frac{2\rho R_1 R_2}{\rho_0}\right) = \frac{1}{\pi}\int_0^{\pi} \cos(\theta)e^{\frac{2\rho R_1 R_2}{\rho_0}\cos(\theta)}\mathrm{d}\theta \tag{A.21}$$

since the integrand is a periodic function, we also may write

$$\frac{1}{\pi}\int_0^{2\pi} e^{j\theta}e^{z\cos(\theta)}\mathrm{d}\theta = \frac{1}{\pi}\int_0^{2\pi} \left(\cos(\theta) + j\sin(\theta)\right)e^{z\cos(\theta)}\mathrm{d}\theta \tag{A.22}$$

and the double integral in (A.19) can be written as

$$\int_0^{2\pi}\int_0^{2\pi} \cos(\varphi_1 - \varphi_2 + \phi)e^{\frac{2\rho R_1 R_2\cos(\varphi_1-\varphi_2+\phi)}{\rho_0}}\mathrm{d}\varphi_1\mathrm{d}\varphi_2 = 4\pi^2 I_1\left(\frac{2\rho R_1 R_2}{\rho_0}\right) \tag{A.23}$$

thus, (A.19) becomes

$$R_y(\tau) = \frac{2e^{-j\phi}}{\sigma^2\rho_0}\int_0^{+\infty}\int_0^{+\infty} f(R_1)f^*(R_2)R_1R_2e^{-\frac{R_1^2+R_2^2}{\rho_0}} I_1\left(\frac{2\rho R_1 R_2}{\rho_0}\right)\mathrm{d}R_1\mathrm{d}R_2 \tag{A.24}$$

Using the Laguerre polynomial series expansion (see [37], Equation (5.11.3.7)), we can write

$$\sum_{\gamma=0}^{+\infty}\frac{\gamma}{(\alpha+1)_\gamma}t^\gamma L_\gamma^{(\alpha)}(x)L_\gamma^{(\alpha+n)}(y) = \tag{A.25}$$

$$\Gamma(\alpha+1)(1-t)^{-n-1}(txy)^{-\frac{\alpha}{2}}e^{\frac{x+y}{t-1}t}$$
$$\sum_{\gamma=0}^{n}(-1)^\gamma\binom{n}{\gamma}\left(\frac{tx}{y}\right)^{\frac{\gamma}{2}} I_{\gamma+\alpha}\left(\frac{2\sqrt{txy}}{1-t}\right) \tag{A.26}$$

considering $n = 0$, $\alpha = 1$, and

$$(A)_k = \frac{\Gamma(A+k)}{\Gamma(A)}, \tag{A.27}$$

where, $\Gamma(A)$ is the Gamma function that is defined as

$$\Gamma(A) = (A-1)! \tag{A.28}$$

we note that

$$(\alpha+1)_\gamma = 2_\gamma = \frac{\Gamma(2+\gamma)}{\Gamma(2)} = \frac{(\gamma+1)!}{1!} = (\gamma+1)! \tag{A.29}$$

and (A.25) becomes

$$\sum_{\gamma=0}^{+\infty} \frac{1}{\gamma+1} t^\gamma L_\gamma^{(1)}(x) L_\gamma^{(1)}(y) = \frac{1}{(1-t)\sqrt{txy}} e^{\frac{x+y}{t-1}t} I_1\left(\frac{2\sqrt{txy}}{1-t}\right) \tag{A.30}$$

making $t=\rho^2$, $x=\frac{R_1^2}{2\sigma^2}$ and $y=\frac{R_2^2}{2\sigma^2}$, we can write (A.30) as

$$\begin{aligned}\sum_{\gamma=0}^{+\infty} \frac{1}{\gamma+1} \rho^{2\gamma} L_\gamma^{(1)}\left(\frac{R_1^2}{2\sigma^2}\right) L_\gamma^{(1)}\left(\frac{R_2^2}{2\sigma^2}\right) &= \frac{1}{(1-\rho^2)\sqrt{\rho^2 \frac{R_1^2}{2\sigma^2}\frac{R_2^2}{2\sigma^2}}} e^{\frac{\frac{R_1^2}{2\sigma^2}+\frac{R_2^2}{2\sigma^2}}{\rho^2-1}\rho^2} I_1\left(\frac{2\sqrt{\rho^2 \frac{R_1^2}{2\sigma^2}\frac{R_2^2}{2\sigma^2}}}{1-\rho^2}\right) \\ &= \frac{2\sigma^2}{(1-\rho^2)\rho R_1 R_2} e^{-\frac{R_1^2+R_2^2}{\rho_0}\rho^2} I_1\left(\frac{2\rho R_1 R_2}{\rho_0}\right)\end{aligned} \tag{A.31}$$

where $L_\gamma^{(1)}$ denotes the generalized Laguerre polynomial of order γ, defined as

$$L_\gamma^{(1)}(x) = \frac{1}{\gamma!} x^{-1} e^x \frac{d^\gamma}{dx^\gamma}\left(e^{-x} x^{\gamma+1}\right) \tag{A.32}$$

Replacing (A.31) in (A.24) we get

$$\begin{aligned}
R_y(\tau) = \frac{2e^{-j\phi}}{\sigma^2\rho_0}\frac{\rho(1-\rho^2)}{2\sigma^2}\int_0^{+\infty}\int_0^{+\infty} f(R_1)f^*(R_2)R_1^2R_2^2 e^{-\frac{R_1^2+R_2^2}{\rho_0}} e^{-\frac{R_1^2+R_2^2}{\rho_0}\rho^2} \\
\cdot\frac{2\sigma^2}{(1-\rho^2)\rho R_1R_2} e^{-\frac{R_1^2+R_2^2}{\rho_0}\rho^2} I_1\left(\frac{2\rho R_1R_2}{\rho_0}\right)\mathrm{d}R_1\mathrm{d}R_2 \\
= \frac{\rho}{2\sigma^6}e^{-j\phi}\int_0^{+\infty}\int_0^{+\infty} f(R_1)f^*(R_2)R_1^2R_2^2 e^{\frac{-(1-\rho^2)(R_1^2+R_2^2)}{2\sigma^2(1-\rho^2)}} \\
\cdot\frac{2\sigma^2}{(1-\rho^2)\rho R_1R_2} e^{-\frac{R_1^2+R_2^2}{\rho_0}\rho^2} I_1\left(\frac{2\rho R_1R_2}{\rho_0}\right)\mathrm{d}R_1\mathrm{d}R_2 \\
= \frac{1}{2\sigma^6}e^{-j\phi}\int_0^{+\infty}\int_0^{+\infty} f(R_1)f^*(R_2)R_1^2R_2^2 e^{\frac{R_1^2+R_2^2}{2\sigma^2}} \\
\cdot\left(\sum_{\gamma=0}^{+\infty}\frac{1}{\gamma+1}\rho^{2\gamma+1}L_\gamma^{(1)}\left(\frac{R_1^2}{2\sigma^2}\right)L_\gamma^{(1)}\left(\frac{R_2^2}{2\sigma^2}\right)\right)\mathrm{d}R_1\mathrm{d}R_2
\end{aligned} \tag{A.33}$$

Since the double integral in (A.33) is separable in two equal integrals in respect to R_1 and R_2, we can write

$$R_y(\tau) = \frac{1}{2\sigma^6}e^{-j\phi}\sum_{\gamma=0}^{+\infty}\frac{1}{\gamma+1}\rho^{2\gamma+1}\left|\int_0^{+\infty} R^2 f(R)e^{-\frac{R^2}{2\sigma^2}}L_\gamma^{(1)}\left(\frac{R^2}{2\sigma^2}\right)\mathrm{d}R\right|^2 \tag{A.34}$$

or,

$$R_y(\tau) = 2\sum_{\gamma=0}^{+\infty} P_{2\gamma+1}\rho^{2\gamma+1}e^{-j\phi}, \tag{A.35}$$

where $P_{2\gamma+1}$ given by

$$P_{2\gamma+1} = \frac{1}{4\sigma^6(\gamma+1)}\left|\int_0^{+\infty} R^2 f(R)e^{-\frac{R^2}{2\sigma^2}}L_\gamma^{(1)}\left(\frac{R^2}{2\sigma^2}\right)\mathrm{d}R\right|^2 \tag{A.36}$$

These coefficients represents the total power associated to IMP of order $2\gamma+1$. Since

$$\rho^{2\gamma+1}e^{-j\phi} = \frac{R_x(\tau)^{\gamma+1}R_x^*(\tau)^\gamma}{R_x(0)^{2\gamma+1}}, \tag{A.37}$$

we can finally define the autocorrelation of the nonlinearity output as

$$R_y(\tau) = 2\sum_{\gamma=0}^{+\infty} P_{2\gamma+1} \frac{R_x(\tau)^{\gamma+1} R_x^*(\tau)^{\gamma}}{R_x(0)^{2\gamma+1}} \tag{A.38}$$